REDOX SIGNALING THROUGH THE ENDOPLASMIC RETICULUM CHAPERONE BIP

A Dissertation

Presented to the Faculty of the Graduate School

of Cornell University

In Partial Fulfillment of the Requirements for the Degree of

Doctor of Philosophy

by

Kevin David Siegenthaler

May 2019

REDOX SIGNALING THROUGH THE ENDOPLASMIC RETICULUM CHAPERONE BIP

Kevin David Siegenthaler, Ph. D.

Cornell University 2019

The process of oxidative protein folding in the endoplasmic reticulum (ER) generates hydrogen peroxide, a reactive oxygen species (ROS). The secretory load of a cell can vary widely, and cells require mechanisms to maintain folding fidelity within the ER despite fluctuating ROS levels. One such mechanism involves tuning the activity of the ER Hsp70 chaperone, BiP. Our lab established that a conserved cysteine residue within the nucleotide-binding domain of *S. cerevisiae* BiP (Kar2) is oxidized in response to ROS accumulation, and oxidation causes the chaperone to bind peptides with perpetually high affinity. The modified peptide-binding activity of oxidized BiP imparts a protective advantage to cells during oxidative stress by limiting aggregation of proteins damaged by ROS. Although beneficial when ROS levels are high, perpetual BiP modification and the holding of peptides decreases cell fitness under non-stressed conditions. Thus, it is essential that cells coordinate BiP oxidation to maintain folding homeostasis with the changing ER redox status.

Here we uncover roles for the BiP nucleotide exchange factor, Sil1, and the oxidative protein folding enzyme, protein disulfide isomerase (PDI), in controlling the redox state of BiP In Chapter 2, we show that Sil1 possesses a N-terminal cysteine pair capable of reducing the redox-sensitive BiP cysteine. The unexpected reductant

activity of Sil1 enables BiP to resume its non-stressed peptide binding activities. In Chapter 3, we identify PDI as a further regulator of BiP oxidation as PDI reduces BiP both directly and by providing electrons to activate Sil1. Due to its role in oxidative protein folding, the redox state of PDI (and its capacity to give electrons to BiP) is tightly linked to the current redox status of the ER. We suggest that together PDI and Sil1 serve as sensors of the ER redox state that adjust BiP function to match the ER redox status.

BIOGRAPHICAL SKETCH

Kevin Siegenthaler was born on September 5th, 1991 in Syracuse New York and was raised by his family in the nearby town of Verona. He graduated from Vernon-Verona-Sherrill High School as the Valedictorian of the Class of 2009. Kevin attended the State University of New York at Geneseo where he was awarded a Bachelor of Science in Biochemistry. He matriculated *summa cum laude* and was elected to the University chapter of Phi Beta Kappa. During his time at Geneseo, Kevin worked in the laboratory of Dr. Ruel McKnight where he studied the effects of varied substituents on the DNA binding properties of a homologous series of natural products. In addition to this, Kevin spent a summer working in the lab of Dr. James Hougland at Syracuse University where he studied post-translational regulatory mechanisms of a Ghrelin *O*-acyltransferase enzyme. While at Geneseo, Kevin worked as an undergraduate teaching assistant for multiple chemistry courses which started his ambition to pursue a career in education. His interests in research and teaching led Kevin to enroll in a PhD program at Cornell University where he joined the lab of Dr. Carolyn Sevier where he has been conducting his dissertation since. In the lab of Dr. Sevier, Kevin studied the regulation of the endoplasmic reticulum chaperone BiP in response to oxidative stress. Outside of the lab, Kevin is an avid basketball fan, enjoys downhill skiing and playing tennis, and is most often found spending time with his family and friends.

For my family. Thank you for your support along the way.

ACKNOWLEDGMENTS

I am immensely grateful to all who provided me with support during my graduate studies. While completion of my dissertation has been a great challenge, the encouragement of my family, friends and colleagues has been invaluable and has ensured that my time in graduate school has been rewarding.

I must first express my gratitude to Dr. Carolyn Sevier. As my advisor. Carolyn has taught me all of the skills necessary to be a successful scientist. Furthermore, her dedication and persistence have provided me with an example I will to strive to emulate in the future. I also would like to thank all of the members of the Sevier lab during my studies: Heather Marsh, Erin Nicklow, Furkat Mukhtarov, Jie Wang, Kristeen Pareeja, Jinnie Kim, Kie Kawate, and Jewon Sohn. Thank you all for the help and advice you provided throughout my time in the lab, but more importantly, thank you for the countless good memories and funny stories. I am fortunate to have worked with such an amazing group of people. Additionally, I thank my committee members, Dr. John Helmann and Dr. William Brown for their guidance and support.

Last but certainly not least, I am grateful to my mother and brothers for the support they provided during graduate school. While undoubtedly rewarding, my research has also been exacting and has tested my perseverance. The encouragement of my family helped me through the difficult times, and without them, I could not have succeeded.

TABLE OF CONTENTS

LIST OF FIGURES

LIST OF TABLES

CHAPTER 1

INTRODUCTION

Protein Folding in the Endoplasmic Reticulum

Functions of the endoplasmic reticulum

A defining feature of eukaryotes is the presence of an endomembrane system forming distinct organelles. Cellular compartmentalization allows for a division of labor within the cell where processes can be carried out in optimal environments. This is exemplified by the endoplasmic reticulum (ER). The ER maintains an oxidizing environment relative to the cytoplasm, which allows for the introduction of stabilizing disulfide bonds within secretory proteins (Cooper, 2000). Thus, maintenance of a delicate redox balance is essential for the ER to carry out its specialized function of secretory protein formation, and if this balance is disturbed, ER function will be jeopardized. To prevent loss of ER function, regulatory mechanisms exist to both maintain the redox milieu of the ER within a narrow range and facilitate the maintenance of ER processes within an oxidizing environment (Cooper, 2000).

One of the primary functions of the ER is the production of proteins that are secreted from the cell. Secreted proteins may act as signaling molecules, enzymes, agents of immunity, assume a structural role at the exterior of the cell or provide a myriad of other functions (Cooper, 2000). They need to be properly folded within the lumen and then are subjected to a number of post-translational modifications. The majority of secreted proteins will have the signal sequence (which targeted them to the ER) cleaved since signal sequences tend to be hydrophobic and can interfere with folding. Also, most secretory proteins will be N-glycosylated at specific residues. The added sugars can facilitate protein folding, serve as a recognition motifs that enables binding

to receptor proteins, and may increase the stability of the folded protein (Hendershot & Kearney, 1988; Helenius & Aebi, 2004; Hebert, Garman, & Molinari, 2005). Finally, the introduction of disulfide bonds between cysteine residues provides added stability to proteins which may be necessary for proteins secreted into the extracellular environment (Braakman & Hebert, 2013; Zielinska, Gnad, Wiśniewski, & Mann, 2010; Apweiler, Hermjakob, & Sharon, 1999).

In addition to its role in protein production, the ER also is the site of other cell processes. It is a storage site for cellular calcium reserves (Koch, 1990; Cooper, 2000). Regulated uptake and release of ER calcium governs many signaling pathways including muscle contraction and initiation of cell death (Chaube & Werstuck, 2016). The ER also serves as the site of synthesis of cellular lipids, and aids in the detoxification of some toxins (Cooper, 2000).

Chaperone systems within the endoplasmic reticulum

Approximately one third of the human proteome is estimated to be secreted so maintaining the fidelity of secretory protein production is critical for cell viability (Huh et al., 2003). Each of these proteins must be translocated across the ER membrane in an unfolded state and then folded within the lumen (Braakman & Hebert, 2013). While some small proteins can adopt their structure unaided, many require the assistance of molecular chaperones (Radford, 2000; Kim, Hipp, Bracher, Hayer-Hartl, & Hartl, 2013). Molecular chaperones are defined as proteins that form transient interactions with a polypeptide in order to facilitate the folding of a protein (Ellis & Hemmingsen, 1989). The ER possesses chaperones systems that facilitate folding of secretory proteins. Broadly, these chaperones can be categorized into one of two families: carbohydrate binding chaperones and classical chaperones (Braakman & Hebert, 2013; Lamriben, Graham, Adams, & Hebert, 2016).

Carbohydrate binding chaperones fold proteins by temporarily associating with the glycosylation units added to their substrates (Braakman & Hebert, 2013; Lamriben et al., 2016). Thus, they are a unique class of chaperones specific to the ER. Calnexin and calreticulin both contain carbohydrate-binding domains, which imbue them with affinity for maturing proteins within the ER. The activity of these chaperones slows the folding process to ensure fidelity, prevents aggregation of unfolded substrates and retains improperly folded proteins in the ER to allow for subsequent folding attempts. Additionally, they appear to facilitate disulfide bond formation and proline isomerization via their interactions with enzymes that catalyze these processes (Lamriben et al., 2016). Trimming of the branched sugars on the folding proteins also directs the substrates maturation process. Sequential cleavage of the sugars by glucosidases I and II allow for calnexin binding. Subsequent cleavage of additional sugars causes the protein to be released from the chaperone so that it may finish folding and be secreted from the ER (Hebert et al., 2005; Braakman & Hebert, 2013).

In contrast to carbohydrate binding chaperones, classical chaperones fold proteins by directly binding to and obscuring peptide sequences within the substrate. This family is comprised primarily of the heat-shock proteins (Braakman & Hebert, 2013; Lamriben et al., 2016). As the name implies, these proteins were discovered as factors that mitigate proteotoxic stress induced by heat shock. Despite this, these chaperones are expressed constitutively and aid in the folding of proteins all the time not just during heat shock (Lindquist, 1986; Ritossa, 1996). They primarily recognize exposed hydrophobic sequences since such patches are generally hidden within the interior of folded proteins (Flynn, Pohl, Flocco, & Rothman, 1991). The heat shock proteins are further subcategorized into families by their approximate size (e.g. Hsp60, Hsp70 etc.). The different families are highly conserved across all organisms, and in eukaryotes,

some families are present within distinct organelles (Lindquist, 1986). The ER of all eukaryotes possesses Hsp70 chaperones as well as Hsp40 chaperones which assist the Hsp70 system (Braakman & Hebert, 2013). Additionally, some organisms possess Hsp90 chaperones within the ER. While the structures, substrates and detailed mechanisms of Hsp70 and Hsp90 do differ, they both rely on the binding and hydrolysis of adenine nucleotides to dictate their transient binding properties that make them chaperones (Braakman & Hebert, 2013). The contents of this dissertation will focus primarily on the Hsp70 chaperone system and mechanisms which regulate Hsp70 function.

The ER HSP70, BiP

The ER Hsp70 chaperone was originally identified as a 78-kDa protein that was bound to heavy chain precursors of antibody synthesis. For this reason, the protein was dubbed BiP for immunoglobulin heavy-chain binding protein (Haas & Wabl, 1983). Subsequent work revealed that this protein was critical for antibody synthesis hinting at its role as a chaperone (Bole, Hendershot, & Kearney, 1986; Hendershot & Kearney, 1988), and eventually, sequence analysis revealed that BiP was the same protein as GRP78, an ER-localized Hsp70 which is upregulated by glucose starvation (Munro & Pelham, 1986; Shiu, Pouyssegur, & Pastan, 1977; Hendershot, Ting, & Lee, 1988). Shortly thereafter, the *Saccharomyces cerevisiae* gene *KAR2* (named for its essential role in the process of nuclear fusion - karyogamy) was shown to encode for a homologous protein in yeast (Rose, Misra, & Vogel, 1989).

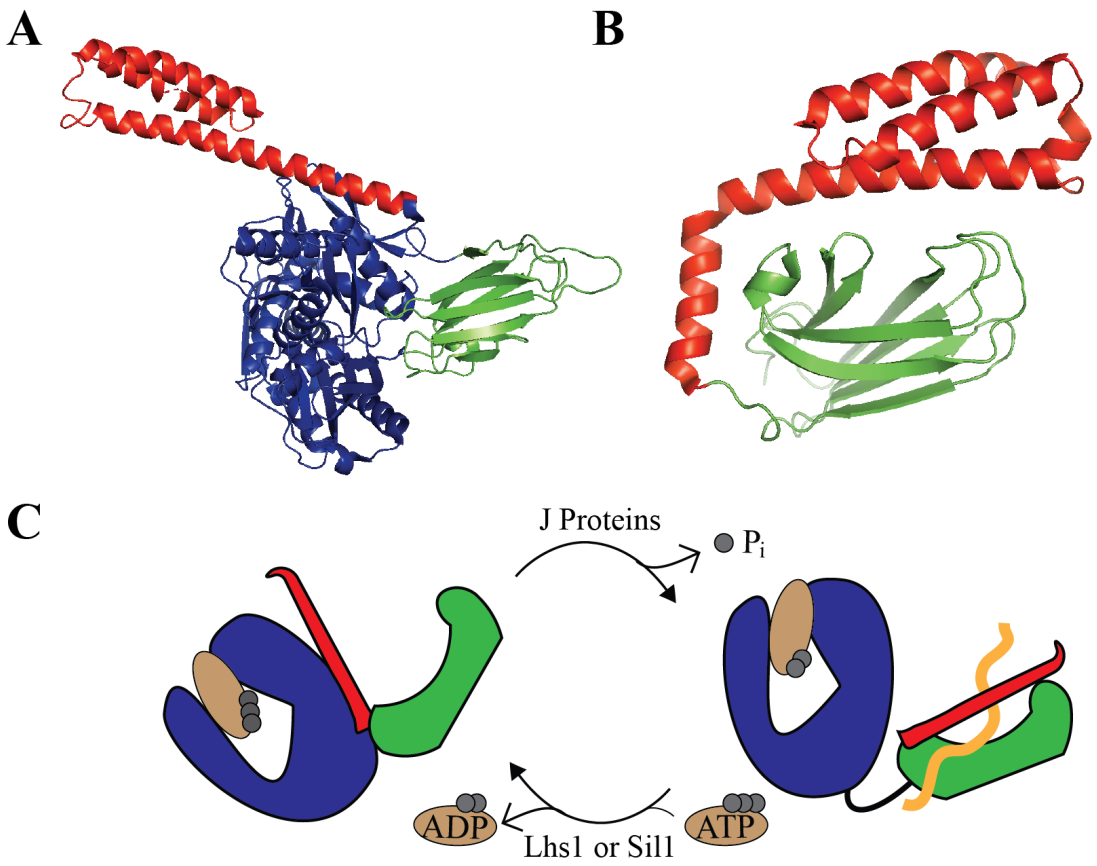

Figure 1.1 BiP peptide binding is allosterically regulated by an ATP hydrolysis cycle. (A) Crystal structure of full length BiP-ATP from (Yang et al., 2015). PDB: 5E84. NBD: blue. SBD: green. SBD lid: red. **(B)** Isolated BiP SBD from (Yang et al., 2015). PDB: 5E85. **(C)** BiP ATP hydrolysis cycle. The NBD of BiP-ATP engages the protein lid leaving the SBD open. J-protein catalyzed hydrolysis of ATP to ADP causes the protein lid to shut allowing BiP to bind peptides with high affinity. ATP/ADP: brown oval. Phosphate: gray circle. Peptide substrate: orange.

BiP mechanism and structure

A detailed understanding of Hsp70 proteins is available owing to a large body of work characterizing various family members, especially the *E. coli* Hsp70 DnaK. While the eukaryotic proteins only share 40-50% sequence identity with DnaK, structural comparisons suggest their peptide binding mechanisms are highly conserved (Yang, Nune, Zong, Zhou, & Liu, 2015). The chaperones are comprised of a substrate-binding domain (SBD) and a nucleotide-binding domain (NBD) joined by a short, flexible linker sequence (**Figure 1.1A**). The coordinated activities of

these domains imbue BiP with transient peptide binding properties necessary for chaperone function as well as for the completion of all other cell tasks carried out by the chaperone (Mayer & Bukau, 2005; Young, 2010; Behnke, Feige, & Hendershot, 2015).

The nucleotide bound within the BiP NBD regulates the affinity of the SBD for substrates (**Figure 1.1B**) (Mayer & Bukau, 2005). When ADP is bound, the NBD and the SBD do not interact. The two domains remain tethered by the linker sequence, but they behave independently of one another. In this state, substrate binding and release are very slow as a lid-like structure within the BiP SBD is closed over the peptide binding site (Buchberger et al., 1995; Bertelsen, Chang, Gestwicki, & Zuiderweg, 2009). Once ATP is exchanged for ADP however, an allosteric relay between the domains changes the peptide binding properties of BiP. The nucleotide binding domain closes tightly around the ATP triggering the docking of the hydrophobic linker sequence within the NBD. These structural changes cause the SBD lid to open leaving the peptide-binding site exposed. In this conformation, peptides bind to and release BiP very quickly (Flynn, Chappell, & Rothman, 1989; Schmid, Baici, Gehring, & Christen, 1994). Upon ATP hydrolysis however, the lid will once again close enabling BiP to bind peptides tightly, thereby completing the cycle (Mayer & Bukau, 2005; Young, 2010; Behnke et al., 2015; Yang et al., 2015). Thus, the energy provided by ATP hydrolysis maintains BiP as a non-equilibrium machine which can modulate its affinity for peptides (De Los Rios & Barducci, 2014).

BiP (and all Hsp70s) possesses low levels of intrinsic ATPase activity, and it relies on multiple cochaperones to catalyze efficient progression through its ATPase cycle. ATP hydrolysis is stimulated by members of the Hsp40 family. As many of these proteins are larger than 40 kDa, they are more commonly referred to as J proteins because of their homologous function to DnaJ in bacteria (**Figure 1.1B**). A large number of proteins across many species

contain J domains which stimulate the ATPase activity of Hsp70s. Each J-protein seems to stimulate ATP hydrolysis in order to facilitate a particular function of BiP while other domains of the protein coordinate other functions that assist with the folding process. For instance, some of these cochaperones are even able to bind and deliver sets of substrates to BiP. Upon transfer of the substrate, the J protein will stimulate ATP hydrolysis thereby closing the SBD lid and enabling BiP to bind the peptide with high affinity (Dong, Bridges, Apsley, Xu, & Weaver, 2008; Ushioda et al., 2008; Kampinga & Craig, 2010; Otero, Lizák, & Hendershot, 2010; Wen & Damania, 2010; Cyr & Ramos, 2015; Melnyk, Rieger, & Zimmermann, 2015; Sevier, 2018). The second step of the BiP ATPase cycle is catalyzed by nucleotide exchange factors, or NEFs. Two NEFs have been identified in the ER, Sil1 (also known as Bap) and Lhs1 (also known as Grp170 or Orp150) (Behnke et al., 2015). Sil1 and Lhs1 appear to have partially redundant function as they can both stimulate ADP exchange for ATP, but they are not completely redundant as Lhs1 is essential in mammals and Sil1 is not (Bracher & Verghese, 2015; Behnke et al., 2015). These NEFs will be discussed in further detail later in this chapter.

Roles of BiP in the ER

The peptide binding properties of BiP allow it to carry out a variety of roles in the ER. In addition to its role in protein folding, BiP has also been shown to maintain the permeability of the ER membrane, facilitate the translocation of proteins into and out of the lumen, regulate induction of the unfolded protein response (UPR) and maintain cellular calcium homeostasis (Gething, 1999; Dudek et al., 2009; Clerico, Tilitsky, Meng, & Gierasch, 2015). Given the numerous functions of BiP in the maintenance of ER homeostasis, the protein is considered the "master regulator of ER function" (Hendershot, 2004).

The role of BiP in ER protein assembly actually begins prior to the folding of a translocated polypeptide. Evidence suggests that BiP assists in the translocation of luminal proteins across the ER membrane (Rapoport, Li, & Park, 2017; Park & Rapoport, 2012). BiP has long been known to associate with Sec61, also known as the translocon (the protein channel through which ER proteins are brought into the ER). Studies showed that BiP is essential for the successful translocation of ER proteins, as depletion of the chaperone prevents the accumulation of mature proteins within the ER (Vogel, Misra, & Rose, 1990). It was later determined that BiP acts as a molecular ratchet preventing backward diffusion of these proteins through the translocon (Matlack, Misselwitz, Plath, & Rapoport, 1999). While initially hypothesized that ATP hydrolysis by BiP could provide the necessary energy to drive protein translocation, this does not appear to be the case. Efficient translocation of the model substrate prepro-α-factor (ppαf) into proteoliposomes was observed when either BiP or antibodies directed against ppαf were included in the liposomes (Matlack et al., 1999). The ability of BiP or the ppαf antibodies to translocate the substrate indicates that no ATP hydrolysis is required for translocation, but rather, a molecule capable of binding the translocating substrates is necessary inside the liposome. Thus, BiP simply acts as a Brownian ratchet by preventing backwards flow of translocating proteins (Matlack et al., 1999).

BiP functions as a chaperone by recognizing and transiently binding diverse peptide sequences (Mayer & Bukau, 2005). Luminal proteins are translocated across the ER membrane in an unfolded state (Behnke et al., 2015). During the translocation and folding processes, hydrophobic residues which will be buried within the core of the final protein structure are temporarily exposed. These residues will tend to cluster with other hydrophobic sequences, leading to protein aggregation. BiP prevents this by binding to and sequestering such residues

until a time when they can assume their proper position within the folded protein (Bukau & Horwich, 1998; Clerico et al., 2015). Thus, repeated rounds of peptide binding and release improve the probability that a protein will achieve its native structure (Mayer & Bukau, 2005).

As would be expected of a chaperone that assists the folding of so many proteins, BiP is able to recognize a multitude of different peptide sequences (Behnke, Mann, Scruggs, Feige, & Hendershot, 2016). The consensus sequence for BiP binding is fairly non-specific. The sequence has been loosely defined as the presence of hydrophobic or aromatic residues in alternating positions (Bukau & Horwich, 1998; Clerico et al., 2015). The binding cleft within the BiP SBD is hydrophobic appearing to mimic the interior of a folded protein and thus provides a temporary interacting platform for these aggregation-prone sequences (Flynn et al., 1991).

BiP is also critical to the retrotranslocation of proteins that fail to fold properly. Despite BiP chaperone activity, inevitably some proteins will be unable to adopt their native conformation. When this occurs, cells must utilize the ubiquitin proteasome system within the cytosol to degrade these substrates necessitating the ejection of these proteins back into the cytosol (Meusser, Hirsch, Jarosch, & Sommer, 2005). This process of ER-associated degradation (ERAD) again relies on the substrate binding capabilities of BiP. In short, misfolded proteins are recognized within the ER and brought to a channel for retrotranslocation. Once moved back into the cytosol, the proteins are ubiquitinated and targeted for proteasomal degradation. It has been suggested that BiP is necessary to maintain ERAD substrates in a soluble state until they can be fed back into the cytosol (Kabani et al., 2003; Meusser et al., 2005). Without the activity of BiP, these proteins would likely aggregate before they have the chance to be degraded.

The presence of channels that are wide enough for polypeptides to pass through present a potential problem when it comes to maintaining a permeability barrier between the ER and the

cytosol. Proper function of the ER requires a lumenal chemical environment that differs from that of the cytosol which includes factors such as distinct ion concentrations and ratios of oxidized and reduced glutathione. Structures of secretory channels suggest that the pore size of these proteins range from ~9 Å in a closed state to ~60 Å in an actively translocating state (Voorhees & Hegde, 2016; Wu, Cabanos, & Rapoport, 2019). While the presence of a substrate within the channel along with a ribosome at the cytosolic opening would prevent diffusion of molecules during translocation, the inactive pore is wide enough to permit diffusion of calcium ions and glutathione molecules. It seems that BiP rectifies this issue by binding at the luminal side of these inactive pores to prevent the entry of small molecules (Hamman, Hendershot, & Johnson, 1998). This gating function of BiP has been proposed to allow ER to maintain ion gradients and distinct glutathione ratios that are essential to its function (Hamman et al., 1998; Ponsero et al., 2017). As BiP is key in the translocation of polypeptides across the translocon, its presence at the pore of inactive channels enables a quick transition from an inactive to an engaged pore.

BiP extends its governance of lumenal protein folding by regulating the signaling of the unfolded protein response [reviewed in (Walter & Ron, 2011)]. In *S. cerevisiae*, when unfolded proteins begin to accumulate in the ER lumen, the UPR is activated by the activity of the transmembrane receptors IRE1. In addition to Ire1, metazoans also activate the UPR via two additional transmembrane receptors, PERK and ATF6. All three proteins detect unfolded proteins via their interactions with BiP. In the absence of proteotoxic stress in the ER, unoccupied BiP molecules are available to bind and sequester these receptors. When protein aggregates start to form, BiP molecules disengage the receptors to assist with protein folding thereby letting the UPR inducers activate. IRE1 and PERK form homodimers in the absence of

BiP, activating kinase domains on the cytosolic sides of these proteins. The dimers then autophosphorylate to become active. This triggers IRE1 to function as an endoribonuclease that can splice the Xbp1 transcript (Hac1 in yeast). Xbp1 or Hac1 then induce expression of ER chaperones to improve the folding capacity of the ER. Upon activation, PERK phosphorylates the translation factor eIF2α. This causes a global attenuation of protein translation thereby reducing the folding burden placed on the ER. ATF6 employs a slightly different activation mechanism whereby BiP dissociation allows secretion of the receptor to the Golgi. Upon transit to the Golgi, the cytosolic domain of ATF6 is cleaved from the transmembrane domain and can act as a transcription factor that promotes the restoration of ER proteostasis. One of the proteins upregulated by the UPR transcription factors is BiP. The increased BiP levels serve to assuage the proteotoxic stress in the lumen. The newly translated BiP molecules also serve to once again bind and deactivate the UPR transmitters thus acting as a negative feedback mechanism (Walter & Ron, 2011).

BiP Regulation

Aside from progression through its ATPase cycle, elaborate regulatory mechanisms exist that enable BiP to carry out its numerous functions in accordance with the temporal needs of the cell. At an estimated concentration of up to 5 μM in pancreatic cells, BiP is among the most abundant cellular proteins (particularly in cells optimized for secretion) (Weitzmann, Baldes, Dudek, & Zimmermann, 2007). As the steady state BiP concentration likely exceeds the normal lumenal requirements, several post-translational modifications have been proposed to temporarily inactivate BiP (Carlsson & Lazarides, 1983; Preissler et al., 2015a; Preissler et al., 2015b; Cha-Molstad et al., 2015). Total BiP expression is increased by cell stress such as the

accumulation of unfolded proteins, but post-translational modulation of BiP activity enables a faster response to an increased folding demand than transcriptional changes.

Shortly after the discovery of BiP, it was reported that the mammalian protein may be phosphorylated and/or ADP-ribosylated (Carlsson & Lazarides, 1983; Hendershot et al., 1988; Satoh, Nakai, Sokawa, Hirayoshi, & Nagata, 1993). These conclusions were drawn based on data showing that ^{32}P or ^{3}H from ATP could be incorporated into BiP, but no direct detection of these species was observed nor were any enzymes discovered capable of adding these modifications to BiP. In subsequent decades, it was determined that BiP could be AMPylated in insect and human cell lines (Sanyal et al., 2015; Preissler et al., 2015b). Given this new discovery, it is now believed that BiP is not phosphorylated or ADP-ribosylated. The observed incorporation of ^{32}P or ^{3}H from ATP into BiP can be explained by AMPylation of Thr-518 in BiP (Preissler et al., 2015a). Notably, there is no evidence thus far that BiP is AMPylated in yeast.

The effects of this BiP AMPylation have been somewhat controversial. The first report of BiP AMPylation displayed decreased ATP hydrolysis by the modified chaperone (Ham et al., 2014), but a report the following year showed that AMPylated BiP has a greater tendency to turnover ATP (Sanyal et al., 2015). Subsequent studies seem to support the former conclusion including the solution of the crystal structure of AMPylated BiP (Preissler et al., 2017). The modified chaperone has decreased affinity for J proteins and therefore resides in a conformation similar to that of the ATP-bound form (Preissler et al., 2017). The resultant decrease in activity is consistent with the idea that this is a deactivating modification that can be reversed when the ER client load increases (Preissler et al., 2017). The same research group provided further evidence

for this claim by showing that FICD, the enzyme that adds this modification to BiP is also capable of removing the AMP (Preissler, Rato, Perera, Saudek, & Ron, 2017).

Another mechanism of BiP inactivation has been proposed whereby the SBD of one BiP monomer will bind to the linker region of another BiP molecule. This enables the formation of large BiP oligomers that are temporarily inactive as chaperones. Induction of ER protein folding burden was shown to reverse BiP oligomerization yielding a pool of BiP monomers that can assist in protein folding (Preissler et al., 2015a). Similar to AMPylation, this inactivation mechanism enables equilibration of ER folding capacity to secretory protein flux on a rapid timescale (Preissler et al., 2015a). Notably, BiP oligomerization occurs much faster than AMPylation (Preissler et al., 2015a). The ability to activate or inactivate BiP through multiple mechanisms which work on different timescales seemingly allows for optimal mobilization of the chaperone in response to a greater range of folding loads in the ER (Preissler et al., 2015a).

It has been reported that BiP can also be modified by the addition of an arginine residue at its N-terminus which acts as a degron and influences BiP half-life (Cha-Molstad et al., 2015). BiP Arginylation was shown to increase in response to ER stress, but paradoxically, it caused apparent relocation of BiP into the cytosol and eventually proteasomal degradation of the chaperone (Cha-Molstad et al., 2015; Shim et al., 2018). While it has been shown that BiP and other ER chaperones can relocalize to different cell compartments, these findings remain poorly understood (Zhang, Liu, Ni, Gill, & Lee, 2010). It has been suggested that cytosolic relocalization of BiP may serve to assist clearance of misfolded proteins in the ER by activating autophagy (Cha-Molstad et al., 2015). However, more studies are needed to solidify the purpose(s) of BiP arginylation.

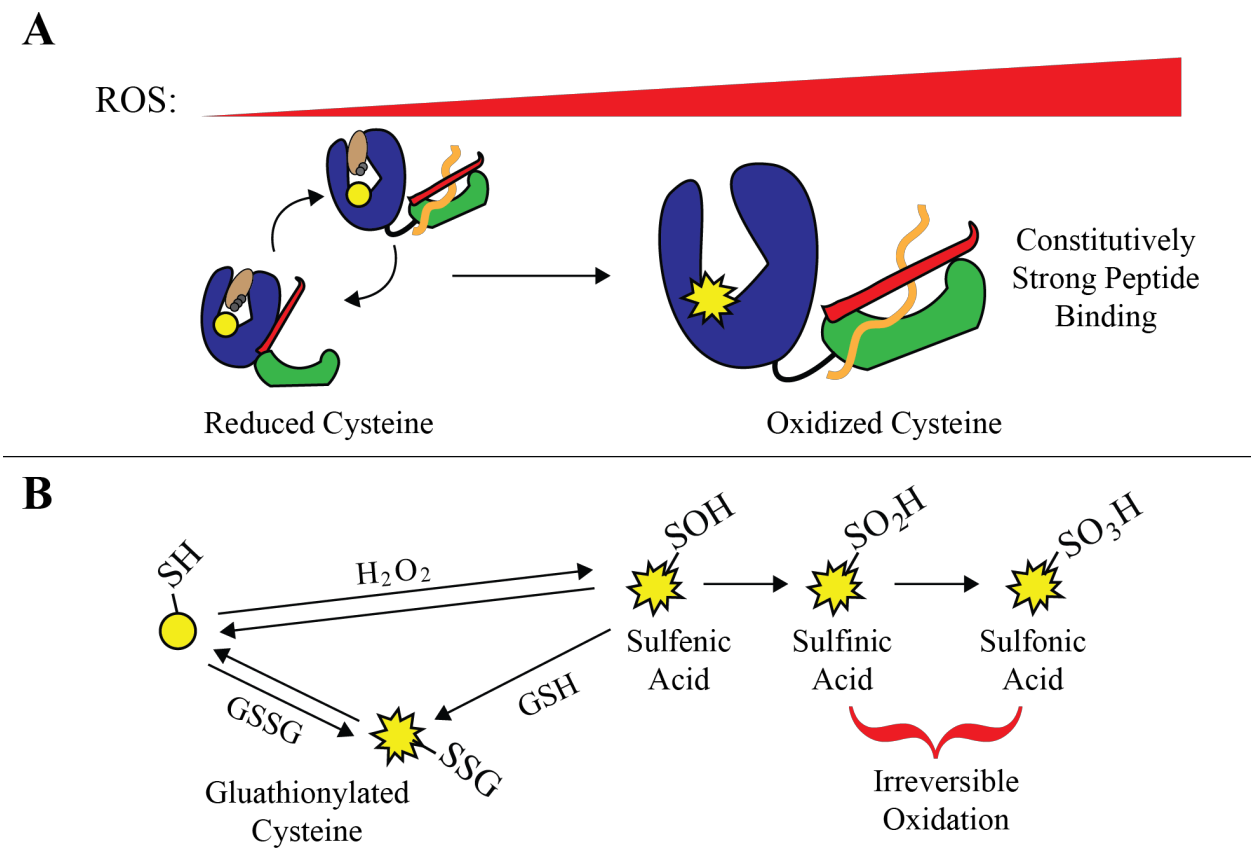

Figure 1.2 Oxidation of BiP alters peptide binding properties. (A) Upon ROS accumulation, a conserved cysteine in the BiP NBD becomes oxidized. Modification of the BiP cysteine decouples peptide binding activity from ATP hydrolysis and locks the chaperone in a high affinity state for peptides. Reduced cysteine: yellow circle. Oxidized cysteine: yellow star. **(B)** The BiP cysteine can be oxidized by hydrogen peroxide to form sulfenic acid. Alternatively, the cysteine can become glutathionylated either by reaction of reduced cysteine with oxidized glutathione (GSSG) or by the reaction of sulfenylated cysteine with reduced glutathione. Glutathionylation of BiP likely prevents the overoxidation of BiP to the irreversible sulfinic and sulfonic acid forms.

Recent evidence suggests that BiP may also be post-translationally modified in response to the fluctuating redox environment of the ER lumen (Lind et al., 2002; Wei et al., 2012; Wang, Pareja, Kaiser, & Sevier, 2014; Wang & Sevier, 2016; Wang, Lee, Liem, & Ping, 2017). The process of oxidative protein folding generates reactive oxygen species (ROS) as a byproduct (Bulleid, 2012; Braakman & Hebert, 2013). These molecules can disrupt the folding process by

aberrantly oxidizing proteins and preventing them from reaching or maintaining their native structure. It seems that redox modification of BiP aims to stem the accumulation of damaged proteins when the redox status of the ER deteriorates.

BiP contains a nearly universally conserved cysteine residue within its nucleotide-binding domain that we have shown is susceptible to oxidation (**Figure 1.2A**) (Wang et al., 2014). Redox modification of this cysteine has been best characterized for the *S. cerevisiae* BiP (Kar2p). Initial reports showed that BiP cysteine-63 was essential for cell viability upon induction of oxidative stress. Further characterization showed that Cys-63 is oxidized to sulfenic acid, and the oxidative stress was hypothesized to mitigate protein aggregation as the modified BiP would bind to and sequester unfolded proteins (Wang et al., 2014). However, with the numerous functions BiP has in the ER, it remains likely that oxidation impacts other BiP mediated processes. It has been suggested that BiP oxidation alters its ability to gate the translocon thereby impacting the exchange of oxidized and reduced glutathione between the ER and cytosol (Ponsero et al., 2017). Additionally, cells possessing BiP Cys-63 mutants displayed induction of the UPR suggesting that redox regulation of BiP likely alters UPR signaling (Wang et al., 2014; Xu, Marsh, & Sevier, 2016).

Further analysis revealed that the redox sensitive cysteine could not only be oxidized to sulfenic acid but could also become glutathionylated (Wang & Sevier, 2016). Similar to sulfenylation, glutathionylation of Cys-63 decreased the nucleotide hydrolysis capacity of BiP and increased its activity as a protein holdase. Modification with glutathione poses the advantage of stability over sulfenic acid. Sulfenic acid is a relatively labile modification that can easily be further oxidized to the irreversible sulfinic and sulfonic acid forms. Glutathionylated cysteines in contrast cannot be oxidized further and therefore preserves the modified BiP in state that can be

reversed once stress subsides (Dalle-Donne, Rossi, Giustarini, Colombo, & Milzani, 2007; Wang & Sevier, 2016). The oxidized form of BiP may also relate to the particular oxidative stress the cell is experiencing. The BiP cysteine is sulfenylated via the reaction of hydrogen peroxide. Similarly, BiP can be glutathionylated by either reaction of a sulfenylated cysteine with reduced glutathione (GSH) or by direct reaction of a reduced cysteine with oxidized glutathione (GSSG) (**Figure 1.2B**). Therefore, glutathionylation may predominate when oxidative stress skews the typical lumenal ratios of oxidized and reduced glutathione (Dalle-Donne et al., 2007; Wang & Sevier, 2016).

While sulfenylated BiP has never been detected in the mammalian protein, several lines of evidence support the idea that this is a conserved modification. First, the redox labile cysteine in the yeast BiP NBD is very highly conserved. It has been demonstrated that the E. coli Hsp70 DnaK is also subjected to several forms of oxidative modification including glutathionylation, sulfenylation and nitrosylation (Winter, Linke, Jatzek, & Jakob, 2005; Williams, Inoue, Chen, & Tsai, 2015; Zhang et al., 2016). These modifications have been proposed to alter the regulation of a heat shock sigma factor by DnaK thereby coordinating the heat shock response with the oxidative stress response. Additionally, the mammalian BiP protein has been shown to form an intramolecular disulfide bond between the NBD cysteine and a cysteine residue in the SBD (Wei et al., 2012). While BiP oxidation has not been characterized as extensively in mammals, we believe the aforementioned modifications likely serve to regulate the mammalian chaperones activity during oxidative stress as is the case in yeast.

All current evidence supports the notion that oxidation of BiP enhances cell viability during oxidative stress (Wang et al., 2014), but constitutive modification of BiP is likely not desirable. BiP mutants that mimic the proteins oxidized form have also been shown to benefit cells

experiencing oxidative stress, but in the absence of stress, these alleles impart a competitive growth disadvantage (Wang & Sevier, 2016). Furthermore, the conservation of a modifiable cysteine implies the benefit of having both oxidized and reduced forms of the protein. While substitution of this cysteine to alanine or valine preserves the ATPase activity of BiP, they do not allow for alteration of BiP activity during stress (Xu et al., 2016). The broadest range of BiP function can only be achieved by inclusion of a redox sensitive cysteine in the BiP NBD explaining the extensive conservation of the residue (Xu et al., 2016). The utility of the BiP cysteine in allowing BiP to respond to a diverse range of cellular conditions highlights the need for a mechanism which reduces BiP after oxidative stress subsides. The reversal of this modification will be the primary focus of Chapters 2 and 3.

Sil1 as a Modulator of BiP Activity

Discovery of Sil1

Efficient progression through the BiP ATPase cycle relies on the presence of nucleotide exchange factors (NEFs) Sil1 and Lhs1. In the late 1990s, the Sil1 protein was identified separately in three different laboratories. Sil1 was first characterized in *Yarrowia lipolytica* where it was pulled out in a screen for proteins involved in translocation of secretory protein in the ER. The investigators sought to identify genes that displayed synthetic leathality with a conditional mutant of the SCR2-encoded 7S RNA component of the signal recognition particle (*sls*). They identified one gene which they dubbed *SLS1* (Boisramé, Beckerich, & Gaillardin, 1996). Later it was shown that the protein encoded by the *SLS1* gene formed a nucleotide-dependent interaction with the Kar2p protein that was necessary for protein

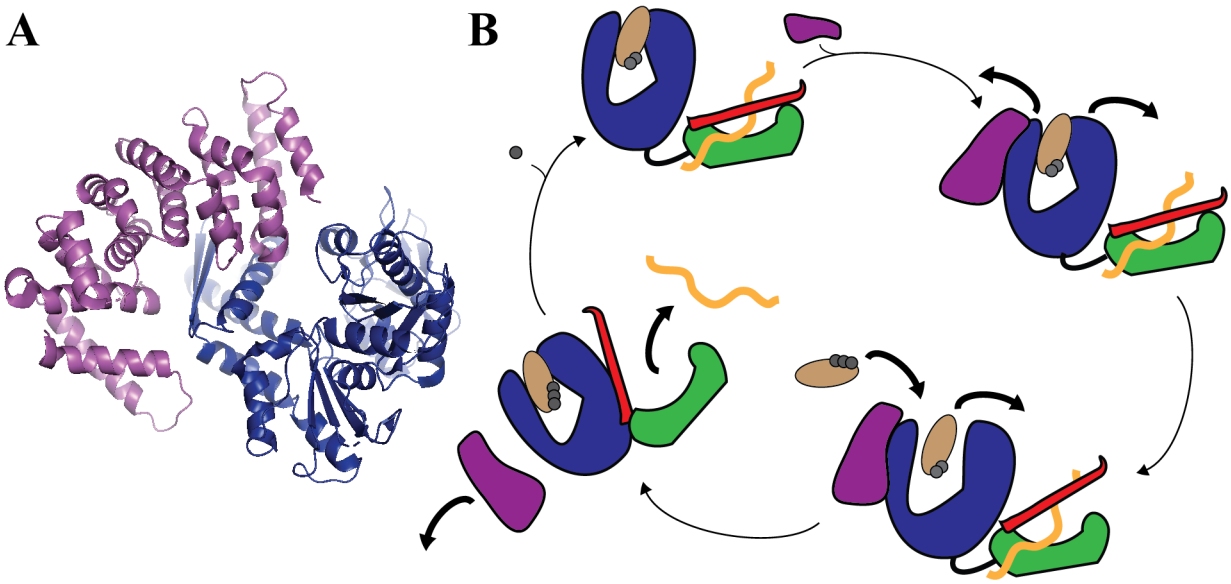

Figure 1.3 Sil1 stimulates ADP release by BiP. (A) Crystal structure of the BiP NBD (blue) bound to Sil1 (purple) from (Yan et al., 2011). PDB: 3QML. **(B)** Cartoon depiction of Sil1 NEF activity. Sil1 binds to the NBD of BiP-ADP and triggers the separation of the NBD lobes. Opening of the nucleotide-binding cleft allows ADP to diffuse from BiP and be replaced by ATP. Nucleotide exchange triggers the opening of the BiP SBD allowing for peptide release. SBD lid: red. SBD: green. ATP/ADP: brown ovals. Phosphate: gray circle. Peptide substrate: orange.

translocation (Boisramé, Kabani, Beckerich, Hartmann, & Gaillardin, 1998; Kabani, Beckerich, & Gaillardin, 2000; Kabani, Beckerich, & Brodsky, 2002).

Around the same time, Sil1 emerged as a hit in a different screen conducted in *S. cerevisiae* (Tyson & Stirling, 2000). The investigators sought to clarify the role of the second Hsp70-related protein in the ER, Lhs1. Building upon the observation that Δ*lhs1* cells have a constitutively activated UPR, the authors deleted the *IRE1* UPR transmitter gene in combination with the *LHS1* gene. The Δ*lhs1* Δ*ire1* strain proved to be inviable, but the cells could be rescued by overexpression of the Sil1p protein which was equivalent to the Sls1 protein in *Y. lipolitica*. The gene was therefore termed *SIL1* for suppressor of the Δ*ire1* Δ*lhs1* strain. This was the first evidence that Sil1 and Lhs1 could provide a redundant function within the ER lumen.

Shortly thereafter, the human Sil1p protein was identified from a yeast-two hybrid screen using variants of the ATPase domain from human BiP as the bait proteins (Chung, Shen, & Hendershot, 2002). The authors identified one protein which they named Bap for BiP-associated protein. Subsequent characterization revealed that Bap bound preferentially to the ADP-bound form of BiP and stimulated nucleotide release of the chaperone (Chung, Shen, & Hendershot, 2002). Sequence analysis showed that Sil1p, Sls1 and Bap were homologous proteins from different species. Today, all forms of the protein are most commonly referred to as Sil1.

Sil1 structure and function

The structure of a Sil1-Kar2 NBD complex provides a mechanistic explanation for the nucleotide exchange capability of Sil1 (**Figure 1.3**) (Yan, Li, & Sha, 2011). The majority of the Sil1 protein is composed of repeated alpha helices which arrange themselves into four armadillo motifs (**Figure 1.3A**). These motifs form a concave "clamp" that wraps itself around a lobe of the BiP NBD and pries the ATPase domain apart (**Figure 1.3B**). The forced separation of the NBD lobes disrupts hydrogen bonds formed between the protein and the nucleotide thereby allowing ADP to be exchanged for ATP. Sil1 also contains an N-terminal domain (NTD) that is absent from the published structure. The N-terminus is predicted to lack major structural elements. Notably, Sil1 bears no structural resemblance to Lhs1 which is a member of the large Hsp70 family. While both proteins can function as a NEF, they appear to bind BiP and catalyze nucleotide exchange by completely different mechanisms (Hale, Lovell, de Keyzer, & Stirling, 2010). In contrast to Sil1, it is believed the Lhs1 NBD makes multiple contacts with the BiP NBD, and this destabilizes BiP causing it to release ADP (Hale et al., 2010; Behnke et al., 2015)

While biochemical and structural data have established that the armadillo repeat core of Sil1 is sufficient to catalyze nucleotide exchange (Yan et al., 2011), recent studies suggest that the presence of the N-terminal domain of Sil1 does influence the BiP ATPase cycle (Rosam et al., 2018). These authors reported that the N-terminal domain of Sil1 functions as a pseudo-substrate that facilitates peptide clearance from BiP. Upon exchange of ADP for ATP, the NTD of Sil1 can bind to the SBD of BiP thereby preventing reassociation of released peptides (Rosam et al., 2018). In further support of this model, an analogous mechanism was proposed for the cytoplasmic Sil1 homologue Fes1 (HspBP1 in humans) (Gowda et al., 2018).

Although Sil1 homologues display low sequence identity among organisms (~15% between yeast and humans), the NTD of Sil1 contains a highly conserved region relative to the rest of the protein. Moreover, it was shown that this conserved sequence can act in an inhibitory manner slowing overall turnover of ATP. Mutations within this region ablated the apparent inhibitory function of the NTD leading to an increased rate of ATP hydrolysis by BiP (Pareja & Sevier, in preparation). The conservation of this inhibitory sequence implies that dampening of BiP ATPase activity is likely beneficial in the long term which is consistent with the numerous mechanisms proposed that inactivate BiP or alter its peptide binding properties. If so, Sil1 inhibition can likely be relieved under certain conditions (such as increased proteotoxic stress) allowing for optimum BiP activity. It has been shown that glycosylation of Sil1 at an asparagine residue (N181 in yeast) also diminishes the protein's function further supporting the need to impede Sil1 NEF activity (Stevens et al., 2017). It remains possible that glycosylation or an alternate post-translational modification governs the coordinated NEF and inhibition function of Sil1 thereby tuning its activity to match the needs of the cell.

Sil1 and disease

Mutations in the Sil1 gene have been linked to multiple diseases in humans, including Marinesco-Sjögren syndrome (MSS), cancer and amyotrophic lateral sclerosis (ALS) (Van Raamsdonk, 2006; Xu, Xu, Zhang, Xin, & Pang, 2018; Filézac de L'Etang et al., 2015). The most common disease associated with impaired Sil1 function is Marinesco-Sjögren syndrome. MSS is an autosomal recessive, multisystem disorder. The hallmark features of the disease include cerebellar ataxia, delayed motor progression, the development of bilateral cataracts in early childhood and varied range of cognitive delay (Van Raamsdonk, 2006; Schulz et al., 2007; Sakai et al., 2008; Inaguma et al., 2014). Consistent with the symptoms, patients exhibit degeneration of Purkinje and granule cells within the brain (Todorov, 1965; Mahloudji, Amirhakimi, Haghighi, & Khodadoust, 1972; Skre & Berg, 1977). To date, there have been a few hundred reported cases globally with the disease oftentimes affecting multiple members of the same family line (Van Raamsdonk, 2006).

While MSS was first described in 1931, it was not until 2005 that disruption of the *SIL1* gene was found to be an underlying cause (Anttonen et al., 2005; Van Raamsdonk, 2006). Four patient mutations were originally described which resulted in frameshift, early termination or point mutations within Sil1(Anttonen et al., 2005). Since this time, numerous subsequent MSS-associated *SIL1* mutations have been identified (Karim et al., 2006; Van Raamsdonk, 2006; Annesi et al., 2007; Anttonen et al., 2008; Eriguchi, Mizuta, Kurohara, Fujitake, & Kuroda, 2008; Riazuddin et al., 2009; Takahata et al., 2010; Howes, Shimizu, Feige, & Hendershot, 2012; Horvers et al., 2013; Krieger et al., 2013; Roos et al., 2014; Cerami et al., 2015; Noreau et al., 2015; Gai et al., 2016; Nair et al., 2016). Notably, Sil1 mutations have been found in about 50% of MSS cases, but it is not currently known which genes are altered in the remaining cases

(Restelli, Masone, Sallese, & Chiesa, 2019). Identification of causative mutations in other genes would enhance our understanding of disease pathophysiology.

MSS progression seems tied to the impaired secretory capacity and subsequent accumulation of protein aggregates within cells lacking functional Sil1 (Anttonen et al., 2008; Buchkremer, González Coraspe, Weis, & Roos, 2016). In 2005, two mouse models for MSS were developed facilitating the study of disease progression. The first mouse generated via transposon insertion in the *SIL1* gene was dubbed "woozy" as it displayed impaired coordination. To verify whether findings from the woozy mouse were resultant from a loss of Sil1, a second model was generated using gene-trap technology and is therefore referred to as a $Sil1^{GT}$ mouse. Mirroring MSS patients, the mice developed ataxia coupled with myopathy at 3-4 months and displayed protein accumulation in the ER and nucleus of Purkinje cells indicative of secretory defects (Zhao, Longo-Guess, Harris, Lee, & Ackerman, 2005; Ichhaporia et al., 2018). Surprisingly, B-cells from the GT mice proved able to efficiently produce and secrete IgG (Ichhaporia, Sanford, Howes, Marion, & Hendershot, 2015). In contrast, $Sil1^{-/-}$ pancreatic beta cells were unable to effectively secrete insulin upon glucose stimulation (Ittner et al., 2014). The discrepancy in ability to secrete these two model cargos suggests that only certain cells and/or secretory cargos are affected by loss of Sil1. In support of the former possibility, a study in yeast showed that overexpression of Sil1 enhanced a cell's ability to secrete ectopically expressed IgG (de Ruijter, Koskela, & Frey, 2016). Furthermore, Northern blot analysis of multiple tissue types revealed that Sil1 expression varies dramatically in different cell types being most highly expressed in placenta, liver, kidney, and skeletal muscle (B cells and pancreatic cells were not assessed) (Chung et al., 2002). Studies have also shown that Sil1 is important for the retrotranslocation of cargos from the ER into the cytosol implying another function for the NEF

which can yield protein aggregation if lost (Williams et al., 2015). Depletion of Sil1 in HEK293 cells yielded structural changes in the ER, widening of the nuclear envelope, mitochondrial degeneration and widespread changes in expression of diverse protein sets displaying that loss of Sil1 can lead to a downstream cellular collapse affecting multiple organelles (Roos et al., 2016).

Currently treatment for MSS patients consists only of palliative care. However, recent therapeutic strategies have focused on the observation that the UPR is upregulated in mammalian cells with loss of Sil1 (Zhao et al., 2005; Zhao, Rosales, Seburn, Ron, & Ackerman, 2010; Grande et al., 2018). Promising preclinical studies have shown that inhibition of the UPR transmitter PERK with GSK2606414 delays the onset of neurodegeneration and enhances coordination in woozy mice (Grande et al., 2018). Interestingly, this implicates UPR activation as a possible cause of MSS symptoms. While UPR activation is intended to alleviate the unfolded protein burden in cells, persistent activation has been shown to induce apoptosis providing a possible explanation for the degeneration of certain tissues lacking Sil1 (Walter & Ron, 2011).

It must be noted that to date, Lhs1 has not been linked to MSS. As mentioned above, although Lhs1 can function as a BiP NEF, it seems to employ an entirely different mechanism of action than Sil1 (Hale et al., 2010). Moreover, as a member of the large Hsp70 family, Lhs1 is thought to have function as a chaperone in addition to serving as a BiP NEF (Behnke et al., 2015). Consistent with this, deletion of *LHS1* in mice is embryonic lethal whereas a deletion of *SIL1* in mammals leads to MSS but is not immediately lethal (Kitao et al., 2001). Thus, it seems likely that Lhs1 can compensate somewhat for Sil1 as NEF, but Sil1 is unable to compensate for the loss of other Lhs1 functions resulting in the inviable phenotype of $Lhs1^{-/-}$ mice (Weitzmann, Volkmer, & Zimmermann, 2006).

In addition to its role in MSS, *SIL1* has been linked to other disorders. Sil1 expression was observed to correlate with the degeneration of motor neurons. ALS-resistant slow motor neurons robustly expressed Sil1 while stress-prone fast fatigable motor neurons were deficient in Sil1 expression (Filézac de L'Etang et al., 2015). While more research is needed to solidify the connection between *SIL1* and ALS, neurodegenerative disorders have long been linked to protein aggregation which is expected upon disruption of the Hsp70 chaperone system (Soto & Pritzkow, 2018). Additionally, a recent study demonstrated a link between Sil1 expression and glioma progression (Xu et al., 2018). However, the correlative nature of the study necessitates further investigation before *SIL1* can be considered an oncogene.

Oxidative Protein Folding and ER ROS Maintenance

Oxidative folding

As stated above, the endoplasmic reticulum provides an oxidizing environment relative to the cytosol as indicated by differing ratios of the oxidized and reduced forms of the cellular redox buffer glutathione (Oka & Bulleid, 2018). Glutathione is the predominant low-molecular weight thiol found in cells. Capable of existing in a reduced (GSH) and oxidized (GSSG) form, glutathione can act as both an electron source and sink to regulate the redox state of cell (Chakravarthi, Jessop, & Bulleid, 2006; Appenzeller-Herzog, 2011). Glutathione is distributed among all cell compartments, but as suggested above, the ratios of oxidized and reduced forms differ between organelles. The cytosol possesses a reduced to oxidized glutathione ratio (GSH:GSSG) of ~100:1 (Hwang, Sinskey, & Lodish, 1992; Chai, Ashraf, Rokutan, Johnston, & Thomas, 1994). This ratio is maintained by a glutathione reductase enzyme which utilizes electrons from NADPH to regenerate GSH from GSSG (Chakravarthi et al., 2006). In contrast,

the GSH:GSSG ratio in the ER lies on the oxidizing side of the spectrum ranging from 1:1 to 35:1(Hwang et al., 1992). Glutathione is constantly oxidized by the activities of the ER disulfide bond formation machinery, and unlike in the cytosol, the endoplasmic reticulum does not possess a system for reducing glutathione (Chakravarthi et al., 2006). Instead, it seems GSH must be imported into the ER while GSSG is either exported back to the cytosol in order to be reduced or else is secreted from the cell (Chakravarthi et al., 2006; Appenzeller-Herzog, 2011).

As GSH antagonizes the formation of disulfide bonds, the low GSH:GSSG ratio maintained by the ER allows for the introduction of disulfide bonds in secreted substrates (Pace, Grimsley, Thomson, & Barnett, 1988). Disulfide bonds are covalent links between the sulfur atoms of two cysteine residues. The bonds can serve both structural and functional roles. They provide extra stability for proteins secreted into the harsh conditions outside of a cell, allow for the assembly of multi-protein complexes, and change the conformation of proteins in ways which affect their activity (Pace et al., 1988; Linke & Jakob, 2003). While the formation of disulfide bonds is spontaneous in the presence of molecular oxygen, the ER is equipped with enzymes that speed up and ensure the fidelity of this process (Anfinsen, Haber, Sela, & White, 1961; Goldberger, Epstein, & Anfinsen, 1963). Disulfides are added to folding proteins by members of the protein disulfide isomerase family (termed PDIs for short). Upon oxidation of ER substrates, PDI will become reduced. The primary pathway for reoxidation of PDI utilizes the activity of the ER oxidoreductase (Ero1) (Sevier & Kaiser, 2002; Sevier & Kaiser, 2006).

PDI and Ero1

Disulfide bonds are added to proteins primarily through the activity of protein disulfide isomerase (PDI) (Hatahet & Ruddock, 2009). PDI belongs to thioredoxin superfamily. It

contains four, tandem thioredoxin-like domains denoted as a, b, b' and a' followed by an acidic, C-terminal tail (Edman, Ellis, Blacher, Roth, & Rutter, 1985; Hatahet & Ruddock, 2009). The domains arrange themselves into a "twisted U" shape with the a and a' domains arranged opposite each other and the b/b' domain form the cleft of the "U" (Tian, Xiang, Noiva, Lennarz, & Schindelin, 2006). Alternatively, rotation of the a domain relative to the remainder of the molecule causes the protein to adopt a more extended "boat" conformation (Tian et al., 2008). The a and a' domains each possess an active site which contains a catalytic CXXC motif. This dicysteine motif is common to numerous redox active proteins. The ability to transition between a reduced dithiol and oxidized disulfide state enable many proteins with these motifs to accept or donate electrons (Edman et al., 1985; Hatahet & Ruddock, 2009). While both active sites are capable of catalyzing disulfide bond formation, they have been shown to possess slightly different reduction potentials in *S. cerevisiae* (Vitu et al., 2010). The b and b' domains lack a CXXC motif but do seem to play a role in the binding and folding of substrates (Cai, Wang, & Tsou, 1994; Wilson, Lees, & Bulleid, 1998; Tian et al., 2006; Wang et al., 2012).

PDI catalyzes the formation of disulfide bonds in folding proteins via a thiol-disulfide exchange reaction (**Figure 1.4A**) (Sevier & Kaiser, 2002; Nagy, 2013). In this mechanism, a reduced cysteine thiolate present in the substrate protein acts as a nucleophile and attacks the oxidized sulfur atom of a PDI disulfide. This step results in the formation of a transient, mixed disulfide bond between PDI and the substrate protein. The intermediate is resolved when a second reduced cysteine from the substrate protein attacks the newly oxidized cysteine residue. This results in the formation of a disulfide bond between the two substrate cysteines and leaves the catalytic cysteine residues of PDI in a reduced dithiol state (Sevier & Kaiser, 2002; Nagy, 2013).

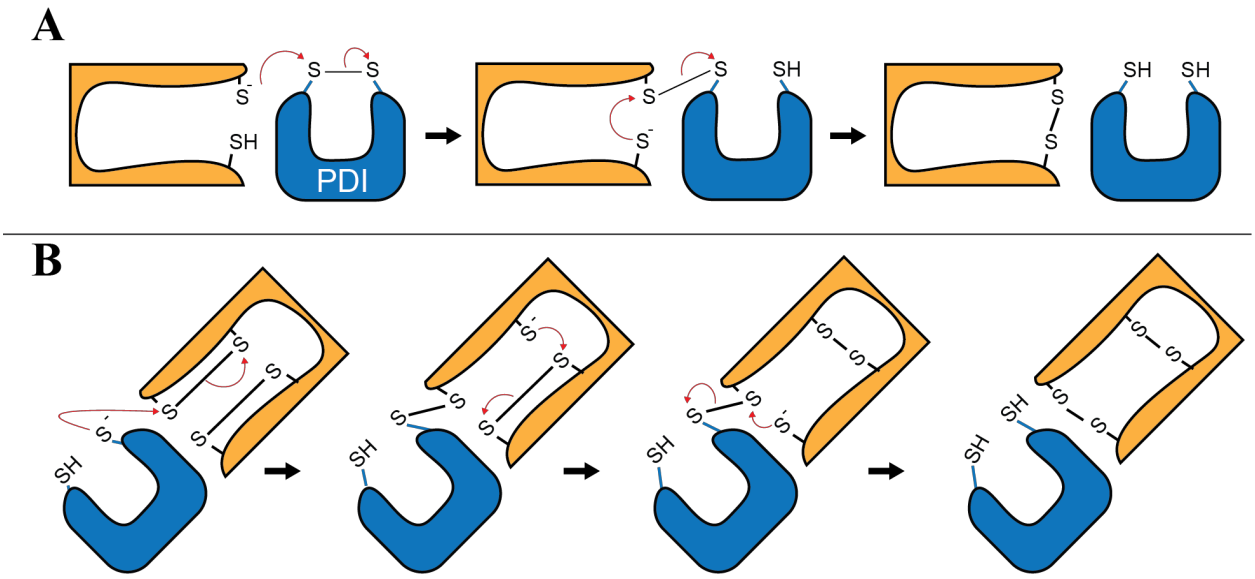

Figure 1.4 Mechanism of disulfide addition and isomerization by PDI. (A) Disulfide addition. A reduced cysteine thiol/thiolate attacks an oxidized cysteine in the active site of oxidized PDI. A transient mixed disulfide bond is formed between a substrate protein (orange) and PDI (blue). Attack of a second reduced thiol/thiolate in the substrate protein at the newly formed disulfide bond resolves the mixed disulfide intermediate leaving the substrate oxidized and PDI reduced. **(B)** Disulfide isomerization. A reduced cysteine within PDI attacks at the incorrect disulfide bond within a substrate protein. A transient mixed disulfide bond is formed between PDI and the substrate. A newly reduced cysteine within the substrate then attacks another substrate cysteine engaged in an incorrect disulfide bond resulting in the formation of a new disulfide bond between the nucleophilic cysteine and its electrophilic counterpart. A newly reduced cysteine then attacks the cysteine engaged in the mixed disulfide bond, collapsing the intermediate.

Significantly, PDI not only adds disulfides to proteins but also isomerizes bonds formed between incorrect cysteine pairs. This similarly utilizes a thiol disulfide exchange mechanism. In this case, a reduced PDI cysteine acts as the original nucleophile and attacks the substrate protein's cysteine (**Figure 1.4B**). The reaction reduces the improperly oxidized cysteines and oxidizes the PDIs active site. PDI can then act as an oxidant and transfer a correct disulfide bond to the folding substrate. It has been speculated that the disulfide isomerase activity of PDI constitutes its essential function in cells as opposed to its ability to oxidize proteins, but this has

persisted as a controversial claim (Lamantia & Lennarz, 1993; Laboissiere, Sturley, & Raines, 1995; Chivers, Laboissière, & Raines, 1996; Frand & Kaiser, 2000; Hatahet & Ruddock, 2009).

Upon oxidizing a substrate, PDI is left in a reduced dithiol state and must be reoxidized before it can add another disulfide bond to folding protein. While it was originally hypothesized that glutathione would accomplish this, PDI is primarily oxidized by the ER oxidoreductase, Ero1 (Frand & Kaiser, 1998; Pollard, Travers, & Weissman, 1998; Frand & Kaiser, 1999; Tu, Ho-Schleyer, Travers, & Weissman, 2000). Ero1 is a flavoprotein that is able to generate disulfide bonds *de novo* by reducing molecular oxygen (Tu & Weissman, 2002). It contains two pairs of cysteines that are essential to the reoxidation of PDI. The active site cysteines are adjacent to the Ero1 flavin and can therefore pass electrons to the cofactor to become oxidized. The second set of cysteines resides on a flexible loop at the surface of the protein. The mobility of this polypeptide segment enables the cysteines to approach the active site and become oxidized via an intramolecular disulfide exchange reaction. The newly oxidized cysteines then "shuttle" the disulfide bond to PDI facilitating the continuation of oxidative protein folding (Frand & Kaiser, 2000; Gross, Kastner, Kaiser, & Fass, 2004; Heldman et al., 2010).

Eukaryotic organisms usually contain several different PDI family members. For example, *S. cerevisiae* contain 5 different PDIs while humans possess more than 20 such proteins (Nørgaard et al., 2001; Galligan & Petersen, 2012). However, only a subset of PDI family members actually retains the ability to catalyze disulfide transfer. The PDI family members that are active as isomerases differ slightly in domain organization, expression patterns and catalytic properties but share a similar mechanism of action (Galligan & Petersen, 2012). The first described and by far the best studied family member is encoded by the *P4HB* gene in humans (*PDI1* in yeast) and is usually just referred to as PDI (Edman et al., 1985; Pihlajaniemi et al.,

1987; Tasanen, Parkkonen, Chow, Kivirikko, & Pihlajaniemi, 1988). In contrast to many other family members, PDI is essential and therefore often considered the major disulfide isomerase in cells (Farquhar et al., 1991; LaMantia et al., 1991; Tachikawa, Miura, Katakura, & Mizunaga, 1991).

Oxidative stress

While Ero1 is essential to drive the process of oxidative protein folding, its activity is not without consequence. The reduction of molecular oxygen generates hydrogen peroxide which is a reactive oxygen species (ROS) (**Figure 1.5**) (Tu & Weissman, 2002). Accumulation of ROS can be toxic for a number of reasons. Various ROS can damage or fragment proteins ultimately causing them to misfold and aggregate (Dalle-Donne, Rossi, Giustarini, Milzani, & Colombo, 2003). Furthermore, the hydroxyl radical can react with cellular lipids disrupting membrane fluidity and can oxidize DNA bases yielding mutations (Marnett, 1999). They can also alter cellular redox potential by oxidizing reduced glutathione pools (Thannickal & Fanburg, 2000; Apel & Hirt, 2004; Birben, Sahiner, Sackesen, Erzurum, & Kalayci, 2012). Considering the many harmful effects of ROS, oxidative protein folding has the potential to greatly burden the cell. For instance, it has been estimated that a beta-cell would produce three million molecules of hydrogen peroxide per minute upon induction of insulin secretion (Shimizu & Hendershot, 2009). While it is possible that Ero1 can utilize an alternative electron acceptor to oxygen in order to offset peroxide production, no such candidate has been found under aerobic conditions.

Given the capacity of the cell to generate copious levels of ROS through disulfide bond generation (and other processes), it is necessary that the cell possess mechanisms for coping with these oxidants. One solution to this is the detoxification of ROS molecules with cellular

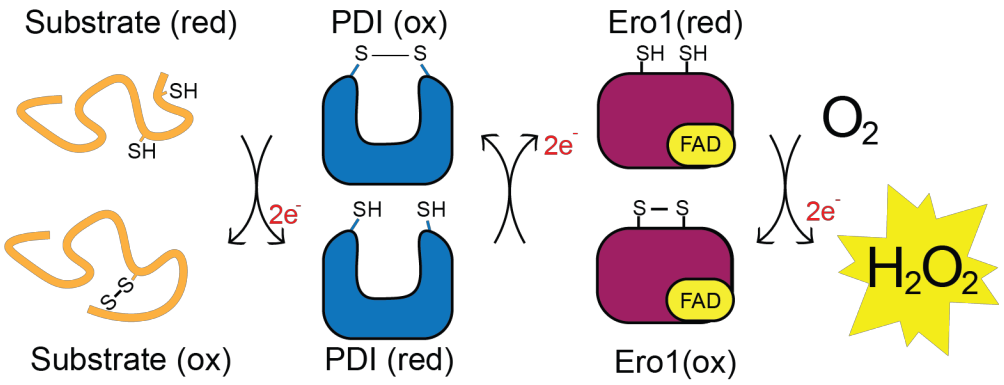

Figure 1.5 Oxidative protein folding in the ER. PDI adds a disulfide bond into a folding substrate. Oxidized PDI is regenerated by participating in a disulfide exchange with oxidized Ero1. Ero1 generates a disulfide bond de novo by passing an electron pair to a molecular oxygen via a flavin cofactor (FAD). The reduction of oxygen by Ero1 generates a molecule of hydrogen peroxide.

reductants. H_2O_2 can react with GSH to produce GSSG. In the cytosol, GSSG is then reduced by glutathione reductase and the thioredoxin system. Additionally, some enzymes consume ROS within the cell. Multiple peroxiredoxins capable of scavenging ROS are found in different organelles, including within the ER of mammalian cells (Birben et al., 2012).

Cells have also evolved mechanisms to sense ROS and induce changes that increase tolerance to the oxidants. For instance, multiple transcription factors that control the cellular antioxidant system are activated by hydrogen peroxide (Turpaev, 2002). Additionally, feedback mechanisms exist in which increasing ROS levels deactivate the cellular sources of ROS. An example of this is found in the feedback regulation of Ero1. When peroxide accumulates in the ER, PDI will oxidize regulatory cysteine pairs in Ero1. This results in a conformational change which inactivates the enzyme and stems peroxide production (Sevier et al., 2007). Once oxidative stress passes, PDI can reduce the Ero1 regulatory bonds reactivating oxidative folding (Kim, Sideris, Sevier, & Kaiser, 2012).

Redox Regulation of BiP in Response to Oxidative Stress

As discussed in an earlier section, increasing ROS levels in the ER cause oxidation of the molecular chaperone BiP. This signaling event helps the cell cope with the harmful effects of ROS by converting the normally ATPase-driven Hsp70 chaperone to an ATP-independent protein holdase. The increased affinity for peptides alleviates the burden of oxidative stress by allowing BiP to sequester ER substrates until optimal ER folding conditions are restored and likely by impacting the numerous other processes BiP oversees in the ER (Wang et al., 2014; Wang & Sevier, 2016). However, prolonged BiP oxidation impedes the folding of proteins in the ER and is therefore detrimental to cell fitness (Wang & Sevier, 2016). Oxidation of BiP must therefore be tightly regulated to match the current conditions of the ER. BiP needs to be oxidized in response to excessive ROS produced by the oxidative protein folding machinery, but a means of reducing BiP is necessary also so that protein folding in the ER can resume when ROS levels subside.

The overarching question addressed here concerns the mechanisms by which BiP oxidation (and the associated holdase activity) is tuned to the current environment of the ER. In Chapter 2, we identify a role for Sil1, one of the NEFs that works on BiP, in regulating the redox state of the chaperone. Sil1 possesses an N-terminal cysteine pair capable of reducing the BiP cysteine and restoring the ATPase-driven protein folding of the chaperone. Chapter 3 builds upon the preceding section by exploring the regulatory mechanisms which link Sil1 reduction to the ER redox poise. Specifically, we show that PDI can both reduce and oxidize Sil1 thereby governing the reductant function of Sil1. As the redox poise of PDI is tightly coupled to the ER redox poise, the oxidoreductase serves as the link between the oxidative status of the ER and redox state of BiP.

REFERENCES

Anfinsen, C. B., Haber, E., Sela, M., & White, F. H. (1961). The kinetics of formation of native ribonuclease during oxidation of the reduced polypeptide chain. *Proc Natl Acad Sci USA*, *47*, 1309-1314.

Annesi, G., Aguglia, U., Tarantino, P., Annesi, F., De Marco, E. V., Civitelli, D. et al. (2007). SIL1 and SARA2 mutations in Marinesco-Sjögren and chylomicron retention diseases. *Clin Genet*, *71*(3), 288-289.

Anttonen, A. K., Mahjneh, I., Hämäläinen, R. H., Lagier-Tourenne, C., Kopra, O., Waris, L. et al. (2005). The gene disrupted in Marinesco-Sjögren syndrome encodes SIL1, an HSPA5 cochaperone. *Nat Genet*, *37*(12), 1309-1311.

Anttonen, A. K., Siintola, E., Tranebjaerg, L., Iwata, N. K., Bijlsma, E. K., Meguro, H. et al. (2008). Novel SIL1 mutations and exclusion of functional candidate genes in Marinesco-Sjögren syndrome. *Eur J Hum Genet*, *16*(8), 961-969.

Apel, K., & Hirt, H. (2004). Reactive oxygen species: metabolism, oxidative stress, and signal transduction. *Annu Rev Plant Biol*, *55*, 373-399.

Appenzeller-Herzog, C. (2011). Glutathione- and non-glutathione-based oxidant control in the endoplasmic reticulum. *J Cell Sci*, *124*(Pt 6), 847-855.

Apweiler, R., Hermjakob, H., & Sharon, N. (1999). On the frequency of protein glycosylation, as deduced from analysis of the SWISS-PROT database. *Biochim Biophys Acta*, *1473*(1), 4-8.

Behnke, J., Feige, M. J., & Hendershot, L. M. (2015). BiP and its nucleotide exchange factors Grp170 and Sil1: mechanisms of action and biological functions. *J Mol Biol*, *427*(7), 1589-1608.

Behnke, J., Mann, M. J., Scruggs, F. L., Feige, M. J., & Hendershot, L. M. (2016). Members of the Hsp70 Family Recognize Distinct Types of Sequences to Execute ER Quality Control. *Mol Cell*, *63*(5), 739-752.

Bertelsen, E. B., Chang, L., Gestwicki, J. E., & Zuiderweg, E. R. (2009). Solution conformation of wild-type E. coli Hsp70 (DnaK) chaperone complexed with ADP and substrate. *Proc Natl Acad Sci USA*, *106*(21), 8471-8476.

Birben, E., Sahiner, U. M., Sackesen, C., Erzurum, S., & Kalayci, O. (2012). Oxidative stress and antioxidant defense. *World Allergy Organ J*, *5*(1), 9-19.

Boisramé, A., Beckerich, J. M., & Gaillardin, C. (1996). Sls1p, an endoplasmic reticulum component, is involved in the protein translocation process in the yeast Yarrowia lipolytica. *J Biol Chem*, *271*(20), 11668-11675.

Boisramé, A., Kabani, M., Beckerich, J. M., Hartmann, E., & Gaillardin, C. (1998). Interaction of Kar2p and Sls1p is required for efficient co-translational translocation of secreted proteins in the yeast Yarrowia lipolytica. *J Biol Chem*, *273*(47), 30903-30908.

Bole, D. G., Hendershot, L. M., & Kearney, J. F. (1986). Posttranslational association of immunoglobulin heavy chain binding protein with nascent heavy chains in nonsecreting and secreting hybridomas. *J Cell Biol*, *102*(5), 1558-1566.

Braakman, I., & Hebert, D. N. (2013). Protein folding in the endoplasmic reticulum. *Cold Spring Harb Perspect Biol*, *5*, a013201.

Bracher, A., & Verghese, J. (2015). The nucleotide exchange factors of Hsp70 molecular chaperones. *Front Mol Biosci*, *2*, 10.

Buchberger, A., Theyssen, H., Schröder, H., McCarty, J. S., Virgallita, G., Milkereit, P. et al. (1995). Nucleotide-induced conformational changes in the ATPase and substrate binding domains of the DnaK chaperone provide evidence for interdomain communication. *J Biol Chem*, *270*(28), 16903-16910.

Buchkremer, S., González Coraspe, J. A., Weis, J., & Roos, A. (2016). Sil1-Mutant Mice Elucidate Chaperone Function in Neurological Disorders. *J Neuromuscul Dis*, *3*(2), 169-181.

Bukau, B., & Horwich, A. L. (1998). The Hsp70 and Hsp60 chaperone machines. *Cell*, *92*(3), 351-366.

Bulleid, N. J. (2012). Disulfide bond formation in the mammalian endoplasmic reticulum. *Cold Spring Harb Perspect Biol*, *4*(11).

Cai, H., Wang, C. C., & Tsou, C. L. (1994). Chaperone-like activity of protein disulfide isomerase in the refolding of a protein with no disulfide bonds. *J Biol Chem*, *269*(40), 24550-24552.

Carlsson, L., & Lazarides, E. (1983). ADP-ribosylation of the Mr 83,000 stress-inducible and glucose-regulated protein in avian and mammalian cells: modulation by heat shock and glucose starvation. *Proc Natl Acad Sci USA*, *80*(15), 4664-4668.

Cerami, C., Tarantino, P., Cupidi, C., Annesi, G., Lo Re, V., Gagliardi, M. et al. (2015). Marinesco-Sjögren syndrome caused by a new SIL1 frameshift mutation. *J Neurol Sci*, *354*(1-2), 112-113.

Cha-Molstad, H., Sung, K. S., Hwang, J., Kim, K. A., Yu, J. E., Yoo, Y. D. et al. (2015). Amino-terminal arginylation targets endoplasmic reticulum chaperone BiP for autophagy through p62 binding. *Nat Cell Biol*, *17*(7), 917-929.

Chai, Y. C., Ashraf, S. S., Rokutan, K., Johnston, R. B., & Thomas, J. A. (1994). S-thiolation of individual human neutrophil proteins including actin by stimulation of the respiratory burst: evidence against a role for glutathione disulfide. *Arch Biochem Biophys*, *310*(1), 273-281.

Chakravarthi, S., Jessop, C. E., & Bulleid, N. J. (2006). The role of glutathione in disulphide bond formation and endoplasmic-reticulum-generated oxidative stress. *EMBO Rep*, *7*(3), 271-275.

Chaube, R., & Werstuck, G. H. (2016). Mitochondrial ROS versus ER ROS: Which Comes First in Myocardial Calcium Dysregulation. *Front Cardiovasc Med*, *3*, 36.

Chivers, P. T., Laboissière, M. C., & Raines, R. T. (1996). The CXXC motif: imperatives for the formation of native disulfide bonds in the cell. *EMBO J*, *15*(11), 2659-2667.

Chung, K. T., Shen, Y., & Hendershot, L. M. (2002). BAP, a mammalian BiP-associated protein, is a nucleotide exchange factor that regulates the ATPase activity of BiP. *J Biol Chem*, *277*(49), 47557-47563.

Clerico, E. M., Tilitsky, J. M., Meng, W., & Gierasch, L. M. (2015). How hsp70 molecular machines interact with their substrates to mediate diverse physiological functions. *J Mol Biol*, *427*(7), 1575-1588.

Cooper, G. M. (2000). The Endoplasmic Reticulum. In *The Cell: A Molecular Approach* (2nd ed.). Sunderland (MA): Sinauer Associates.

Cyr, D. M., & Ramos, C. H. (2015). Specification of Hsp70 function by Type I and Type II Hsp40. *Subcell Biochem*, *78*, 91-102.

Dalle-Donne, I., Rossi, R., Giustarini, D., Colombo, R., & Milzani, A. (2007). S-glutathionylation in protein redox regulation. *Free Radic Biol Med*, *43*(6), 883-898.

Dalle-Donne, I., Rossi, R., Giustarini, D., Milzani, A., & Colombo, R. (2003). Protein carbonyl groups as biomarkers of oxidative stress. *Clin Chim Acta*, *329*(1-2), 23-38.

De Los Rios, P., & Barducci, A. (2014). Hsp70 chaperones are non-equilibrium machines that achieve ultra-affinity by energy consumption. *Elife*, *3*, e02218.

de Ruijter, J. C., Koskela, E. V., & Frey, A. D. (2016). Enhancing antibody folding and secretion by tailoring the Saccharomyces cerevisiae endoplasmic reticulum. *Microb Cell Fact*, *15*, 87.

Dong, M., Bridges, J. P., Apsley, K., Xu, Y., & Weaver, T. E. (2008). ERdj4 and ERdj5 are required for endoplasmic reticulum-associated protein degradation of misfolded surfactant protein C. *Mol Biol Cell*, *19*(6), 2620-2630.

Dudek, J., Benedix, J., Cappel, S., Greiner, M., Jalal, C., Müller, L. et al. (2009). Functions and pathologies of BiP and its interaction partners. *Cell Mol Life Sci*, *66*(9), 1556-1569.

Edman, J. C., Ellis, L., Blacher, R. W., Roth, R. A., & Rutter, W. J. (1985). Sequence of protein disulphide isomerase and implications of its relationship to thioredoxin. *Nature*, *317*(6034), 267-270.

Ellis, R. J., & Hemmingsen, S. M. (1989). Molecular chaperones: proteins essential for the biogenesis of some macromolecular structures. *Trends Biochem Sci*, *14*(8), 339-342.

Eriguchi, M., Mizuta, H., Kurohara, K., Fujitake, J., & Kuroda, Y. (2008). Identification of a new homozygous frameshift insertion mutation in the SIL1 gene in 3 Japanese patients with Marinesco-Sjögren syndrome. *J Neurol Sci*, *270*(1-2), 197-200.

Farquhar, R., Honey, N., Murant, S. J., Bossier, P., Schultz, L., Montgomery, D. et al. (1991). Protein disulfide isomerase is essential for viability in Saccharomyces cerevisiae. *Gene*, *108*(1), 81-89.

Filézac de L'Etang, A., Maharjan, N., Cordeiro Braña, M., Ruegsegger, C., Rehmann, R., Goswami, A. et al. (2015). Marinesco-Sjögren syndrome protein SIL1 regulates motor neuron subtype-selective ER stress in ALS. *Nat Neurosci*, *18*(2), 227-238.

Flynn, G. C., Chappell, T. G., & Rothman, J. E. (1989). Peptide binding and release by proteins implicated as catalysts of protein assembly. *Science*, *245*(4916), 385-390.

Flynn, G. C., Pohl, J., Flocco, M. T., & Rothman, J. E. (1991). Peptide-binding specificity of the molecular chaperone BiP. *Nature*, *353*(6346), 726-730.

Frand, A. R., & Kaiser, C. A. (1998). The ERO1 gene of yeast is required for oxidation of protein dithiols in the endoplasmic reticulum. *Mol Cell*, *1*(2), 161-170.

Frand, A. R., & Kaiser, C. A. (1999). Ero1p oxidizes protein disulfide isomerase in a pathway for disulfide bond formation in the endoplasmic reticulum. *Mol Cell*, *4*, 469-477.

Frand, A. R., & Kaiser, C. A. (2000). Two pairs of conserved cysteines are required for the oxidative activity of Ero1p in protein disulfide bond formation in the endoplasmic reticulum. *Mol Biol Cell*, *11*(9), 2833-2843.

Gai, N., Jiang, C., Zou, Y. Y., Zheng, Y., Liang, D. S., & Wu, L. Q. (2016). Novel SIL1 nonstop mutation in a Chinese consanguineous family with Marinesco-Sjögren syndrome and Dandy-Walker syndrome. *Clin Chim Acta*, *458*, 1-4.

Galligan, J. J., & Petersen, D. R. (2012). The human protein disulfide isomerase gene family. *Hum Genomics*, *6*, 6.

Gething, M. J. (1999). Role and regulation of the ER chaperone BiP. *Semin Cell Dev Biol*, *10*(5), 465-472.

Goldberger, R. F., Epstein, C. J., & Anfinsen, C. B. (1963). Acceleration of reactivation of reduced bovine pancreatic ribonuclease by a microsomal system from rat liver. *J Biol Chem*, *238*, 628-635.

Gowda, N. K. C., Kaimal, J. M., Kityk, R., Daniel, C., Liebau, J., Öhman, M. et al. (2018). Nucleotide exchange factors Fes1 and HspBP1 mimic substrate to release misfolded proteins from Hsp70. *Nat Struct Mol Biol*, *25*(1), 83-89.

Grande, V., Ornaghi, F., Comerio, L., Restelli, E., Masone, A., Corbelli, A. et al. (2018). PERK inhibition delays neurodegeneration and improves motor function in a mouse model of Marinesco-Sjögren syndrome. *Hum Mol Genet*, *27*(14), 2477-2489.

Gross, E., Kastner, D. B., Kaiser, C. A., & Fass, D. (2004). Structure of Ero1p, source of disulfide bonds for oxidative protein folding in the cell. *Cell*, *117*(5), 601-610.

Haas, I. G., & Wabl, M. (1983). Immunoglobulin heavy chain binding protein. *Nature*, *306*(5941), 387-389.

Hale, S. J., Lovell, S. C., de Keyzer, J., & Stirling, C. J. (2010). Interactions between Kar2p and its nucleotide exchange factors Sil1p and Lhs1p are mechanistically distinct. *J Biol Chem*, *285*(28), 21600-21606.

Ham, H., Woolery, A. R., Tracy, C., Stenesen, D., Krämer, H., & Orth, K. (2014). Unfolded protein response-regulated Drosophila Fic (dFic) protein reversibly AMPylates BiP chaperone during endoplasmic reticulum homeostasis. *J Biol Chem*, *289*(52), 36059-36069.

Hamman, B. D., Hendershot, L. M., & Johnson, A. E. (1998). BiP maintains the permeability barrier of the ER membrane by sealing the lumenal end of the translocon pore before and early in translocation. *Cell*, *92*(6), 747-758.

Hatahet, F., & Ruddock, L. W. (2009). Protein disulfide isomerase: a critical evaluation of its function in disulfide bond formation. *Antioxid Redox Signal*, *11*, 2807-2850.

Hebert, D. N., Garman, S. C., & Molinari, M. (2005). The glycan code of the endoplasmic reticulum: asparagine-linked carbohydrates as protein maturation and quality-control tags. *Trends Cell Biol*, *15*(7), 364-370.

Heldman, N., Vonshak, O., Sevier, C. S., Vitu, E., Mehlman, T., & Fass, D. (2010). Steps in reductive activation of the disulfide-generating enzyme Ero1p. *Protein Sci*, *19*(10), 1863-1876.

Helenius, A., & Aebi, M. (2004). Roles of N-linked glycans in the endoplasmic reticulum. *Annu Rev Biochem*, *73*, 1019-1049.

Hendershot, L. M. (2004). The ER function BiP is a master regulator of ER function. *Mt Sinai J Med*, *71*(5), 289-297.

Hendershot, L. M., & Kearney, J. F. (1988). A role for human heavy chain binding protein in the developmental regulation of immunoglobin transport. *Mol Immunol*, *25*(6), 585-595.

Hendershot, L. M., Ting, J., & Lee, A. S. (1988). Identity of the immunoglobulin heavy-chain-binding protein with the 78,000-dalton glucose-regulated protein and the role of posttranslational modifications in its binding function. *Mol Cell Biol*, *8*(10), 4250-4256.

Horvers, M., Anttonen, A. K., Lehesjoki, A. E., Morava, E., Wortmann, S., Vermeer, S. et al. (2013). Marinesco-Sjögren syndrome due to SIL1 mutations with a comment on the clinical phenotype. *Eur J Paediatr Neurol*, *17*(2), 199-203.

Howes, J., Shimizu, Y., Feige, M. J., & Hendershot, L. M. (2012). C-terminal mutations destabilize SIL1/BAP and can cause Marinesco-Sjögren syndrome. *J Biol Chem*, *287*(11), 8552-8560.

Huh, W. K., Falvo, J. V., Gerke, L. C., Carroll, A. S., Howson, R. W., Weissman, J. S. et al. (2003). Global analysis of protein localization in budding yeast. *Nature*, *425*(6959), 686-691.

Hwang, C., Sinskey, A. J., & Lodish, H. F. (1992). Oxidized redox state of glutathione in the endoplasmic reticulum. *Science*, *257*(5076), 1496-1502.

Ichhaporia, V. P., Kim, J., Kavdia, K., Vogel, P., Horner, L., Frase, S. et al. (2018). SIL1, the endoplasmic-reticulum-localized BiP co-chaperone, plays a crucial role in maintaining skeletal muscle proteostasis and physiology. *Dis Model Mech*, *11*(5).

Ichhaporia, V. P., Sanford, T., Howes, J., Marion, T. N., & Hendershot, L. M. (2015). Sil1, a nucleotide exchange factor for BiP, is not required for antibody assembly or secretion. *Mol Biol Cell*, *26*(3), 420-429.

Inaguma, Y., Hamada, N., Tabata, H., Iwamoto, I., Mizuno, M., Nishimura, Y. V. et al. (2014). SIL1, a causative cochaperone gene of Marinesco-Söjgren syndrome, plays an essential role in establishing the architecture of the developing cerebral cortex. *EMBO Mol Med*, *6*(3), 414-429.

Ittner, A. A., Bertz, J., Chan, T. Y., van Eersel, J., Polly, P., & Ittner, L. M. (2014). The nucleotide exchange factor SIL1 is required for glucose-stimulated insulin secretion from mouse pancreatic beta cells in vivo. *Diabetologia*, *57*(7), 1410-1419.

Kabani, M., Beckerich, J. M., & Brodsky, J. L. (2002). Nucleotide exchange factor for the yeast Hsp70 molecular chaperone Ssa1p. *Mol Cell Biol*, *22*(13), 4677-4689.

Kabani, M., Beckerich, J. M., & Gaillardin, C. (2000). Sls1p stimulates Sec63p-mediated activation of Kar2p in a conformation-dependent manner in the yeast endoplasmic reticulum. *Mol Cell Biol*, *20*(18), 6923-6934.

Kabani, M., Kelley, S. S., Morrow, M. W., Montgomery, D. L., Sivendran, R., Rose, M. D. et al. (2003). Dependence of endoplasmic reticulum-associated degradation on the peptide binding domain and concentration of BiP. *Mol Biol Cell*, *14*(8), 3437-3448.

Kampinga, H. H., & Craig, E. A. (2010). The HSP70 chaperone machinery: J proteins as drivers of functional specificity. *Nat Rev Mol Cell Biol*, *11*(8), 579-592.

Karim, M. A., Parsian, A. J., Cleves, M. A., Bracey, J., Elsayed, M. S., Elsobky, E. et al. (2006). A novel mutation in BAP/SIL1 gene causes Marinesco-Sjögren syndrome in an extended pedigree. *Clin Genet*, *70*(5), 420-423.

Kim, S., Sideris, D. P., Sevier, C. S., & Kaiser, C. A. (2012). Balanced Ero1 activation and inactivation establishes ER redox homeostasis. *J Cell Biol*, *196*(6), 713-725.

Kim, Y. E., Hipp, M. S., Bracher, A., Hayer-Hartl, M., & Hartl, F. U. (2013). Molecular chaperone functions in protein folding and proteostasis. *Annu Rev Biochem*, *82*, 323-355.

Kitao, Y., Ozawa, K., Miyazaki, M., Tamatani, M., Kobayashi, T., Yanagi, H. et al. (2001). Expression of the endoplasmic reticulum molecular chaperone (ORP150) rescues hippocampal neurons from glutamate toxicity. *J Clin Invest*, *108*(10), 1439-1450.

Koch, G. L. (1990). The endoplasmic reticulum and calcium storage. *Bioessays*, *12*(11), 527-531.

Krieger, M., Roos, A., Stendel, C., Claeys, K. G., Sonmez, F. M., Baudis, M. et al. (2013). SIL1 mutations and clinical spectrum in patients with Marinesco-Sjogren syndrome. *Brain*, *136*(Pt 12), 3634-3644.

Laboissiere, M. C., Sturley, S. L., & Raines, R. T. (1995). The essential function of protein-disulfide isomerase is to unscramble non-native disulfide bonds. *J Biol Chem*, *270*(47), 28006-28009.

Lamantia, M., & Lennarz, W. J. (1993). The essential function of yeast protein disulfide isomerase does not reside in its isomerase activity. *Cell*, *74*, 899-908.

LaMantia, M., Miura, T., Tachikawa, H., Kaplan, H. A., Lennarz, W. J., & Mizunaga, T. (1991). Glycosylation site binding protein and protein disulfide isomerase are identical and essential for cell viability in yeast. *Proc Natl Acad Sci USA*, *88*(10), 4453-4457.

Lamriben, L., Graham, J. B., Adams, B. M., & Hebert, D. N. (2016). N-Glycan-based ER Molecular Chaperone and Protein Quality Control System: The Calnexin Binding Cycle. *Traffic*, *17*(4), 308-326.

Lind, C., Gerdes, R., Hamnell, Y., Schuppe-Koistinen, I., von Löwenhielm, H. B., Holmgren, A. et al. (2002). Identification of S-glutathionylated cellular proteins during oxidative stress and constitutive metabolism by affinity purification and proteomic analysis. *Arch Biochem Biophys*, *406*(2), 229-240.

Lindquist, S. (1986). The heat-shock response. *Annu Rev Biochem*, *55*, 1151-1191.

Linke, K., & Jakob, U. (2003). Not every disulfide lasts forever: disulfide bond formation as a redox switch. *Antioxid Redox Signal*, *5*(4), 425-434.

Mahloudji, M., Amirhakimi, G. H., Haghighi, P., & Khodadoust, A. A. (1972). Marinesco-Sjögren syndrome. Report of an autopsy. *Brain*, *95*(4), 675-680.

Marnett, L. J. (1999). Lipid peroxidation-DNA damage by malondialdehyde. *Mutat Res*, *424*(1-2), 83-95.

Matlack, K. E., Misselwitz, B., Plath, K., & Rapoport, T. A. (1999). BiP acts as a molecular ratchet during posttranslational transport of prepro-alpha factor across the ER membrane. *Cell*, *97*(5), 553-564.

Mayer, M. P., & Bukau, B. (2005). Hsp70 chaperones: cellular functions and molecular mechanism. *Cell Mol Life Sci*, *62*(6), 670-684.

Melnyk, A., Rieger, H., & Zimmermann, R. (2015). Co-chaperones of the mammalian endoplasmic reticulum. *Subcell Biochem*, *78*, 179-200.

Meusser, B., Hirsch, C., Jarosch, E., & Sommer, T. (2005). ERAD: the long road to destruction. *Nat Cell Biol*, *7*(8), 766-772.

Munro, S., & Pelham, H. R. (1986). An Hsp70-like protein in the ER: identity with the 78 kd glucose-regulated protein and immunoglobulin heavy chain binding protein. *Cell*, *46*(2), 291-300.

Nagy, P. (2013). Kinetics and mechanisms of thiol-disulfide exchange covering direct substitution and thiol oxidation-mediated pathways. *Antioxid Redox Signal*, *18*(13), 1623-1641.

Nair, P., Hamzeh, A. R., Mohamed, M., Tawfiq, N., Al-Ali, M. T., & Bastaki, F. (2016). Marinesco-Sjögren Syndrome in an Emirati Child with a Novel Mutation in SIL1 Affecting the 5' Untranslated Region. *Med Princ Pract*, *25*(6), 580-582.

Noreau, A., La Piana, R., Marcoux, C., FORGE, C., Dion, P. A., Brais, B. et al. (2015). Novel SIL1 mutations cause cerebellar ataxia and atrophy in a French-Canadian family. *Neurogenetics*, *16*(4), 315-318.

Nørgaard, P., Westphal, V., Tachibana, C., Alsøe, L., Holst, B., & Winther, J. R. (2001). Functional differences in yeast protein disulfide isomerases. *J Cell Biol*, *152*(3), 553-562.

Oka, B. V. O., & Bulleid, N. J. (2018). Disulfide Bond Formationin the Endoplasmic Reticulum. In M. J. Feige (Ed.), *Oxidative Folding of Proteins: Basic Principles, Cellular Regulationa nd Engineering. Vol. 9* (pp. 306-333). Royal Society of Chemistry.

Otero, J. H., Lizák, B., & Hendershot, L. M. (2010). Life and death of a BiP substrate. *Semin Cell Dev Biol*, *21*(5), 472-478.

Pace, C. N., Grimsley, G. R., Thomson, J. A., & Barnett, B. J. (1988). Conformational stability and activity of ribonuclease T1 with zero, one, and two intact disulfide bonds. *J Biol Chem*, *263*(24), 11820-11825.

Pareja, K. A., & Sevier, C. S. (in preparation). Auto-inhibition of Sil1 nucleotide exchange factor activity through a conserved N-terminal region.

Park, E., & Rapoport, T. A. (2012). Mechanisms of Sec61/SecY-mediated protein translocation across membranes. *Annu Rev Biophys*, *41*, 21-40.

Pihlajaniemi, T., Helaakoski, T., Tasanen, K., Myllylä, R., Huhtala, M. L., Koivu, J. et al. (1987). Molecular cloning of the beta-subunit of human prolyl 4-hydroxylase. This subunit and protein disulphide isomerase are products of the same gene. *EMBO J*, *6*(3), 643-649.

Pollard, M. G., Travers, K. J., & Weissman, J. S. (1998). Ero1p: a novel and ubiquitous protein with an essential role in oxidative protein folding in the endoplasmic reticulum. *Mol Cell*, *1*(2), 171-182.

Ponsero, A. J., Igbaria, A., Darch, M. A., Miled, S., Outten, C. E., Winther, J. R. et al. (2017). Endoplasmic Reticulum Transport of Glutathione by Sec61 Is Regulated by Ero1 and Bip. *Mol Cell*, *67*(6), 962-973.e5.

Preissler, S., Chambers, J. E., Crespillo-Casado, A., Avezov, E., Miranda, E., Perez, J. et al. (2015a). Physiological modulation of BiP activity by trans-protomer engagement of the interdomain linker. *Elife*, *4*, e08961.

Preissler, S., Rato, C., Chen, R., Antrobus, R., Ding, S., Fearnley, I. M. et al. (2015b). AMPylation matches BiP activity to client protein load in the endoplasmic reticulum. *Elife*, *4*, e12621.

Preissler, S., Rato, C., Perera, L., Saudek, V., & Ron, D. (2017). FICD acts bifunctionally to AMPylate and de-AMPylate the endoplasmic reticulum chaperone BiP. *Nat Struct Mol Biol*, *24*(1), 23-29.

Preissler, S., Rohland, L., Yan, Y., Chen, R., Read, R. J., & Ron, D. (2017). AMPylation targets the rate-limiting step of BiP's ATPase cycle for its functional inactivation. *Elife*, *6*.

Radford, S. E. (2000). Protein folding: progress made and promises ahead. *Trends Biochem Sci*, *25*(12), 611-618.

Rapoport, T. A., Li, L., & Park, E. (2017). Structural and Mechanistic Insights into Protein Translocation. *Annu Rev Cell Dev Biol*, *33*, 369-390.

Restelli, E., Masone, A., Sallese, M., & Chiesa, R. (2019). Neuroprotective modulation of the unfolded protein response in Marinesco-Sjögren syndrome: PERK signaling inhibition and beyond. *Neural Regen Res*, *14*(1), 62-64.

Riazuddin, S. A., Amiri-Kordestani, L., Kaul, H., Butt, T., Jiao, X., Riazuddin, S. et al. (2009). Novel SIL1 mutations in consanguineous Pakistani families mapping to chromosomes 5q31. *Mol Vis*, *15*, 1050-1056.

Ritossa, F. (1996). Discovery of the heat shock response. *Cell Stress Chaperones*, *1*(2), 97-98.

Roos, A., Buchkremer, S., Kollipara, L., Labisch, T., Gatz, C., Zitzelsberger, M. et al. (2014). Myopathy in Marinesco-Sjögren syndrome links endoplasmic reticulum chaperone dysfunction to nuclear envelope pathology. *Acta Neuropathol*, *127*(5), 761-777.

Roos, A., Kollipara, L., Buchkremer, S., Labisch, T., Brauers, E., Gatz, C. et al. (2016). Cellular Signature of SIL1 Depletion: Disease Pathogenesis due to Alterations in Protein Composition Beyond the ER Machinery. *Mol Neurobiol*, *53*(8), 5527-5541.

Rosam, M., Krader, D., Nickels, C., Hochmair, J., Back, K. C., Agam, G. et al. (2018). Bap (Sil1) regulates the molecular chaperone BiP by coupling release of nucleotide and substrate. *Nat Struct Mol Biol*, *25*(1), 90-100.

Rose, M. D., Misra, L. M., & Vogel, J. P. (1989). KAR2, a karyogamy gene, is the yeast homolog of the mammalian BiP/GRP78 gene. *Cell*, *57*(7), 1211-1221.

Sakai, K., Tada, M., Yonemochi, Y., Nakajima, T., Onodera, O., Takahashi, H. et al. (2008). Marinesco-Sjögren syndrome with atrophy of the brain stem tegmentum and dysplastic cytoarchitecture in the cerebral cortex. *Neuropathology*, *28*(5), 541-546.

Sanyal, A., Chen, A. J., Nakayasu, E. S., Lazar, C. S., Zbornik, E. A., Worby, C. A. et al. (2015). A novel link between Fic (filamentation induced by cAMP)-mediated adenylylation/AMPylation and the unfolded protein response. *J Biol Chem*, *290*(13), 8482-8499.

Satoh, M., Nakai, A., Sokawa, Y., Hirayoshi, K., & Nagata, K. (1993). Modulation of the phosphorylation of glucose-regulated protein, GRP78, by transformation and inhibition of glycosylation. *Exp Cell Res*, *205*(1), 76-83.

Schmid, D., Baici, A., Gehring, H., & Christen, P. (1994). Kinetics of molecular chaperone action. *Science*, *263*(5149), 971-973.

Schulz, S., Vielhaber, S., Muschke, P., Mohnike, K., Gooding, R., & Wieacker, P. (2007). Congenital cataract, ataxia, external ophthalmoplegia and dysphagia in two siblings. A Marinesco-Sjögren-like syndrome. *Neuropediatrics*, *38*(2), 88-90.

Sevier, C. S. (2018). Redox Regulation of Hsp70 Chaperone Function in the Endoplasmic Reticulum. In M. J. Feige (Ed.), *Oxidative Folding of Proteins: Basic Principles, Cellular Regulation and Engineering. Vol. 9* (pp. 334-354). Royal Society of Chemistry.

Sevier, C. S., & Kaiser, C. A. (2002). Formation and transfer of disulphide bonds in living cells. *Nat Rev Mol Cell Biol*, *3*(11), 836-847.

Sevier, C. S., & Kaiser, C. A. (2006). Conservation and diversity of the cellular disulfide bond formation pathways. *Antioxid Redox Signal*, *8*(5-6), 797-811.

Sevier, C. S., Qu, H., Heldman, N., Gross, E., Fass, D., & Kaiser, C. A. (2007). Modulation of cellular disulfide-bond formation and the ER redox environment by feedback regulation of Ero1. *Cell*, *129*(2), 333-344.

Shim, S. M., Choi, H. R., Sung, K. W., Lee, Y. J., Kim, S. T., Kim, D. et al. (2018). The endoplasmic reticulum-residing chaperone BiP is short-lived and metabolized through N-terminal arginylation. *Sci Signal*, *11*(511).

Shimizu, Y., & Hendershot, L. M. (2009). Oxidative folding: cellular strategies for dealing with the resultant equimolar production of reactive oxygen species. *Antioxid Redox Signal*, *11*(9), 2317-2331.

Shiu, R. P., Pouyssegur, J., & Pastan, I. (1977). Glucose depletion accounts for the induction of two transformation-sensitive membrane proteinsin Rous sarcoma virus-transformed chick embryo fibroblasts. *Proc Natl Acad Sci USA*, *74*(9), 3840-3844.

Skre, H., & Berg, K. (1977). Linkage studies on Marinesco-Sjøgren syndrome and hypergonadotropic hypogonadism. *Clin Genet*, *11*(1), 57-66.

Soto, C., & Pritzkow, S. (2018). Protein misfolding, aggregation, and conformational strains in neurodegenerative diseases. *Nat Neurosci*, *21*(10), 1332-1340.

Stevens, K. L. P., Black, A. L., Wells, K. M., Yeo, K. Y. B., Steuart, R. F. L., Stirling, C. J. et al. (2017). Diminished Ost3-dependent N-glycosylation of the BiP nucleotide exchange factor Sil1 is an adaptive response to reductive ER stress. *Proc Natl Acad Sci USA*, *114*(47), 12489-12494.

Tachikawa, H., Miura, T., Katakura, Y., & Mizunaga, T. (1991). Molecular structure of a yeast gene, PDI1, encoding protein disulfide isomerase that is essential for cell growth. *J Biochem*, *110*(2), 306-313.

Takahata, T., Yamada, K., Yamada, Y., Ono, S., Kinoshita, A., Matsuzaka, T. et al. (2010). Novel mutations in the SIL1 gene in a Japanese pedigree with the Marinesco-Sjögren syndrome. *J Hum Genet*, *55*(3), 142-146.

Tasanen, K., Parkkonen, T., Chow, L. T., Kivirikko, K. I., & Pihlajaniemi, T. (1988). Characterization of the human gene for a polypeptide that acts both as the beta subunit of prolyl 4-hydroxylase and as protein disulfide isomerase. *J Biol Chem*, *263*(31), 16218-16224.

Thannickal, V. J., & Fanburg, B. L. (2000). Reactive oxygen species in cell signaling. *Am J Physiol Lung Cell Mol Physiol*, *279*(6), L1005-28.

Tian, G., Kober, F. X., Lewandrowski, U., Sickmann, A., Lennarz, W. J., & Schindelin, H. (2008). The catalytic activity of protein-disulfide isomerase requires a conformationally flexible molecule. *J Biol Chem*, *283*(48), 33630-33640.

Tian, G., Xiang, S., Noiva, R., Lennarz, W. J., & Schindelin, H. (2006). The crystal structure of yeast protein disulfide isomerase suggests cooperativity between its active sites. *Cell*, *124*(1), 61-73.

Todorov, A. (1965). [Marinesco-Sjogren syndrome. 1st anatomo-clinical study]. *J Genet Hum*, *14*(2), 197-233.

Tu, B. P., Ho-Schleyer, S. C., Travers, K. J., & Weissman, J. S. (2000). Biochemical basis of oxidative protein folding in the endoplasmic reticulum. *Science*, *290*(5496), 1571-1574.

Tu, B. P., & Weissman, J. S. (2002). The FAD- and O(2)-dependent reaction cycle of Ero1-mediated oxidative protein folding in the endoplasmic reticulum. *Mol Cell*, *10*(5), 983-994.

Turpaev, K. T. (2002). Reactive oxygen species and regulation of gene expression. *Biochemistry (Mosc)*, *67*(3), 281-292.

Tyson, J. R., & Stirling, C. J. (2000). LHS1 and SIL1 provide a lumenal function that is essential for protein translocation into the endoplasmic reticulum. *EMBO J*, *19*(23), 6440-6452.

Ushioda, R., Hoseki, J., Araki, K., Jansen, G., Thomas, D. Y., & Nagata, K. (2008). ERdj5 is required as a disulfide reductase for degradation of misfolded proteins in the ER. *Science*, *321*(5888), 569-572.

Van Raamsdonk, J. M. (2006). Loss of function mutations in SIL1 cause Marinesco-Sjögren syndrome. *Clin Genet*, *69*(5), 399-400.

Vitu, E., Kim, S., Sevier, C. S., Lutzky, O., Heldman, N., Bentzur, M. et al. (2010). Oxidative activity of yeast Ero1p on protein disulfide isomerase and related oxidoreductases of the endoplasmic reticulum. *J Biol Chem*, *285*(24), 18155-18165.

Vogel, J. P., Misra, L. M., & Rose, M. D. (1990). Loss of BiP/GRP78 function blocks translocation of secretory proteins in yeast. *J Cell Biol*, *110*(6), 1885-1895.

Voorhees, R. M., & Hegde, R. S. (2016). Structure of the Sec61 channel opened by a signal sequence. *Science*, *351*(6268), 88-91.

Walter, P., & Ron, D. (2011). The unfolded protein response: from stress pathway to homeostatic regulation. *Science*, *334*(6059), 1081-1086.

Wang, C., Yu, J., Huo, L., Wang, L., Feng, W., & Wang, C. C. (2012). Human protein-disulfide isomerase is a redox-regulated chaperone activated by oxidation of domain a'. *J Biol Chem*, *287*(2), 1139-1149.

Wang, J., Lee, J., Liem, D., & Ping, P. (2017). HSPA5 Gene encoding Hsp70 chaperone BiP in the endoplasmic reticulum. *Gene*, *618*, 14-23.

Wang, J., Pareja, K. A., Kaiser, C. A., & Sevier, C. S. (2014). Redox signaling via the molecular chaperone BiP protects cells against endoplasmic reticulum-derived oxidative stress. *Elife*, *3*, e03496.

Wang, J., & Sevier, C. S. (2016). Formation and Reversibility of BiP Protein Cysteine Oxidation Facilitate Cell Survival during and post Oxidative Stress. *J Biol Chem*, *291*(14), 7541-7557.

Wei, P. C., Hsieh, Y. H., Su, M. I., Jiang, X., Hsu, P. H., Lo, W. T. et al. (2012). Loss of the oxidative stress sensor NPGPx compromises GRP78 chaperone activity and induces systemic disease. *Mol Cell*, *48*(5), 747-759.

Weitzmann, A., Baldes, C., Dudek, J., & Zimmermann, R. (2007). The heat shock protein 70 molecular chaperone network in the pancreatic endoplasmic reticulum - a quantitative approach. *FEBS J*, *274*(19), 5175-5187.

Weitzmann, A., Volkmer, J., & Zimmermann, R. (2006). The nucleotide exchange factor activity of Grp170 may explain the non-lethal phenotype of loss of Sil1 function in man and mouse. *FEBS Lett*, *580*(22), 5237-5240.

Wen, K. W., & Damania, B. (2010). Hsp90 and Hsp40/Erdj3 are required for the expression and anti-apoptotic function of KSHV K1. *Oncogene*, *29*(24), 3532-3544.

Williams, J. M., Inoue, T., Chen, G., & Tsai, B. (2015). The nucleotide exchange factors Grp170 and Sil1 induce cholera toxin release from BiP to enable retrotranslocation. *Mol Biol Cell*, *26*(12), 2181-2189.

Wilson, R., Lees, J. F., & Bulleid, N. J. (1998). Protein disulfide isomerase acts as a molecular chaperone during the assembly of procollagen. *J Biol Chem*, *273*(16), 9637-9643.

Winter, J., Linke, K., Jatzek, A., & Jakob, U. (2005). Severe oxidative stress causes inactivation of DnaK and activation of the redox-regulated chaperone Hsp33. *Mol Cell*, *17*(3), 381-392.

Wu, X., Cabanos, C., & Rapoport, T. A. (2019). Structure of the post-translational protein translocation machinery of the ER membrane. *Nature*, *566*(7742), 136-139.

Xu, H., Xu, S., Zhang, R., Xin, T., & Pang, Q. (2018). SIL1 functions as an oncogene in glioma by AKT/mTOR signaling pathway. *Onco Targets Ther*, *11*, 3775-3783.

Xu, M., Marsh, H. M., & Sevier, C. S. (2016). A Conserved Cysteine within the ATPase Domain of the Endoplasmic Reticulum Chaperone BiP is Necessary for a Complete Complement of BiP Activities. *J Mol Biol*, *428*(20), 4168-4184.

Yan, M., Li, J., & Sha, B. (2011). Structural analysis of the Sil1-Bip complex reveals the mechanism for Sil1 to function as a nucleotide-exchange factor. *Biochem J*, *438*(3), 447-455.

Yang, J., Nune, M., Zong, Y., Zhou, L., & Liu, Q. (2015). Close and Allosteric Opening of the Polypeptide-Binding Site in a Human Hsp70 Chaperone BiP. *Structure*, *23*(12), 2191-2203.

Young, J. C. (2010). Mechanisms of the Hsp70 chaperone system. *Biochem Cell Biol*, *88*(2), 291-300.

Zhang, H., Yang, J., Wu, S., Gong, W., Chen, C., & Perrett, S. (2016). Glutathionylation of the Bacterial Hsp70 Chaperone DnaK Provides a Link between Oxidative Stress and the Heat Shock Response. *J Biol Chem*, *291*(13), 6967-6981.

Zhang, Y., Liu, R., Ni, M., Gill, P., & Lee, A. S. (2010). Cell surface relocalization of the endoplasmic reticulum chaperone and unfolded protein response regulator GRP78/BiP. *J Biol Chem*, *285*(20), 15065-15075.

Zhao, L., Longo-Guess, C., Harris, B. S., Lee, J. W., & Ackerman, S. L. (2005). Protein accumulation and neurodegeneration in the woozy mutant mouse is caused by disruption of SIL1, a cochaperone of BiP. *Nat Genet*, *37*(9), 974-979.

Zhao, L., Rosales, C., Seburn, K., Ron, D., & Ackerman, S. L. (2010). Alteration of the unfolded protein response modifies neurodegeneration in a mouse model of Marinesco-Sjögren syndrome. *Hum Mol Genet*, *19*(1), 25-35.

Zielinska, D. F., Gnad, F., Wiśniewski, J. R., & Mann, M. (2010). Precision mapping of an in vivo N-glycoproteome reveals rigid topological and sequence constraints. *Cell*, *141*(5), 897-907.

CHAPTER 2

AN UNEXPECTED ROLE FOR THE YEAST NUCLEOTIDE EXCHANGE FACTOR SIL1 AS A REDUCTANT ACTING ON THE MOLECULAR CHAPERONE BIP

ABSTRACT

Unfavorable redox conditions in the endoplasmic reticulum (ER) can decrease the capacity for protein secretion, altering vital cell functions. While systems to manage reductive stress are well-established, how cells cope with an overly oxidizing ER remains largely undefined. In previous work (Wang, Pareja, Kaiser, & Sevier, 2014), we demonstrated that the chaperone BiP is a sensor of overly oxidizing ER conditions. We showed that modification of a conserved BiP cysteine during stress beneficially alters BiP chaperone activity to cope with suboptimal folding conditions. How this cysteine is reduced to reestablish 'normal' BiP activity post-oxidative stress has remained unknown. Here we demonstrate that BiP's nucleotide exchange factor – Sil1 – can reverse BiP cysteine oxidation. This previously unexpected reductant capacity for yeast Sil1 has potential implications for the human ataxia Marinesco-Sjögren, where it is interesting to speculate that a disruption in ER redox-signaling (due to genetic defects in SIL1) may influence disease pathology.

± The following sections are reproduced from Siegenthaler, K.D., Pareja, K.A., Wang, J. and Sevier, C.S. "An unexpected role for the yeast nucleotide exchange factor Sil1 as a reductant acting on the molecular chaperone BiP." *Elife*, *6* (2017): p.e24141.

INTRODUCTION

In eukaryotes, the oxidizing environment of the endoplasmic reticulum (ER) facilitates the folding and secretion of approximately a third of the cellular proteome. Protein flux through the ER varies widely, and transient increases in oxidative folding both deplete reduced glutathione and generate hydrogen peroxide, which can disrupt protein structure, folding, and secretion (Bulleid & Ellgaard, 2011; Kakihana, Nagata, & Sitia, 2012). We have shown in yeast that a conserved cysteine in the nucleotide-binding domain of the Hsp70 chaperone BiP (Kar2) senses alterations in levels of both glutathione and peroxide in the ER. As ER levels of these small molecules rise, the BiP cysteine becomes oxidized, converting the normally ATP-driven chaperone into an ATP-independent protein holdase (Wang et al., 2014; Wang & Sevier, 2016). A similar system has been proposed for mammals, where formation of an intramolecular disulfide bond in the presence of increased oxidants augments BiP chaperone function (Wei et al., 2012). The increased chaperone activity of oxidized BiP is proposed to promote cell survival by limiting polypeptide aggregation during suboptimal folding conditions (Wang et al., 2014).

A hallmark of thiol-redox switches is their reversibility, which allows for a reversion to 'normal' activity when oxidative stress subsides. Yet how BiP reduction is achieved within cells has remained unclear. The ER contains multiple members of the thioredoxin superfamily with the capacity to reduce oxidized thiols; yet the relatively buried location of the redox-sensitive cysteine in BiP suggests that BiP is a poor candidate substrate for these reductases. Here we identify Sil1, BiP's nucleotide exchange factor (NEF), as an unexpected reductant of oxidized BiP. We propose that a redox-active cysteine pair within a flexible N-terminal polypeptide domain of Sil1 facilitates reduction of the relatively buried BiP cysteine.

RESULTS AND DISCUSSION

A role for Sil1 in controlling the redox state of the BiP cysteine emerged from a genetic screen designed to isolate yeast BiP alleles that increase the viability of cells exposed to oxidative ER stress conditions. This screen took advantage of our prior observations that (i) a yeast strain unable to undergo BiP oxidation (a *kar2-C63A* strain) was inviable when cells were subject to oxidative ER stress and (ii) an ectopic BiP allele that functionally mimics oxidized BiP allows for robust growth of the compromised *kar2-C63A* strain (Wang et al., 2014). Building upon these phenotypes, we randomly mutagenized BiP and screened for alleles that allowed for robust growth of a *kar2-C63A* yeast strain expressing a hyper-active mutant of the oxidoreductase Ero1 (Ero1*), which we used as proxy for physiological ER oxidative stress (Sevier et al., 2007). We aimed to isolate BiP mutants that either stabilized the oxidized BiP form or phenotypically mimicked the oxidized form, without necessarily impacting BiP oxidation. Our screen identified a BiP-K314E mutant allele. BiP is an essential gene in yeast. We observed that the K314E mutation does not compromise essential BiP activity; a BiP-K314E allele can support cell viability as the sole cellular BiP (**Figure 2.1A**). Yet, in keeping with the original screen design, a strain containing a BiP-K314E mutant was able to more efficiently manage oxidative stress, exhibiting a greater resistance to the small molecule oxidant diamide (**Figure 2.1A**).

The redox-active BiP cysteine (Cys63) and Lys314 are both located in the BiP ATPase domain; Cys63 is relatively hidden within a cleft that forms the nucleotide-binding pocket while Lys314 is sur- face exposed, found at the interface formed between BiP and its NEF Sil1 (**Figure 2.2)** (Yan, Li, & Sha, 2011). Although mutation of the surface exposed Lys314 could alter the

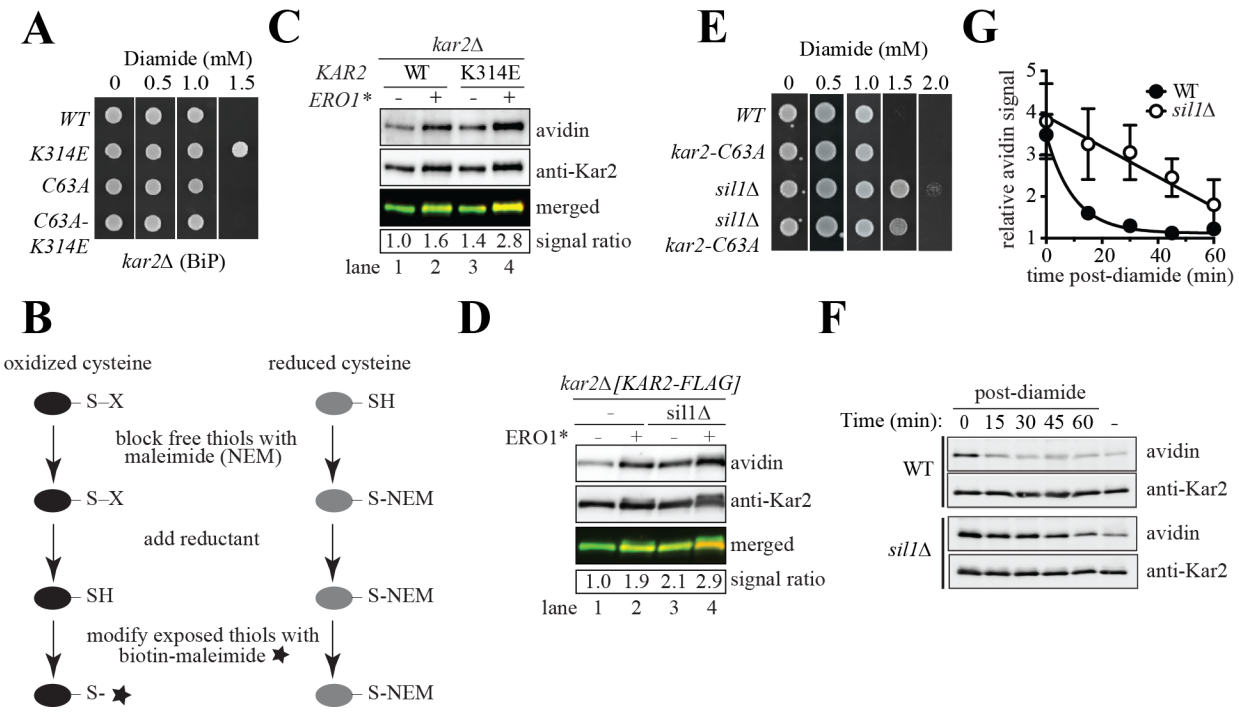

Figure 2.1 Sil1 regulates BiP oxidation state in cells. (A) Yeast strains (CSY289, 290, 612, 689) were spotted onto SMM plates containing 0–1.5 mM diamide and incubated for 2 d at 30˚C. (B) Schematic for the biotin-switch procedure. (C) Yeast strains deleted for endogenous BiP (*kar2*Δ) containing plasmids encoding FLAG-tagged BiP were assayed for oxidized BiP levels using the biotin-switch protocol. Oxidative stress was generated by overexpression of Ero1*. BiP was immunoprecipitated, and total and oxidized BiP were detected by Western blotting. The relative levels of oxidized BiP are expressed as the ratio of the intensity of the avidin and anti-BiP signals. The signal ratio was set to 1.0 for wild-type cells grown in the absence of Ero1*. (D) Lysates were prepared from the indicated yeast after Ero1* induction. Oxidized BiP levels were detected and quantified as in C. (E) Yeast strains (CSY5, 275, 448, 449) were spotted onto YPD plates containing 0–2.0 mM diamide and were incubated for 2 d at 30˚C. (F) Cells were treated with 5 mM diamide for 15 min, diamide was removed, and cells were returned to 30˚C until harvest. Oxidized BiP levels were determined as in C. (G) Plot of the averaged quantified data ± SEM from F and a second independent experiment using the same protocol. For each strain, the signal ratio was set to 1.0 for cells grown without diamide.

local cysteine environment to modulate cysteine oxidation, we were more intrigued by the possibility that introduction of a negative charge a position 314 may weaken the interaction between BiP and Sil1, which could beneficially alter BiP activity during oxidative stress. Using a GST-pulldown assay, we confirmed a clear disruption in the physical association between Sil1

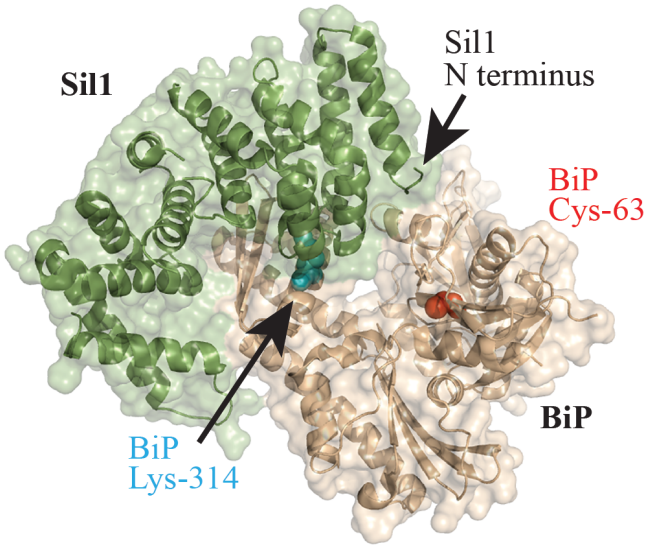

Figure 2.2 Sil1-BiP complex. Sil1-BiP complex structure (PBD ID: 3QML) encompassing the armadillo repeats from yeast Sil1 (residues 113–421) and the yeast BiP ATPase domain (residues 43–426) (Yan et al., 2011). BiP is shown in wheat; Sil1 is colored green. The redox-active BiP cysteine is shown as a red sphere. BiP lysine-314 is shown as a cyan sphere.

and recombinant BiP-K314E (**Figure 2.3A)**. A disruption in the interaction between BiP-K314E and Sil1 in vivo was also implied by the equivalent phenotypes observed with BiP-K314E and *sil1*Δ alleles. BiP utilizes two NEFs, and a strain lacking both NEFs (*lhs1*Δ *sil1*Δ) is inviable (Tyson & Stirling, 2000); a BiP-K314E allele behaved like a *sil1*Δ allele, showing inviability in combination with *lhs1*Δ (**Figure 2.3B)**. Given these data, we initially speculated that the resistance to oxidant observed for the BiP-K314E alleles was due to the loss of NEF interaction, letting BiP dwell longer in an ADP/peptide-bound state, enhancing holdase activity like oxidized BiP (Wang et al., 2014). Yet, while such a mechanism may contribute to some of the beneficial impact of the BiP-K314E allele during stress, we observed that the resistance to diamide conferred by the K314E mutation was largely abolished upon mutation of BiP Cys63 (a C63A-K314E mutation; **Figure 2.1A**). Curiously, these data implied that the K314E alteration may influence BiP cysteine oxidation despite the lack of proximity between Lys314 and Cys63.

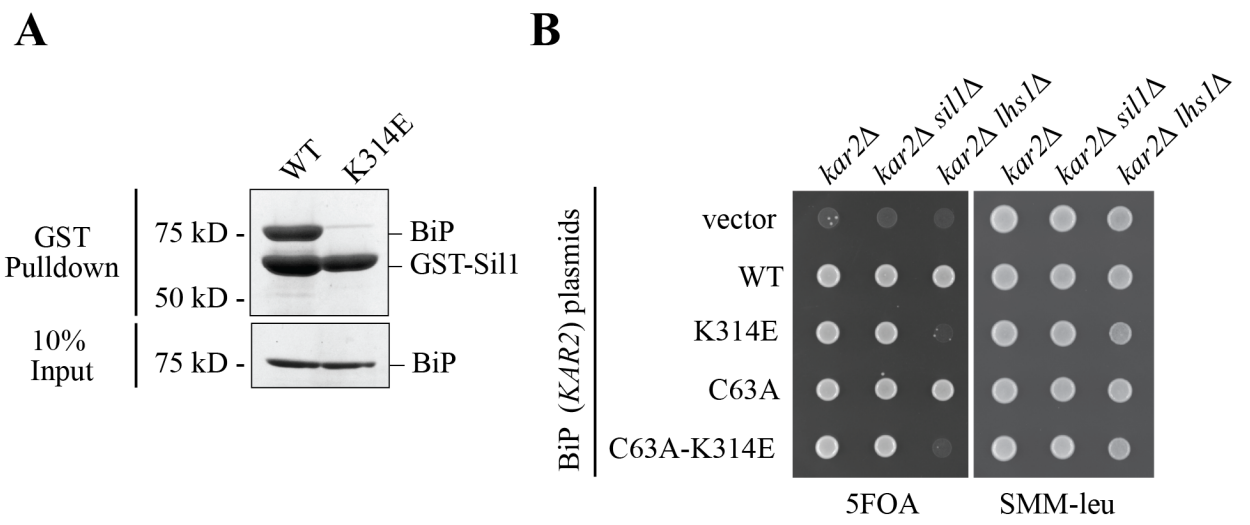

Figure 2.3 A BiP K314E mutation disrupts Sil1 binding. (**A**) GST-Sil1, bound to glutathione-agarose beads, was incubated with recombinant wild-type BiP or mutant BiP-K314E proteins for 1 hr Bound proteins were eluted from the agarose beads with SDS, and proteins were resolved by SDS-PAGE and visualized using a Coomassie blue stain. (**B**) CSY214 (*kar2*Δ [pCS623]), CSY594 (*kar2*Δ *sil1*Δ [pCS623]), and CSY595 (*kar2*Δ *lhs1*Δ [pCS623]) strains were transformed with *LEU2*-marked plasmids coding for the indicated BiP alleles (pCS681, pKP37, pCS685, pKP97) or empty vector. Transformants were spotted onto SMM plates containing 5-FOA (to select against wild-type BiP plasmid pCS623) or SMM minus leucine plates (to confirm successful transformation with the *LEU2*-marked plasmid). A *sil1*Δ *lhs1*Δ yeast strain is inviable; the observed inviability of the BiP-K314E mutant in the *lhs1*Δ strain background is consistent with an inability of the BiP-K314E mutant to associate with Sil1, which phenocopies a *sil1* null strain.

To directly test the influence of the K314E mutation on BiP cysteine oxidation, we performed a biotin-switch procedure that allows for the conversion of oxidized cysteine adducts to biotinylated cysteines, which are readily detectable with an avidin probe (**Figure 2.1B**). Yeast BiP contains a single cysteine (Cys63), and any avidin signal in this switch assay has been traced to Cys63 oxidation (Wang et al., 2014). Confirming our prior results, approximately two-fold more oxidized BiP was recovered from cells grown under conditions of ER stress (**Figure 2.1C**) (Wang et al., 2014). Strikingly, a BiP-K314E allele further enhanced the recovery of oxidized BiP from stressed cells (**Figure 2.1C**). If the enhanced oxidation of BiP-K314E is a consequence of disrupted Sil1 binding, a similar increase in BiP oxidation levels should be observed in cells

lacking Sil1. Indeed, a *sil1*Δ strain not only accumulated more oxidized BiP than a wild-type strain under stress but also showed a higher basal level of oxidized BiP in the absence of stressor (**Figure 2.1D**). A *sil1*Δ strain also exhibited an increased ability to survive in the presence of diamide, relative to a wild-type strain (**Figure 2.1E**); the increased resistance to diamide for a *sil1*Δ strain mirrors the increased diamide resistance observed for a strain containing BiP-K314E (**Figure 2.1A**). Together, these data are consistent with a model wherein a disruption in the association between BiP and Sil1 in cells results in an increased level of oxidized BiP under stress conditions. We propose that it is the accumulation of more oxidized BiP in these cells that contributes towards the increase in cell survival observed for these strains when grown in the presence of oxidant (diamide). In keeping with this model, the resistance of a *sil1*Δ strain to diamide was lessened when the BiP cysteine was mutated to alanine (**Figure 2.1E**). However, it is important to note that the increased diamide resistance observed for the *sil1*Δ strain cannot be attributed exclusively to a role for Sil1 in modulating BiP's redox state; a *sil1*Δ *kar2-C63A* strain displays more resistance to diamide than a *kar2-C63A* strain (**Figure 2.1E**). These data suggest that there is also some benefit for loss of *SIL1* during oxidative stress independent of BiP cysteine oxidation; we suggest that changes in BiP function in cells as a consequence of a loss of Sil1 NEF activity also facilitate diamide resistance.

The increased level of oxidized BiP observed in both a BiP-K314E mutant and *sil1*Δ strain implies that the normal association of BiP and Sil1 either (i) inhibits adduct formation or (ii) facilitates adduct reduction. We have shown previously that when stress conditions subside, the BiP cysteine-adduct is reduced (removed) with a half-life of less than 10 min (Wang & Sevier, 2016). To determine if Sil1 facilitates BiP reduction, we monitored whether an absence of Sil1 slowed the removal of the BiP cysteine-adduct post-oxidative stress. Utilizing the biotin-

switch assay, we observed a rapid decrease in oxidized BiP levels in a wild-type strain post-oxidant removal ($t_{1/2}$ ~6 min) (**Figure 2.1F, G**). In contrast, the stability of the BiP cysteine-adduct was markedly enhanced in a strain lacking Sil1 (*sil1*Δ), demonstrating a half-life of greater than 45 min (**Figure 2.1F, G**). Sil1 has been implicated in the retrotranslocation of cholera toxin (Williams, Inoue, Chen, & Tsai, 2015). However, the relatively constant and similar levels of total BiP in the wild-type and *sil1*Δ strains suggests that changes in ER-associated degradation do not account for the stabilization of oxidized BiP. Of note, the level of oxidized BiP in a *sil1*Δ strain was restored to wild-type levels 1 hr post-oxidant removal (**Figure 2.1F, G**), demonstrating that other (slower) mechanisms exist for BiP reduction in the absence of Sil1. The presence of compensatory reduction systems is consistent with the viability of the *sil1*Δ strain. If Sil1 were the sole facilitator of BiP reduction, loss of Sil1 activity might be expected to be lethal to cells; we have shown previously that a strain containing a mimetic allele of constitutively oxidized BiP (as the sole copy of cellular BiP) is inviable under non-stress conditions (Wang et al., 2014).

We initially reasoned that the documented ability of Sil1 to ratchet open the nucleotide-binding cleft (Yan et al., 2011) could allow a reductant access to the cysteine. However, we were struck by the presence of a pair of cysteines in the N-terminal domain of Sil1 separated by four intervening residues (Cys-52 and Cys-57), which suggested the intriguing alternative that Sil1 itself could be an oxidoreductase. These cysteine residues are absent in the BiP-Sil1 structure (Yan et al., 2011), yet it is easy to envision how a polypeptide sequence extending from the most N-terminal residue of Sil1 in the structure could reach into the BiP nucleotide-binding cleft to allow for thiol-disulfide exchange between Sil1 and oxidized BiP (**Figure 2.2**).

To determine if Sil1 has the capacity to reduce oxidized BiP, we purified recombinant BiP and Sil1 from bacteria and assayed for Sil1 activity as a reductant in vitro. In cells, BiP is oxidized by peroxide and glutathione, forming either a sulfenic acid or glutathione adduct (Wang et al., 2014; Wang & Sevier, 2016). To facilitate monitoring of oxidized BiP in vitro, we reacted BiP with Ellman's reagent (DNTB), which results in a BiP-TNB disulfide linkage similar to the BiP-glutathione disulfide link; a protein-TNB substrate has also been utilized as an effective substrate for an enzyme that reverses sulfenic acid adducts (Depuydt et al., 2009). A BiP-TNB adduct is colorless, yet reduction of BiP liberates the TNB anion, allowing for spectroscopic monitoring (**Figure 2.4A**). Strikingly, Sil1 reduced the otherwise stable BiP-TNB adduct (**Figure 2.4B**). Sil1 reducing activity required the presence of either Cys52 or Cys57; a C52A-C57A mutant showed no capacity to facilitate BiP reduction (**Figure 2.4B**). Interestingly, the presence of a single N-terminal cysteine (either Cys-52 or Cys-57) was sufficient to release TNB, demonstrating that each cysteine can act as the attacking nucleophile (**Figure 2.4B**). Such a mechanism is distinct from that used by the well-characterized reductase thioredoxin, where only the first cysteine in the active site Cys-X-X-Cys motif is able to serve as an attacking nucleophile (Lu & Holmgren, 2014). However enzymes containing redox-active cysteine pairs that do not adopt a thioredoxin fold have shown a behavior similar to what is seen with Sil1, including the ER- localized oxidase Erv2 (Gross, Sevier, Vala, Kaiser, & Fass, 2002). Sil1 contains two additional cysteines within the armadillo repeats (Cys-203 and Cys-373); we observed that these cysteines were dispensable for Sil1 reducing activity (**Figure 2.4B**).

Disruption of residues at the contact sites formed between BiP and Sil1 also hindered BiP-TNB reduction. Sil1 His163 has been shown to be critically involved in the association of Sil1 with BiP (Yan et al., 2011), and we observed that a Sil1-H163E mutant was unable to

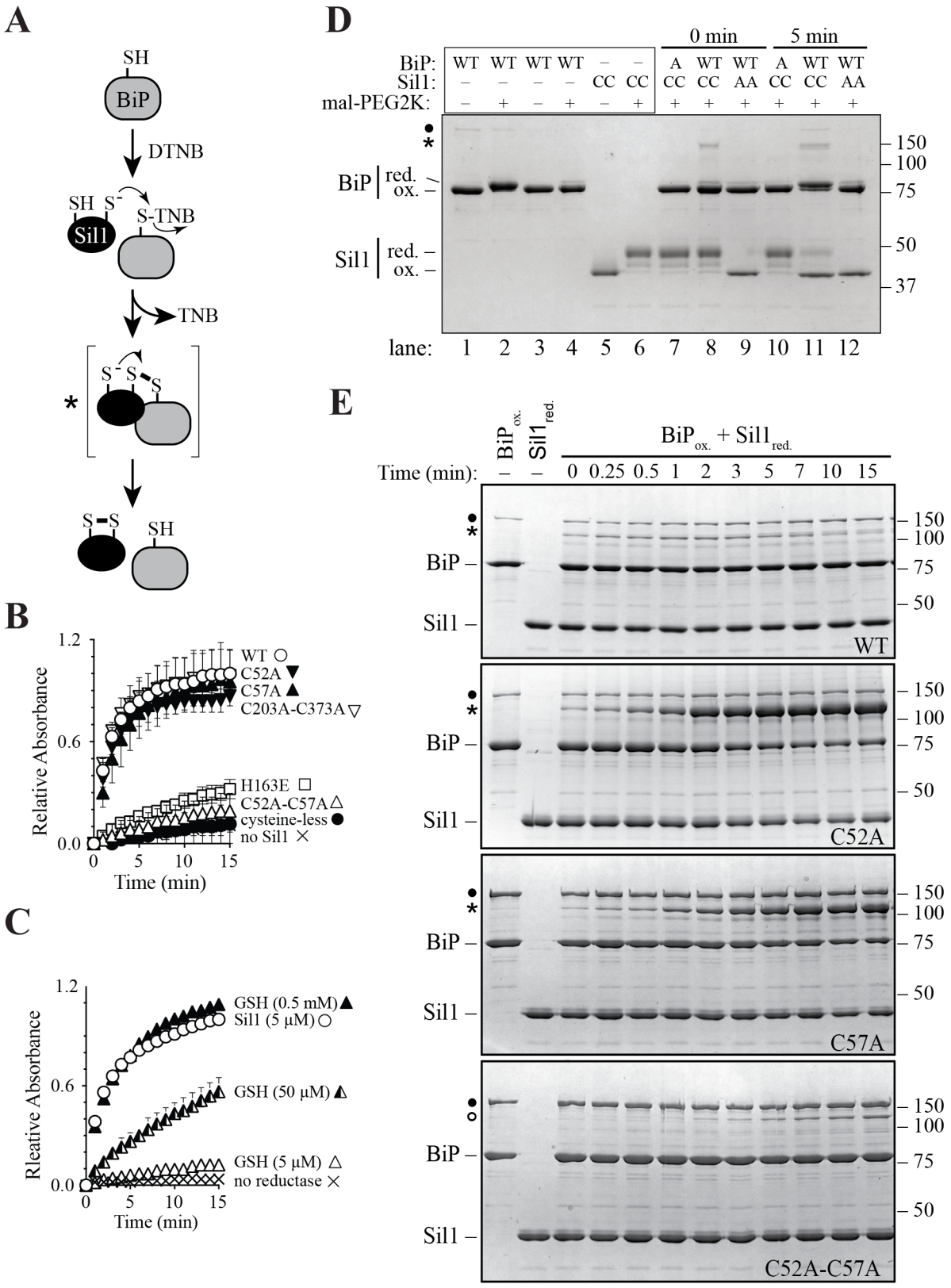
A
SH
BiP
DTNB
SH S⁻
S-TNB
Sil1
TNB
S⁻ S S
*
S-S
SH
B
1.2
0.6
0.0
Relative Absorbance
0 5 10 15
Time (min)
WT ○
C52A ▼
C57A ▲
C203A-C373A ▽
H163E □
C52A-C57A △
cysteine-less ●
no Sil1 ×
C
1.2
0.6
0.0
Rleative Absorbance
0 5 10 15
Time (min)
GSH (0.5 mM) ▲
Sil1 (5 μM) ○
GSH (50 μM) ◭
GSH (5 μM) △
no reductase ×
D
0 min
5 min
BiP: WT WT WT WT – – A WT WT A WT WT
Sil1: – – – – CC CC CC CC AA CC CC AA
mal-PEG2K: – + – + – + + + + + + +
BiP red.
ox.
Sil1 red.
ox.
150
100
75
50
37
lane: 1 2 3 4 5 6 7 8 9 10 11 12
E
BiP ox.
Sil1 red.
BiP ox. + Sil1 red.
Time (min): – – 0 0.25 0.5 1 2 3 5 7 10 15
BiP
Sil1
WT
C52A
C57A
C52A-C57A
150
100
75
50

Figure 2.4 Sil1 N-terminal cysteines facilitate reduction of oxidized recombinant BiP in vitro. (A) Schematic for monitoring Sil1 activity as a BiP-cysteine reductant. (B) Reduction of recombinant BiP oxidized by DTNB (BiP-TNB), in the presence of recombinant wild-type or mutant Sil1, was monitored by following the change in absorbance at 412 nm (indicative of TNB release) over time. (C) BiP-TNB reduction by reduced glutathione (GSH) or Sil1 was monitored as in B. Data in B and C represent the mean values from three independent experiments; error bars depict the range. (D) Thiol-disulfide exchange between recombinant wild-type BiP (WT) or a cysteine-less BiP-C63A mutant (A) and Sil1-C203A-C373A (with the N-terminal cysteines; CC) or a cysteine-less Sil1 (lacking the N-terminal cysteines; AA) was monitored by following the presence or absence of free thiols in both proteins. BiP and/or Sil1 were incubated for the indicated times, and reactions were quenched with the addition of the thiol-modifying agent mal-PEG2K. Samples were separated by non-reducing SDS-PAGE and visualized with Coomassie blue. Lanes 1–6 are shown as mobility controls. Lanes 1 and 2 contain BiP that was not reacted with DTNB; all other lanes include BiP incubated with DNTB prior to the addition of Sil1, and later mal-PEG2K. Labels indicate disulfide-linked BiP-Sil1 (asterisk) and BiP-BiP (filled circle) species. (E) Coomassie-stained gels follow recombinant BiP-TNB reaction with wild-type and mutant Sil1 proteins. Samples were quenched at the indicated times with N-ethylmaleimide (NEM) and separated by non-reducing SDS-PAGE. A BiP-Sil1 mixed-disulfide species (asterisk) accumulates with Sil1-C52A and Sil1-C57A. A second BiP-Sil1 species maintained in the absence of the N-terminal Sil1 cysteine pair is noted with an open circle.

effectively reduce BiP- TNB (**Figure 2.4B**). Similarly, mutation of BiP Lys314 (a BiP-K314E mutant) lessened the removal of the TNB adduct by wild-type Sil1 (**Figure 2.5**). Some modest release of TNB from oxidized BiP-K314E by Sil1 was observed (**Figure 2.5**), and we suggest that the limited reductant activity observed with BiP-K314E reflects some productive association of BiP-K314E and Sil1 at the high BiP:Sil1 ratio required for this single-turnover assay. Notably, the release of TNB from BiP-K314E by Sil1 was lost when the Sil1 N-terminal cysteines were mutated to alanine (**Figure 2.5)**

To test Sil1 activity relative to a characterized reductant, we compared the activity of Sil1 to reduced glutathione (GSH). Surprisingly, GSH showed negligible activity when tested at an equivalent concentration to Sil1 (**Figure 2.4C**). In fact, a 100-fold excess of GSH was required to recapitulate comparable Sil1 activity (**Figure 2.4C**). We expect that the high affinity reported for Sil1 towards BiP likely accounts for the increased reducing capacity observed for Sil1 relative to GSH (Yan et al., 2011). Given the abundant (millimolar) amounts of glutathione present in the ER, it remains an open question whether GSH contributes to BiP reduction *in vivo*.

We expect that BiP-TNB reduction by Sil1 proceeds through a dithiol-disulfide exchange reaction, wherein recovery of the BiP cysteine thiol is coincident with oxidation of the N-terminal Sil1 cysteines (**Figure 2.4A**). To confirm that oxidation of the Sil1 cysteines is concomitant with BiP reduction, we monitored the Sil1 cysteine redox state using a 2-kD maleimide-PEG reagent (mal-PEG2K), which will react with reduced thiols resulting in a mobility shift detectable by SDS-PAGE. In order to specifically follow the N-terminal cysteine pair, we used a Sil1-C203A-C373A mutant. We first determined the relative mobility on a SDS-polyacrylamide gel for the oxidized and reduced forms of BiP and Sil1 after mal-PEG2K addition. Modification of the free thiol in reduced BiP with mal-PEG2K resulted in a slower

migrating species (**Figure 2.4D**, lane 2) that could be clearly distinguished from oxidized BiP (BiP-TNB), which was not susceptible to alkylation by mal-PEG2K and migrated similarly to BiP not treated with mal-PEG2K (**Figure 2.4D**, lane 4 versus 3). Likewise, alkylation of the two free thiols in reduced Sil1 resulted in a slow migrating species relative to untreated Sil1 (**Figure 2.4D**, lane 6 versus 5) or Sil1 lacking any thiols (**Figure 2.4D**, lane 9). We suggest that the minor Sil1 species migrating between the oxidized and reduced forms, observed when reduced Sil1 was treated with mal-PEG2K (**Figure 2.4D**, lane 6), indicates partial alkylation, wherein only one of the two Sil1 thiols is alkylated (likely a consequence of the steric hindrance for two mal-PEG2K modifications in such close proximity). Consistent with the TNB release observed spectroscopically (**Figure 2.4B**), treatment with mal- PEG2K indicated that BiP transitioned from an oxidized (**Figure 2.4D**, lane 8) to a reduced form (**Figure 2.4D**, lane 11) in the presence of Sil1-C203A-C373A. Importantly, in keeping with the proposed thiol-disulfide exchange reaction, Sil1 concomitantly transitioned from a reduced (**Figure 2.4D**, lane 8) to oxidized (**Figure 2.4D**, lane 11) state. Here Sil1 contains only the two N-terminal cysteines, and these data reflect redox changes in the Sil1 Cys52/Cys57 pair. The oxidation state of BiP-TNB did not change when BiP-TNB was reacted with Sil1 lacking the N-terminal cysteine pair, confirming that the N-terminal cysteines are necessary for efficient BiP-TNB reduction (**Figure 2.4D**, lane 9 and 12). No change in reduced Sil1 mobility was observed when Sil1 was incubated with a cysteine-less BiP (**Figure 2.4D**, lane 7 and 10) demonstrating that Sil1 was not becoming air-oxidized over time.

A transient high molecular weight band was also observed upon incubation of BiP-TNB and Sil1- C203A-C373A (**Figure 2.4D**, asterisk). The molecular weight of this band is consistent with a BiP-Sil1 mixed-disulfide intermediate (**Figure 2.4A**, asterisk), and interestingly the

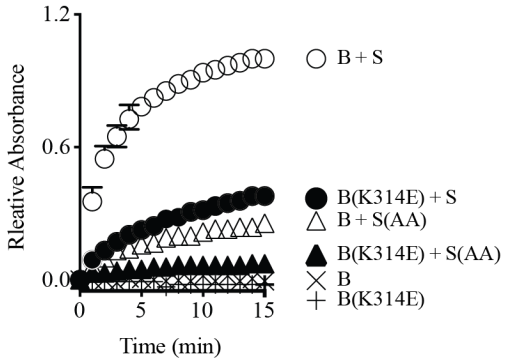

Figure 2.5 Oxidized BiP-K314E is a relatively poor substrate for Sil1. Recombinant wild-type BiP or BiP-K314E were oxidized with DTNB, and the ability of wild-type Sil1 or mutant Sil1 (C52A-C57A) to reduce the oxidized BiP proteins was monitored by following the change in absorbance at 412 nm over time. Data represent the mean values from three independent experiments; error bars depict the range. Equivalent maximal absorbance values (equal amounts of TNB release) were observed when the reductant DTT was added in excess to the oxidized wild-type BiP or BiP-K314E proteins (data not shown), confirming that wild-type BiP and BiP-K314E were both equally oxidized by DTNB.

formation of the band was rapid and readily apparent immediately upon mixing (**Figure 2.4D**, t = 0, lane 8). These data are again consistent with a direct exchange of electrons between oxidized BiP and Sil1. Of note, a minor high molecular weight species was also seen in the BiP prep (**Figure 2.4D**, black circle), which we expect is a BiP-BiP disulfide-bonded dimer. We have observed a disulfide-linked BiP dimer previously in vitro with unknown significance in vivo (Wang & Sevier, 2016).

Intrigued by the potential visualization of the BiP-Sil1 disulfide-bonded intermediate formed during a thiol-disulfide exchange reaction (**Figure 2.4A**, asterisk), we sought to confirm the identity and requirements for formation of this transient species. We repeated the alkylation assay using both wild-type Sil1 and N-terminal Sil1 cysteine mutants. Here we used *N*-ethylmaleimide (NEM) as the alkylating agent, which due to its smaller size will prevent any overlapping migrating species and confounding size shifts associated with the larger mal-

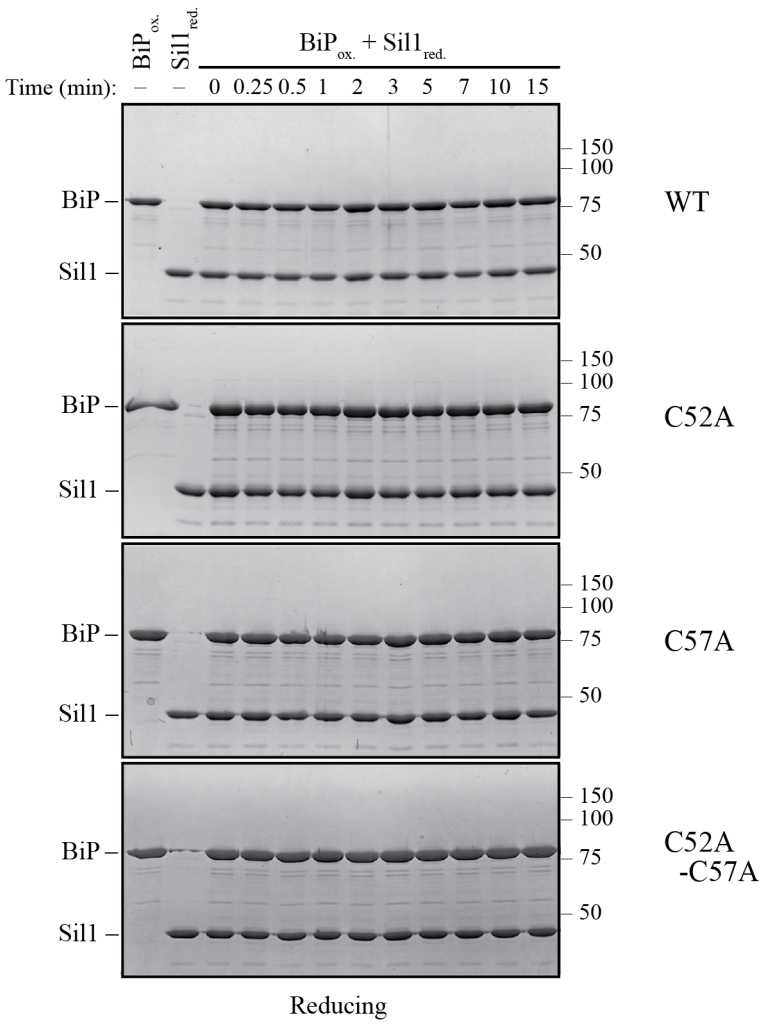

Figure 2.6 High molecular weight protein species are resolved by reducing SDS-PAGE. Samples from Figure 2.2E were treated with BME (5%) prior to electrophoresis, and proteins were visualized with a Coomassie blue stain. The disappearance of the high molecular weight bands present under non-reducing conditions is consistent with the designation of these bands in Figure 2.2E as disulfide-bonded BiP-BiP (filled circle) and BiP-Sil1 (asterisk) species.

PEG2K. As observed with Sil1-C203A-C373A in **Figure 2.4D**, a modest level of a transient high molecular weight species was observed when BiP- TNB was incubated with wild-type Sil1 (**Figure 2.4E**, asterisk). Use of a Sil1 single cysteine mutant (Sil1-C52A or -C57A) as reductant enhanced recovery of the mixed-disulfide species (**Figure 2.4E)**. The stabilization ('trapping') of the BiP-Sil1 intermediate in the absence of a resolving cysteine was expected; with a single

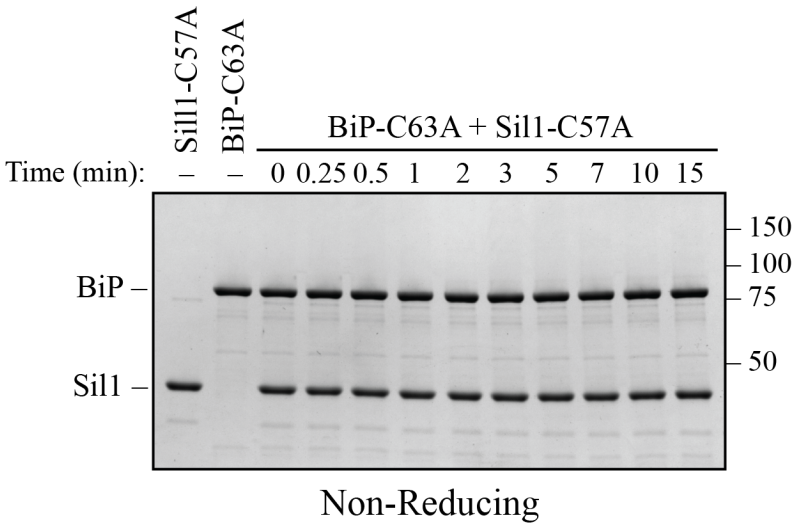

Figure 2.7 BiP's cysteine is required to form the disulfide-bonded species observed with Sil1-C57A. Reduced recombinant Sil1-C57A was mixed with an equal concentration of a cysteine-less BiP protein (BiP-C63A), which was mock treated with DTNB. At the indicated times, sample buffer containing NEM was added to quench any reactive thiols as in Figure 2.2E. Proteins were resolved by non-reducing SDS-PAGE, and the gel was stained with Coomassie blue. In contrast to the strong disulfide-bonded species observed upon mixing Sil1-C57A mutant and wild-type BiP, no high molecular weight bands were observed at any point during the reaction of Sil1-C57A and cysteine-less BiP. These data are consistent with the identification of the strong high molecular weight disulfide-bonded species in Figure 2.2E (denoted with an asterisk) as a BiP-Sil1 mixed-disulfide pair. No high molecular weight species were observed for the BiP-C63A protein reacted with DTNB, consistent with the identification of the band observed with wild-type BiP after treatment with DTNB as a BiP-BiP disulfide bonded species (Figure 2.2E, filled circle).

cysteine, one anticipates the attack and release of TNB (**Figure 2.4B**) but in the absence of a second resolving thiol, the mixed-disulfide intermediate is poorly resolved. All high molecular weight bands were resolved by reducing SDS-PAGE (**Figure 2.6**), confirming that these bands reflect disulfide-bonded species. Use of various BiP and Sil1 cysteine mutants established that these bands reflect the trapping of a BiP-C63–Sil1-C52/C57 intermediate (**Figure 2.7** and **2.8**). The putative BiP-Sil1 disulfide-bonded species was verified also to contain both Sil1 and BiP by immunoblotting (**Figure 2.8**). We attribute the late appearance of a lesser mixed-disulfide species with Sil1-C52A-C57A (that lacks significant reducing activity) to a modest (catalytically

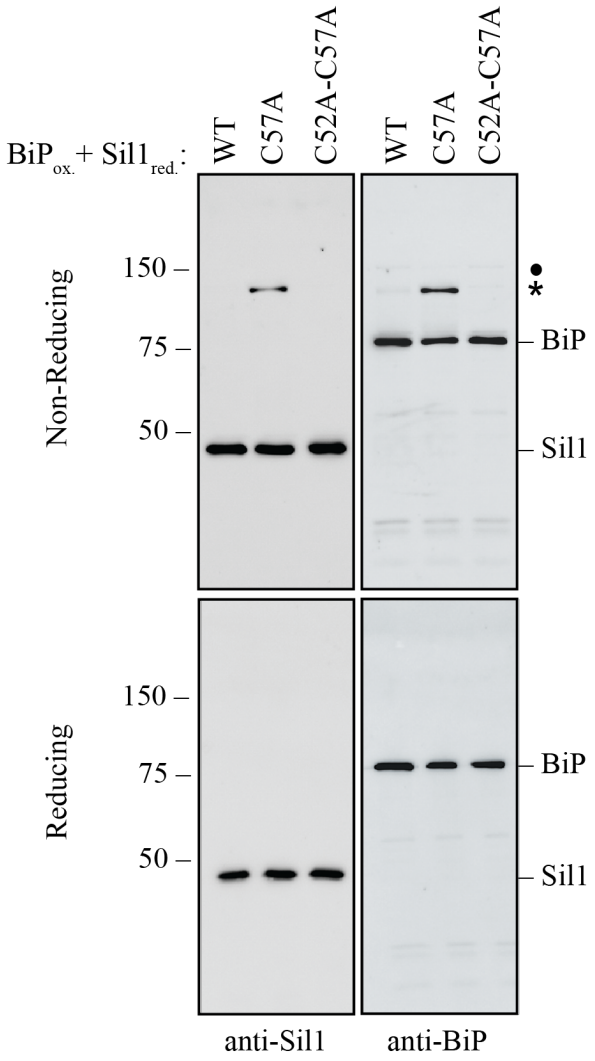

Figure 2.8 High molecular weight species observed under non-reducing conditions (and enhanced when Sil1 contains a single N-terminal cysteine) contain both Sil1 and BiP. Reduced Sil1 (WT), Sil1-C57A, Sil1-C52A-C57A, and BiP-TNB were prepared, and BiP-TNB and the indicated Sil1 proteins were reacted, as in Figure 2.2E. Reactions were quenched 5 min after mixing of the BiP-TNB and Sil1 proteins by the addition of sample buffer containing NEM. Samples were separated by non-reducing or reducing SDS-PAGE; for reducing conditions, BME (5%) was added prior to electrophoresis. Samples were transferred to nitrocellulose, and Sil1 and BiP were detected by immunoblotting with rabbit anti-Sil1 or anti-BiP antibodies. Non-reducing and reducing samples were run on a single gel, and the membrane was cut after transfer prior to the probing with the individual antibodies. Labels indicate disulfide-linked BiP-Sil1 (asterisk) and a weakly detected BiP-BiP dimer (filled circle).

irrelevant) reactivity of the Sil1 armadillo-repeat cysteines with BiP-TNB. Although TNB is a useful experimental proxy for physiological BiP cysteine adduct(s), BiP-TNB is not the substrate for Sil1 in cells. Thus, we sought to determine the reactivity of Sil1 towards a physiologically relevant oxidation adduct. We have shown that BiP is both sulfenylated and glutathionylated in cells (Wang et al., 2014; Wang & Sevier, 2016), and we have established conditions for BiP glutathionylation in vitro (Wang & Sevier, 2016). Building on our prior data, we prepared glutathionylated recombinant BiP by treating reduced BiP with a molar excess of reduced glutathione (GSH) and diamide. We followed the ability of Sil1 to reduce glutathionylated BiP by monitoring the redox state of the BiP cysteine using mal-PEG2K, which will modify BiP thiols uncovered upon glutathione removal. In order to specifically follow the reactivity of the Sil1 N-terminal cysteine pair towards glutathionylated BiP, we made use of the same Sil1 proteins as for **Figure 2.4D**: a Sil1- C203A-C373A mutant (with the N-terminal cysteines; CC) and a cysteine-less Sil1 (lacking the N-terminal cysteines; AA). We observed that Sil1 was able to remove the glutathione adduct from BiP, which was evident in the appearance of the slower migrating reduced BiP species over time (**Figure 2.9**), and that the reduction of the BiP glutathione adduct was dependent on the presence of the Sil1 N-terminal cysteines (**Figure 2.9**). Removal of the glutathione adduct from BiP was coincident with the oxidation of the Sil1 N-terminal cysteines, which was indicated by the appearance of a faster migrating Sil1 species over time (**Figure 2.9**). At present, it remains untested whether sulfenylated BiP is also a substrate for Sil1. We have shown that sulfenylated BiP can condense with GSH to yield a BiP-glutathione adduct (Wang & Sevier, 2016), and we have proposed that glutathionylation of BiP in cells may serve to prevent overoxidation of BiP by peroxide (the transition of a sulfenic acid adduct (-SOH) to irreversible sulfinic (–SO_2H) or sulfonic (–SO_3H) acid adducts)

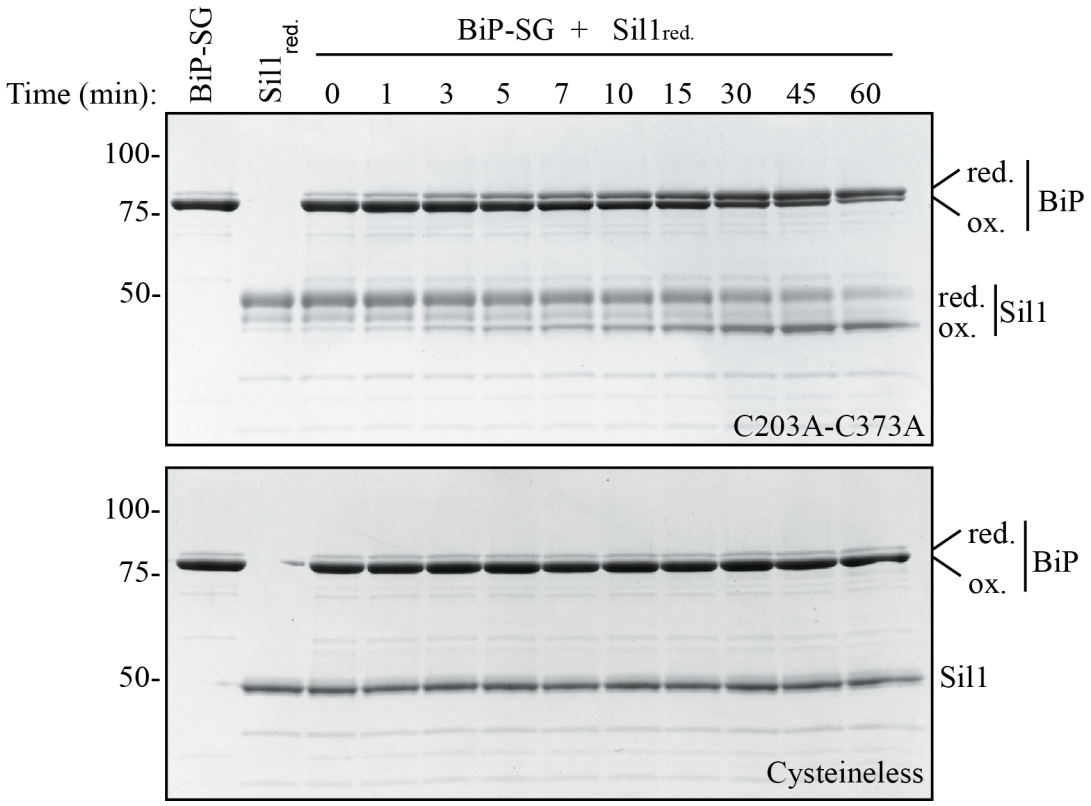

Figure 2.9 Sil1 can reduce glutathionylated BiP. (A) Schematic for formation and reduction of glutathionylated BiP. (B) Glutathionylated BiP was prepared as described in the Materials and Methods. Reduction of glutathionylated BiP by Sil1-C203A-C373A (with the N-terminal cysteines; CC) or a cysteine-less Sil1 (lacking the N-terminal cysteines; AA) was monitored by following the presence or absence of free protein thiols. At the indicated times, reactions were quenched with the addition of the thiol-modifying agent mal-PEG2K, which irreversibly reacts with reduced thiols. Samples were separated by reducing SDS-PAGE and visualized with Coomassie blue. Proteins with free thiols that become modified with mal-PEG2K show a decreased electrophoretic mobility relative to proteins with oxidized cysteines that do not react with mal-PEG2K; the oxidized and reduced forms of each protein are indicated.

(Wang & Sevier, 2016). If Sil1 is unable to reduce a sulfenic acid adduct, we speculate that cells may require both Sil1 and glutathione to prevent irreversible oxidation of BiP.

We initially observed that a yeast strain deficient for Sil1 activity (a *sil1*Δ) showed an enhanced resistance to diamide (**Figure 2.1**), and we reasoned that the observed diamide resistance relates to Sil1's ability to modulate the oxidation state of BiP. Given the clear dependence for recombinant Sil1's reductant activity on its N-terminal Cys52/Cys57 pair, we

expected that the diamide resistance observed for *sil1*Δ cells could be recapitulated also with cells containing a Sil1 mutant lacking the N-terminal cysteines (Sil1-C52A-C57A). In contrast, we observed that a strain possessing a sil1-C52A-C57A allele demonstrated the same sensitivity to diamide as a wild-type strain (**Figure 2.10**). These data suggest that the diamide resistance observed for a *sil1*Δ strain does not depend on Sil1 activity as a reductant, and instead that the diamide resistance observed for a *sil1*Δ strain may be a consequence of the absence of another Sil1 activity, such as a loss of NEF function. However, considering these data (**Figure 2.10**) alongside the diamide resistance phenotypes observed for strains in **Figure 2.1A** and **E**, we suggest a slightly altered interpretation: that the diamide resistance observed for a *sil1*Δ strain does not solely reflect a loss of Sil1 activity as a reductant or as a NEF. We propose that the diamide resistance of a *sil1*Δ strain is a byproduct of both a loss of reductant activity (and increased BiP oxidation) and also a loss of NEF activity (which may also alter BiP activity). We propose that the lack of detectable diamide resistance conferred to cells by a loss of the N-terminal Sil1 cysteines (**Figure 2.10**) could be a consequence of compensatory mechanism activated in the sil1-C52A-C57A strain.

Struck by the potential for Sil1 to impact BiP activity both as a NEF and a reductant, we further explored the relationship between these functions. We observed that the presence of the active-site cysteines does not influence NEF activity. The inviability of a *lhs1*Δ *sil1*Δ strain (ascribed to a loss of NEF function) was rescued by a Sil1 catalytic-cysteine mutant (**Figure 2.11**). Furthermore, both wild- type Sil1 and Sil1-C52A-C57A stimulated ATP turnover by BiP (**Figure 2.11**). In contrast, no activity was observed in either assay for a Sil1-H163E mutant (**Figure 2.11A**, **B**); Sil1-H163E is defective in BiP binding (Yan et al., 2011) and as a consequence is ineffective as a NEF and a reductant (**Figure 2.4B**).

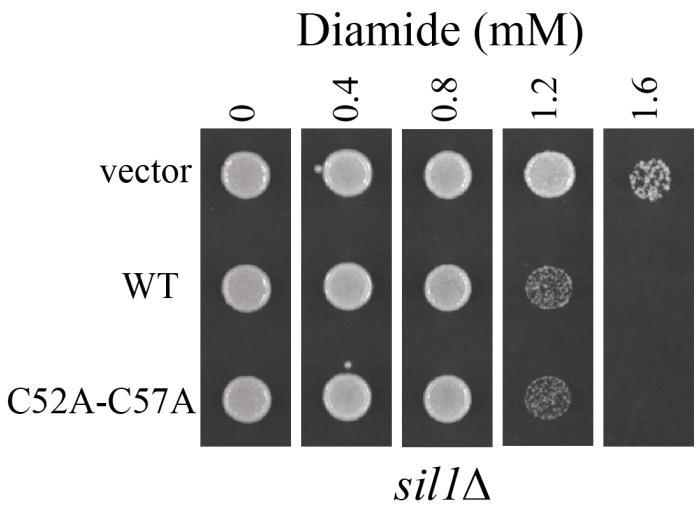

Figure 2.10 A yeast strain expressing a Sil1 mutant that lacks reducing activity (Sil1-C52A-C57A) does not show an increased resistance to diamide. A *sil1*Δ strain (CSY448) transformed with the plasmids pJW7 (*SIL1*), pCS876 (*sil1-C52A-C57A*), or an empty vector was spotted onto SMM plates containing 0–1.6 mM diamide and incubated for 2 d at 30°C.

We have shown previously that recombinant oxidized BiP shows a lower steady-state ATPase rate than reduced BiP (Wang et al., 2014). When Sil1 activity was assessed in the context of modified BiP, we observed that only a Sil1 protein with reducing activity (wild-type Sil1) in combination with a reversible BiP-TNB substrate allowed for measurable BiP ATPase activity (**Figure 2.11C**). We interpret these data to reflect that wild-type Sil1 can reduce a reversible BiP modification to restore BiP ATPase activity; we expect that the restored ATPase activity of reduced BiP is, in turn, stimulated by Sil1 activity as a NEF. We observed that the activity of wild-type Sil1 or a Sil1 cysteine mutant (both functional in their ability to stimulate ATP turnover; **Figure 2.11B**) was insufficient to override the loss of ATPase activity observed with irreversibly oxidized BiP (**Figure 2.11C**, BiP-NEM). Similarly, a Sil1 protein that lacks reducing activity (Sil1-C52A-C57A) was unable to reverse the BiP-TNB adduct and restore measurable ATP hydrolysis (**Figure 2.11C**). In keeping with an importance for BiP-TNB

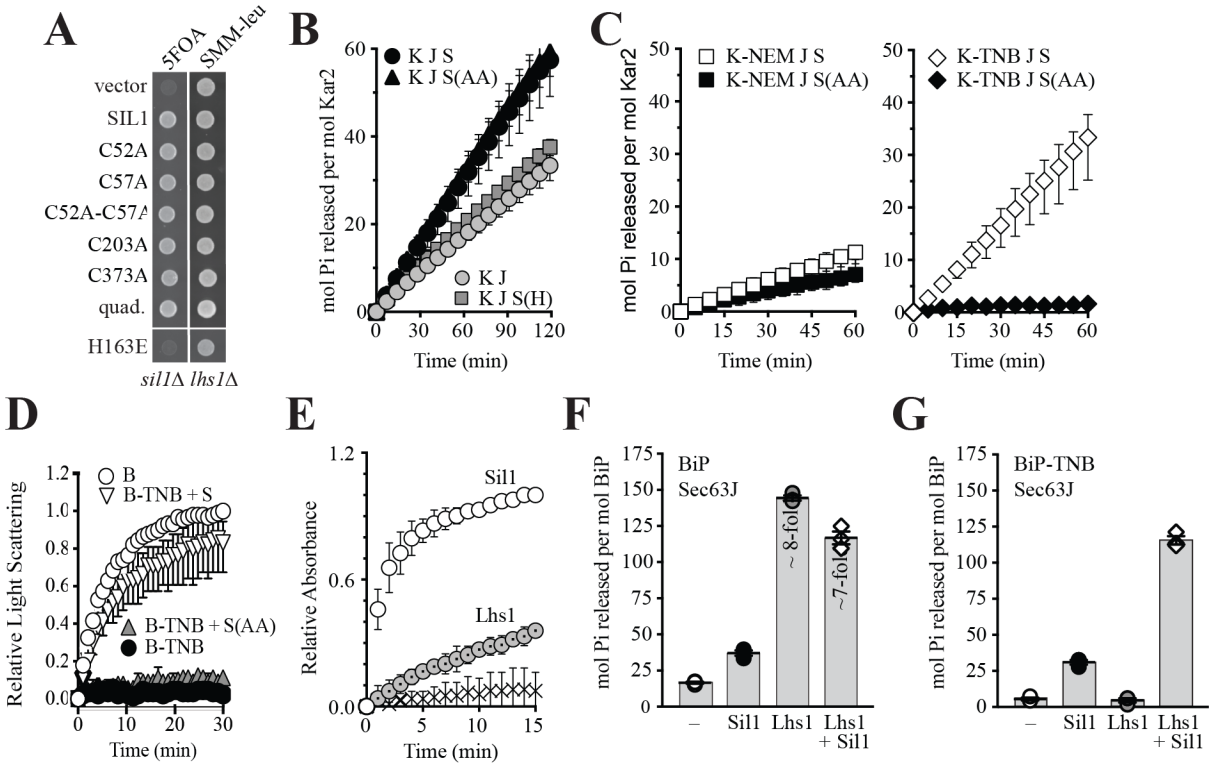

Figure 2.11 Sil1 regulates BiP activity both as a nucleotide exchange factor (NEF) and a reductant. (A) Sil1 cysteine mutants maintain nucleotide exchange activity. A *sil1*Δ *lhs1*Δ strain covered with an *URA3*-marked SIL1 plasmid was transformed with LEU2-marked plasmids encoding the indicated Sil1 proteins. Their ability to substitute for wild-type Sil1 was assessed after counter-selection of the *URA3*-plasmid on 5-FOA. (B) BiP (B) ATPase activity was monitored by following the accumulation of free phosphate in the presence of Sec63J (J) and Sil1 (S), Sil1-C52A-C57A (S(AA)) or Sil1-H163E (S(H)). (C) ATP hydrolysis rates of BiP oxidized with NEM (B-NEM) or DNTB (B-TNB) was monitored in combination with J, S, or S(AA). In B and C, mean values of triplicate experiments are shown; error bars depict the range. (D) Aggregation of denatured rhodanese was assayed by monitoring light scattering (associated with aggregation) over time. Denatured rhodanese was diluted away from denaturant into buffer containing BiP or BiP-TNB that had been pre-incubated in the presence or absence of reduced, recombinant Sil1. Mean values of three independent experiments are shown; error bars depict the range. (E) The accumulation of free phosphate 15 min (left panel) or 30 min (right panel) post-ATP addition was determined for reduced BiP and BiP-TNB incubated with Sil1 (1:1 ratio) and/or Lhs1 (1:0.2 ratio) plus J-protein. Data show the mean rate of phosphate release ± SEM of three independent experiments. (F) Reduction of BiP-TNB by Sil1 or Lhs1 was monitored spectroscopically as in Figure 2.4. Mean values of four independent experiments are shown; error bars depict the range.

reduction in restoring ATPase activity to BiP, a Sil1-H163E mutant (unable to efficiently reduce BiP-TNB; **Figure 2.11B**) was also unable to facilitate an increase in ATP hydrolysis for oxidized BiP (**Figure 2.12A**).

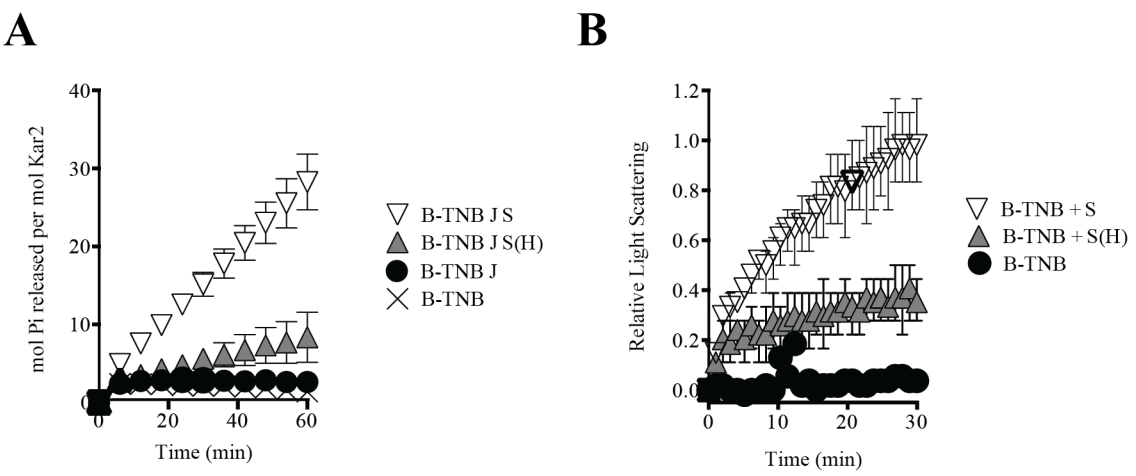

Figure 2.12 Sil1-H163E only modestly reverses the decreased ATPase and increased holdase activities associated with oxidized BiP. (**A**) ATP hydrolysis rates of BiP oxidized with DNTB (B-TNB) were monitored in combination with Sec63J (J) and Sil1 (S) or Sil1-H163E (S(H)). Mean values of duplicate experiments are shown; error bars depict the range. (**B**). Aggregation of denatured rhodanese was assayed as in Figure 2.11D. Denatured rhodanese was diluted away from denaturant into buffer containing BiP-TNB that had been pre-incubated in the presence or absence of reduced, recombinant wild-type Sil1 or Sil1-H163E mutant. Mean values of three independent experiments are shown; error bars depict the range.

The ability of wild-type Sil1 to remove the BiP-TNB adduct and, in turn, stimulate ATPase activity (**Figure 2.11C**), is in keeping with a role for Sil1 activity in reversing and restoring BiP's chaperone function when levels of oxidative stress in the ER subside. Correspondingly, reduction of BiP-TNB by Sil1 reversed the enhanced holdase activity also associated with modified BiP (**Figure 2.11C**). Consistent with our prior reports (Wang et al., 2014), BiP-TNB limited the aggregation of denatured rhodanese relative to unmodified BiP, evident as a decrease in light scattering observed in the presence of BiP- TNB relative to unmodified BiP (**Figure 2.11D**). Reduction of BiP-TNB by wild-type Sil1, but not Sil1- C52A-C57A, resulted in an aggregation profile similar to that observed with unmodified BiP (**Figure 2.11D**). A Sil1-H163E mutant, which shows limited reducing activity (**Figure 2.4B**), behaved similarly to Sil1-C52A-C57A and was unable to markedly reverse the enhanced holdase activity of BiP- TNB (**Figure 2.12B**).

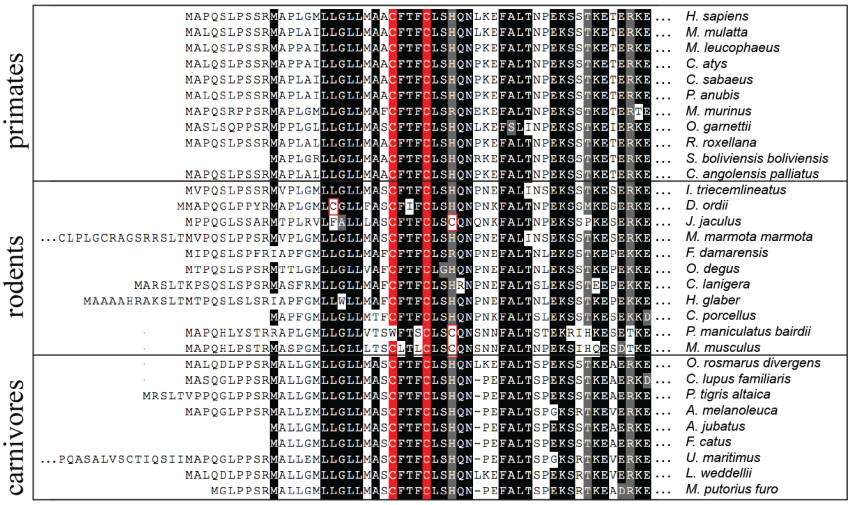

Figure 2.13 Mammalian SIL1 orthologs contain a conserved pair of cysteines within the N-terminal region. An alignment of protein sequences from SIL1 orthologs found in primates, rodents, and carnivores reveals a conserved cysteine pair in the N-terminal region. Sequences are shaded at 90% identity. Cysteines conserved between 90% of the chosen orthologs are highlighted in red; additional cysteine residues are outlined in red.

Given the presence of both Lhs1 and Sil1 within the ER lumen, we sought to determine also how Lhs1 alone and in combination with Sil1 impacts the ATPase activity of oxidized BiP. It has been shown previously that a BiP/J-protein/Sil1 protein mixture shows a lower steady-state ATPase rate relative to a BiP/J-protein/Lhs1 combination (Steel, Fullerton, Tyson, & Stirling, 2004). We observed also that Sil1 only modestly enhanced steady-state BiP ATPase activity relative to Lhs1, which was used at an even lower concentration than Sil1(**Figure 2.11E**). It has been proposed that the enhanced steady-state ATP-hydrolysis with Lhs1 reflects a reciprocal stimulation of Lhs1 ATPase activity by BiP; a difference in the ability of Sil1 and Lhs1 to release nucleotide was not observed under single-turnover conditions (Steel et al., 2004). Focusing on modified BiP, we found that Lhs1 was unable to stimulate the ATPase rate of BiP-TNB, suggesting that Lhs1 is not active as a reductant. Low reducing activity was observed also when TNB release was monitored spectroscopically (**Figure 2.11F**). These data imply that Sil1

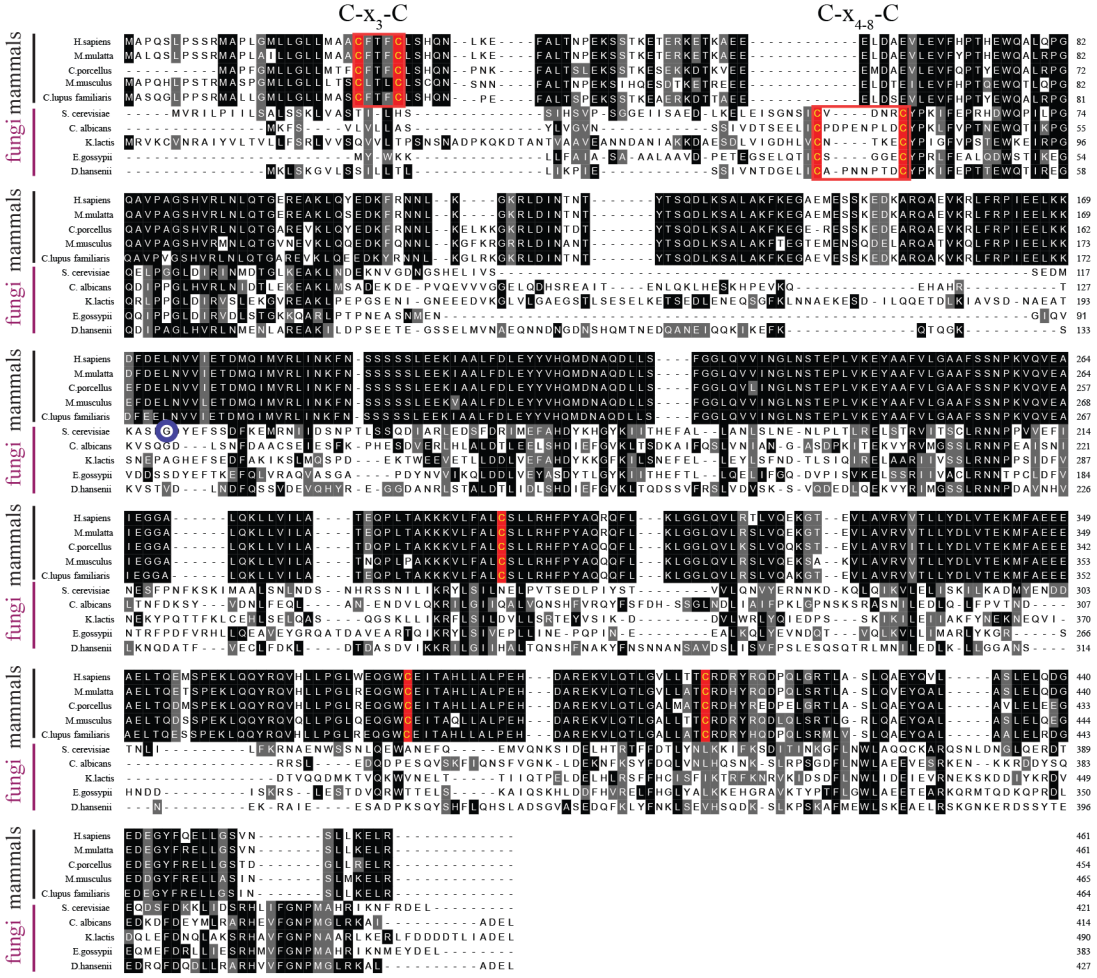

Figure 2.14 Mammalian and fungal proteins contain a conserved N-terminal cysteine pair. Alignment of orthologous Sil1 protein sequences from five mammalian and five fungal species. Protein sequences were aligned using ClustalW (Larkin et al., 2007) and formatted using Multiple Align Show (Stothard, 2000) with a consensus-shading setting of 50% identity (black) or similarity (grey). Cysteines showing a 50% conservation between orthologs are highlighted in red text (instead of black). The N-terminal redox-active cysteine pair identified in *S. cerevisiae* Sil1 and shared between fungal orthologs is boxed in red; conserved N-terminal mammalian cysteines are also boxed in red. A blue circle notes *S. cerevisiae* residue 113, the most N-terminal residue from the Sil1 structure construct Figure 2.2. Note the limited sequence identity observed between the fungal and mammalian Sil1 orthologs, and also among the fungal Sil1 orthologs.

reducing activity is specific to Sil1 and not a common feature of the ER NEFs. Of interest, the low steady-state ATPase rate with modified BiP in the presence of Lhs1 also suggests that

oxidized BiP does not appreciably stimulate Lhs1 ATPase activity. When ATPase activity of BiP- TNB was measured in the presence of both Lhs1 and Sil1, a relatively robust steady-state ATPase rate was observed (**Figure 2.11E**, right panel), which we attribute to the removal of the BiP-TNB adduct by Sil1 and the enhanced rate of ATP-turnover for reduced BiP that is mediated by Lhs1. These data imply a potential advantage for the presence of both Sil1 and Lhs1 in the ER following oxidative stress. Of unclear significance, we also observed a modest decrease in the overall ATPase rate when Sil1 was added to an unmodified-BiP/J/Lhs1 mixture (**Figure 4.11E**, right panel).

Human SIL1 shows functional and structural conservation with yeast Sil1; however, they share limited primary sequence homology (**Figure 2.14**). This is in contrast to mammalian and yeast BiP, which exhibit a high degree of sequence conservation (**Figure 2.15**). Yet strikingly, the N-terminal domain of human SIL1 contains a pair of cysteine residues, which is highly conserved between the mammalian SIL1 orthologs (**Figure 2.13**). The location and spacing of these cysteines in human SIL1 is similar to location and spacing of the redox-active cysteines in yeast Sil1 (**Figure 2.14**). Cysteine is a rare amino acid in proteins, and cysteine conservation likely speaks to an important structural or functional role for these mammalian SIL1 cysteines (Marino & Gladyshev, 2010). While it remains to be determined whether human SIL1 is redox active, it is tempting to speculate that mammalian SIL1 facilitates reduction of the intramolecular disulfide described for mammalian BiP that forms in the presence of peroxide (Wei et al., 2012).

Mutations in human SIL1 are associated with Marinesco-Sjögren syndrome (MSS), an autosomal recessive disorder arising in early childhood that manifests in musculoskeletal defects, cognitive delay, and early onset cataracts (Senderek et al., 2005; Anttonen et al., 2005; Krieger et al., 2013). Recently, a new role for SIL1 as a modifier of the neurodegenerative disorder ALS

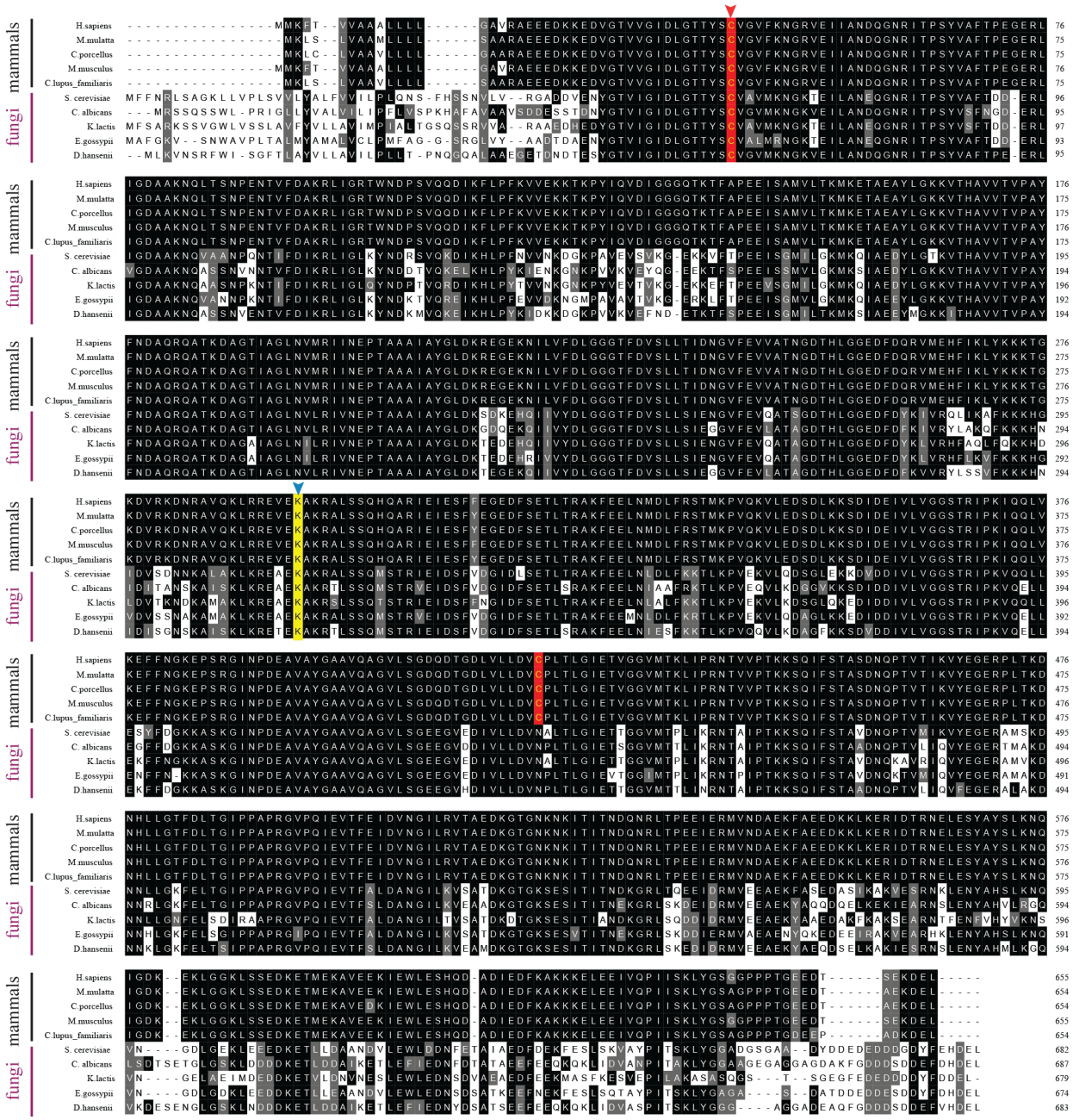

Figure 2.15 Sequence alignment of BiP orthologs. Alignment of BiP ortholog protein sequences from five mammalian and five fungal species. Sil1 proteins from the same species are displayed in Figure 2.14. Protein sequences were aligned and formatted as described for Figure 2.14. In contrast to the low degree of sequence conservation observed between Sil1 orthologs, a high degree of sequence conservation is seen among the BiP orthologs. A red arrow highlights the conserved redox active cysteine within the BiP ATPase domain. A blue arrow and yellow background indicate the position of lysine-314 in yeast BiP, which is conserved across species.

has also been described (de Keyzer, Steel, Hale, Humphries, & Stirling, 2009). It has been assumed that MSS symptoms, and any impact of SIL1 activity in ALS progression, stem from a loss of SIL1 NEF activity and corresponding defects in protein folding and/or secretion. Yet a role for yeast Sil1 as a reductant in the ER implies a potentially important function for redox signaling in disease pathology. A majority of MSS alleles are truncations and deletions (Goto et al., 2014; Ezgu et al., 2014; Krieger et al., 2013), which will impact reducing activity while also destroying NEF function. It will be exciting to explore if and/or how a loss of SIL1 activity as a reductant impacts disease progression.

Currently it is unclear how Sil1 is maintained in a reduced state to facilitate BiP reduction in cells. We expect that a further understanding of the proteins and/or small molecules that donate electrons to maintain Sil1 in a reduced state (allow for Sil1 reducing activity) will provide increased insight into redox signaling within the ER. We speculate that the identification of physiological reductants for Sil1 may also point toward new candidate genetic mutations that account for the onset of disease in the 50% of MSS patients without any SIL1 defect and no characterized genetic cause.

MATERIALS AND METHODS

Plasmid and strain construction

Plasmids are listed in **Table 2.1**. Yeast expression plasmids are derived from the pRS vector series (Sikorski & Hieter, 1989). Plasmids pJW7 and pHS116 contain SIL1 with 720 bp of 5' and 621 bp of 3' untranslated sequence. SIL1 and its flanking sequences were amplified from yeast genomic DNA with engineered restriction sites, and the amplified DNA was digested and ligated into compatible restriction sites in the pRS polylinker. To construct pCS637 (Sil1-His_6), sequence coding for a start methionine and Sil1 residues 20–407 was cloned into pET-21b, generating an in-frame fusion with sequence coding for a C-terminal His_6-tag. Plasmid pKP52 (GST-Sil1) was made by ligating sequence coding for Sil1 residues 22–406 into pGEX-5X-3. QuikChange mutagenesis (Agilent Technologies) was performed to generate amino acid substitution mutants using plasmid pCS757, pCS681, pJW7, pHS116, pCS817, or pCS637 as a template. All mutations were confirmed by sequencing.

Yeast strains used in this study are listed in **Table 2.2** and are of the S288C background. Yeast containing genomic deletions for *SIL1* and *LHS1* were obtained from the *Saccharomyces cerevisiae* genome deletion collection (Brachmann et al., 1998), and deletions were verified by genomic PCR. These yeast strains were backcrossed against *GAL2 ura3-52 leu2-3,112* strains from the Sevier lab collection to generate CSY448 (*sil1*Δ), CSY449 (*sil1*Δ *kar2-C63A*), and CSY581 (*lhs1*Δ). CSY594 and CSY595 were made by crossing CSY214 (*kar2*Δ) with CSY448 and CSY581, respectively. Strains CSY612, CSY622, CSY646, and CSY689 were generated by transformation of CSY214 with pKP37, pCS757, pCS878, or pKP97 followed by counter-selection of pCS623 on plates containing 5-fluoroorotic acid (5-FOA). Similarly, CSY625 was

Table 2.1. Plasmids

Plasmid	Description	Marker	Source
pCS623	*KAR2*	*CEN*, *LEU2*	(Wang, et al., 2014)
pCS757	*KAR2-FLAG*	*CEN*, *LEU2*	(Wang, et al., 2014)
pCS878	*kar2-K314E-FLAG*	*CEN*, *LEU2*	This study
pCS452	P_{GAL1}*-ERO1*-myc*	*CEN*, *URA3*	(Sevier, et al., 2007)
pCS681	*KAR2*	*CEN*, *LEU2*	(Wang, et al., 2014)
pCS685	*kar2-C63A*	*CEN*, *LEU2*	(Wang, et al., 2014)
pKP37	*kar2-K314E*	*CEN*, *LEU2*	This study
pKP97	*kar2-C63A-K314E*	*CEN*, *LEU2*	This study
pJW7	*SIL1*	*CEN*, *URA3*	This study
pCS876	*sil1-C52A-C57A*	*CEN*, *URA3*	This study
pHS116	*SIL1*	*CEN*, *LEU2*	This study
pKS20	*sil1-C52A*	*CEN*, *LEU2*	This study
pKS21	*sil1-C57A*	*CEN*, *LEU2*	This study
pKS24	*sil1-C52A-C57A*	*CEN*, *LEU2*	This study
pKS23	*sil1-C203A*	*CEN*, *LEU2*	This study
pKS22	*sil1-C373A*	*CEN*, *LEU2*	This study
pCS923	*sil1-C52A-C57A-C203A-C373A*	*CEN*, *LEU2*	This study
pCS925	*sil1-H163E*	*CEN*, *LEU2*	This study
pCS817	His_6*-kar2-(42-682)*	KAN	(Wang, et al., 2014)
pCS818	His_6*-kar2-(42-682)-C63A*	KAN	(Wang, et al., 2014)
pKP85	His_6*-kar2-(42-682)-K314#*	KAN	This study
pCS637	*Sil1-(20-407)-*His_6	AMP	This study
pCS870	*Sil1-(20-407)-C52A-*His_6	AMP	This study
pCS871	*Sil1-(20-407)-C57A-*His_6	AMP	This study
pCS875	*Sil1-(20-407)-H163E-*His_6	AMP	This study
pCS877	*Sil1-(20-407)-C52A-C57A-*His_6	AMP	This study
pCS948	*Sil1-(20-407)-C203A-C373A-*His_6	AMP	This study
pCS895	*Sil1-(20-407)-C52A-C57A-C203A-C373A-*His_6	AMP	This study
pKP52	*GST-sil1-(22-406)*	AMP	This study
pHS130	His_6*-lhs1-(21-877)-StrepII*	KAN	(Xu et al., 2016)
pCS675	*GST-sec63J-(121-221)*	AMP	(Wang, et al., 2014)

Table 2.2 Yeast strains

Strain	Genotype	Source
CSY5	*MATa GAL2 ura3-52 leu2-3,112*	(Wang, et al., 2014)
CSY214	*MATa GAL2 ura3-52 leu2-3,112 kar2Δ::KanMX[pCS623]*	(Wang, et al., 2014)
CYS275	*MATa GAL2 ura3-52 leu2-3,112 kar2-C63A*	(Wang, et al., 2014)
CSY278	*MATa GAL2 ura3-52 leu2-3,112 kar2-C63A can1::P_{GAL1}-ERO1*-myc*	(Wang, et al., 2014)
CSY289	*MATa GAL2 ura3-52 leu2-3,112 kar2Δ::KanMX* [pCS681]	(Wang, et al., 2014)
CSY290	*MATa GAL2 ura3-52 leu2-3,112 kar2Δ::KanMX* [pCS685]	(Wang, et al., 2014)
CSY612	*MATa GAL2 ura3-52 leu2-3,112 kar2Δ::KanMX* [pKP37]	This study
CSY689	*MATa GAL2 ura3-52 leu2-3,112 kar2Δ::KanMX* [pKP97]	This study
CSY622	*MATa GAL2 ura3-52 leu2-3,112 kar2Δ::KanMX* [pCS757]	This study
CSY646	*MATa GAL2 ura3-52 leu2-3,112 kar2Δ::KanMX* [pCS878]	This study
CS7448	*MATalpha GAL2 ura3 leu2 sil1Δ::KanMX*	This study
CSY449	*MATalpha GAL2 ura3 leu2 lys2Δ0 kar2-C63A sil1Δ::KanMX*	This study
CSY581	*MATalpha GAL2 ura3 leu2 lhs1Δ::KanMX*	This study
CSY594	*MATa GAL2 ura3 leu2 sil1Δ::KanMX kar2Δ::KanMX*[pCS623]	This study
CSY595	*MATa GAL2 ura3 leu2 lhs1Δ::KanMX kar2Δ::KanMX*[pCS623]	This study
CSY625	*MATa GAL2 ura3 leu2 sil1Δ::KanMX kar2Δ::KanMX*[pCS757]	This study
CSY647	*MATa GAL2 ura3 leu2 sil1Δ::KanMX lhs1Δ::KanMX*[pJW7]	This study

made by transformation of pCS757 into CSY594, and counter-selection of pCS623. Note that CSY622 is genetically equivalent to CSY318 described in Wang and Sevier (2016). To generate CSY647, a heterozygous *SIL1/sil1*Δ *LHS1/lhs1*Δ diploid strain was transformed with pJW7, and the transformants were sporulated and tetrads were dissected. Spores containing *sil1*Δ *lhs1*Δ and pJW7 were unable to grow on medium containing 5-FOA.

Yeast growth conditions

Cultures were grown in rich medium (1% Bacto-yeast extract and 2% Bacto-peptone containing 2% dextrose; YPD) or minimal medium (0.67% nitrogen base without amino acids supplemented with 16 amino acids not including cysteine) containing 2% dextrose (SMM), 2% galactose (SMM Gal) or 2% raffinose (SMM Raf). Uracil or leucine supplements were removed from minimal media to select for plasmids as needed.

BiP mutant screen

Mutations in the BiP gene (*KAR2*) were generated by error-prone PCR using the methods described previously (Sevier & Kaiser, 2006) with some modifications. The entire BiP gene was amplified from pCS681 with Taq DNA Polymerase (New England Biolabs) in the presence of 0.3 mM $MnCl_2$ and an unbalanced dNTP ratio. PCR products and a gapped pRS315 vector (Sikorski & Hieter, 1989) were transformed into CSY278 (*kar2-C63A can1::PGAL-ERO1**), and yeast containing gap- repaired plasmids were isolated by selection for Leu+ transformants. ER-stress resistant transform- ants were identified by the ability to grow on galactose plates at 37˚C.

Protein expression and purification

His_6-tagged BiP proteins (Kar2 residues 42–682) and GST-Sec63J protein were purified as previously described (Wang et al., 2014). GST-Sil1 protein (pKP52) was purified from bacteria as described for GST-Sec63J (Wang et al., 2014) with some adjustments. Induction of GST-Sil1 was carried out at 16˚C overnight, and column washes were limited to 20 column volumes (cv) of PBS with 2 mM EDTA and 10 cv of PBS with 2 mM EDTA, 1 M KCl and 0.1% Triton-X-100. His6/StrepII-tagged Lhs1 was expressed and purified as described previously (Xu,

Marsh, & Sevier, 2016), except that the initial 10 cv wash with lysis buffer was not performed, and the concentration of imidazole in the elution buffer was increased to 50 mM final.

To purify His_6-tagged Sil1, BL21 (DE3) cells containing the appropriate pET-derived plasmid were grown overnight at 37˚C to saturation in Luria-Bertani (LB) medium with 100 mg/mL ampicillin. Cells were diluted 1:200 in LB with fresh ampicillin, and cells were grown at 37˚C for 3–5 hr (until an OD_{600} between 0.5 and 1.0 was reached). Cultures were shifted to 18˚C, and Sil1 expression was induced with a final concentration of 0.2 mM isopropyl-b-D-thiogalactopyranoside (IPTG). Cells were harvested 16–20 hr post-induction, and cell pellets were frozen at -80˚C. Pellets were solubilized in 25 mL of Sil1 lysis buffer (50 mM Na_2HPO_4 pH 7.4, 500 mM NaCl, 10 mM imidazole, 10% glycerol, 1% Triton X-100) plus one EDTA-free protease inhibitor tablet (Pierce) per 1 L of culture, and cells were lysed by treatment with lysozyme followed by sonication. Insoluble material was removed by centrifugation at 23,700 g for 20 min at 4˚C. Soluble material was loaded onto a HiTrap chelating column (GE Healthcare) charged with nickel. The column was washed with 100 cv of Sil1 wash buffer (50 mM Na_2HPO_4 pH 7.4, 500 mM NaCl, 20 mM imidazole, 10% glycerol), and Sil1 protein was eluted with wash buffer containing a final concentration of 0.3 M imidazole. Protein was exchanged into PBS with 10% glycerol using a PD-10 column (GE Healthcare) and concentrated to 10–30 mg/ mL using a vivaspin-15 (GE Healthcare) or an Ultra-4-centrifugal filter (Amicon). Purified proteins were flash frozen in liquid nitrogen and stored at -80˚C. Concentrations were determined by BCA protein assay (Thermo Fisher Scientific) using bovine serum albumin as a standard.

In vitro BiP activity assays

Sil1 reducing activity was measured using recombinant BiP (His_6-BiP) oxidized with DTNB [5,5'- dithio-bis(2-nitrobenzoic acid)] as the substrate (BiP-TNB). Recombinant His_6-BiP, Sil1-His_6, or His_6/ StrepII-Lhs1 were each diluted to 100 mM in the same buffers used for long-term storage of these proteins at -80˚C. To oxidize BiP, a 3–10-fold molar excess of DTNB was added, and samples were incubated for 1–2 hr at room temperature. To reduce Sil1 and Lhs1, proteins were incubated for 1–2 hr at room temperature in the presence of a 10-fold or greater molar excess of DTT. Unreacted DTNB and DTT were removed and buffers were exchanged using NAP-5 columns (GE Healthcare) equilibrated with TNE (10 mM Tris-HCl, pH 7.4, 50 mM NaCl, 1 mM EDTA). Catalyzed release of the TNB-adduct from oxidized BiP was measured by following the change in absorbance at 412 nm with a Beckman Coulter DU730 UV/Vis spectrophotometer. Oxidized BiP (5 mM) was incubated with 5 mM reduced Sil1 or Lhs1 in TNE, and 10 s readings were collected over 15 min. For experiments using reduced glutathione (GSH) as the reductant, oxidized BiP (5 mM) was mixed with 5–500 mM GSH. For samples containing no additional reductant (**Figure 4B,C**, X symbol, or **Figure 5**, + symbol), a DTT mixture equivalent to that used to reduce Sil1 was passed over a NAP-5 column to control for any potential DTT carryover. The initial absorbance for each reaction was set to zero. Data were normalized to a maximal value of 1.0 for wild-type Sil1 after 15 min. Graphs depict the mean normalized values from a minimum of three independent replicates. Error bars depict the range.

To follow the redox state of BiP and Sil1, an equimolar mixture of oxidized BiP and reduced Sil1 (5–20 mM each) was prepared in TNE. At the indicated time, reactions were quenched with an equal volume of buffer containing 100 mM Tris-HCl, pH 6.8, 4% SDS, 40%

glycerol, 0.1% bromophenol blue and a 10-fold molar excess of *N*-ethylmaleimide (NEM), relative to the sample cysteine content. Alternatively, samples were quenched with an equal volume of 80 mM HEPES, pH 7.4, 4.8 M urea, 0.8% SDS, 20% glycerol containing a 10-fold molar excess of a 2 kDa maleimide-PEG (mal-PEG2K; Laysan Bio Inc.). Samples were incubated for 30 min at room temperature, and mal-PEG2K samples were quenched with a molar excess of free cysteine. Proteins were separated by non-reducing SDS- PAGE and visualized with a Coomassie blue stain. Samples run under reducing SDS-PAGE were supplemented with BME (5% final) prior to electrophoresis. Data shown represent a minimum of two independent assays. For detection of BiP and Sil1 by Western blotting, polyclonal antibodies raised against recombinant BiP (Kar2-(60-688)-His_6) or recombinant Sil1 (Sil1-(20-407)-His_6) were used. Anti- serum to yeast BiP (RRID:AB_2636950) or Sil1 (RRID:AB_2636949) were obtained by injection of recombinant protein into rabbits by Covance Inc. (Denver, PA).

Glutathionylated BiP was prepared by reacting 50 mM BiP with 1.5 mM GSH and 750 mM diamide at 30˚C for 1 hr. Unreacted small molecules were removed using a NAP-5 column equilibrated with de-glutathionylation assay buffer (10 mM Tris-HCl, pH 8.0, 50 mM NaCl, 1 mM EDTA). For reduction assays, 5 mM glutathionylated BiP was reacted at 30˚C with 5 mM reduced Sil1 in de-glutathionylation assay buffer. At the indicated times, samples were quenched with an equal volume of 80 mM HEPES, pH 7.4, 4.8 M urea, 0.8% SDS, 20% glycerol containing a 10-fold molar excess of mal-PEG2K. After 30 min, BME was added to 5% final, and proteins were separated by reducing SDS-PAGE and visualized with a Coomassie blue stain.

ATP hydrolysis was monitored using an EnzChek Phosphate Assay Kit (Thermo Fisher Scientific) with user-supplied buffer. BiP (1 mM), GST-Sec63J (2 mM), and Sil1 (0.5 mM) were incubated in ATPase buffer (50 mM Tris-HCl, pH 7.4, 50 mM KCl, 5 mM $MgCl_2$, 1 mM DTT)

with 200 mM 2-amino- 6-mercapto-7-methylpurine riboside (MESG) and 0.2 U/mL purine nucleoside phosphorylase (PNP). Sample volumes were adjusted for a 96-well plate format with a final reaction volume of 200 mL. Approximately 0.3% glycerol final was also present in each reaction due to carryover from the BiP preparation. Prior to the assay, Sil1 proteins were exchanged from phosphate buffer into 2X ATPase buffer using a NAP-5 column. Reactions were initiated with the addition of 5 mM ATP final, and phosphate release was monitored at 360 nm for 1 hour with a BioTek Synergy 2 plate reader. For ATPase assays using oxidized BiP, His_6-BiP (100 mM) was reacted for 2 hours with a 10-fold excess of DTNB or a 50-fold excess of NEM in 10 mM Tris-HCl, pH 7.4, 50 mM NaCl, 10% glycerol. Sil1 was reduced as described above, and both BiP and Sil1 proteins were exchanged into 2X ATPase buffer without DTT using a NAP-5 column. Oxidized BiP (1.3 mM) was pre-incubated for 1 hour with GST- Sec63J (2.6 mM), Sil1 (1.3 mM), and/or Lhs1 (0.3 mM) in a final volume of 150 mL ATPase buffer lacking DTT and containing 200 mM MESG and 0.2 U/mL PNP. Reactions were initiated with 50 mL of 20 mM ATP. Absorbance values were converted to phosphate concentrations using a phosphate standard curve. Figures show the mean phosphate turnover from a minimum of two independent experiments. Error bars depict the range.

Denatured rhodanese was prepared as described previously (Wang et al., 2014), except prior to the assay, rhodanese was exchanged into denaturing buffer lacking DTT using a P6 spin column (Bio-Rad). His_6-BiP (68 mM) was oxidized with a 30-fold excess of DTNB for 1–2 hr at room temperature, and Sil1 was reduced as described above. Each protein was exchanged into rhodanese assay buffer (20 mM HEPES-KOH, pH 7.4, 50 mM KCl) using a NAP-5 column. BiP (2 mM) and Sil1 (4 mM) were pre-incubated in rhodanese assay buffer for 1 hr at room temperature in a 96-well plate (191 mL volume), at which time 5 mM $MgCl_2$ and 1 mM ATP

were added and the assay was started with the addition of 1 mM denatured rhodanese. Aggregation was monitored by following the scattering of light at 300 nm over time with a BioTek Synergy 2 plate reader. The initial timepoints were adjusted to 0 for each sample. All data were normalized to the maximal light scattering at 30 min that was observed with mock-treated BiP (**Figure 2.11D**) or BiP-TNB treated with Sil1 (**Figure 2.12B**) (set to 1.0). Data represent the mean and error bars show the range for three independent experiments.

To assess binding of recombinant BiP and Sil1, GST-Sil1 (10 mg) was incubated with 10 ml glutathione-agarose beads (Gold Biotechnology) in a total volume of 100 mL binding buffer (20 mM HEPES- KOH, pH 7.4, 100 mM KCl, 2 mM $MgCl_2$, 0.1% Igepal CA-630, 2% glycerol, 1 mM DTT, 1 mM pepstatin A). Samples were rotated for 1 hr at 4˚C, and beads were collected by centrifugation at 500 g for 1 min. Beads were washed three times with 200 mL of binding buffer to remove unbound proteins, and washed beads were suspended in a final volume of 100 mL binding buffer. Wild-type or mutant His_6-BiP (10 mg) was added to the beads, and samples were rotated at 4˚C for 1 hr. Beads were pelleted and washed three times with 200 mL of binding buffer. Bound proteins were solubilized in 20 mL of 2X sample buffer (100 mM Tris-HCl, pH 6.8, 4% SDS, 40% glycerol, and 0.1% bromophenol blue) containing 5% BME. Samples were resolved on a SDS-acrylamide gel and visualized with a Coomassie blue stain. Data shown represent a result observed in more than three independent assays.

Biotin-switch assay

CSY622 and CSY625 transformed with pRS316 or pCS452 were grown to late-log phase overnight at 30˚C in SMM Raf. The following morning, cells were diluted into SMM Gal, and cells were grown for 5 hours at 30˚C until harvest by centrifugation. Alternatively, CSY622 and

CSY646 transformed with pRS316 or pCS452 were collected after 6 hours of growth in SMM Gal at 30˚C. The biotin-switch assay was performed as previously described, using BME as the reductant (Wang et al., 2014). The time-course assay was carried out as described in Wang and Sevier (2016). In brief, CSY622 or CSY625 were grown to mid-log phase in SMM at 30˚C and were treated with 5 mM diamide for 15 min. Diamide-containing medium was removed by filtration, and cells were suspended in SMM containing 20 mg/mL cycloheximide. Cells were returned to 30˚C until the time of harvest. BiP-FLAG was immunoisolated from cell lysates using anti-FLAG affinity resin, which was a mixture of five parts anti- FLAG affinity resin (RRID:AB_10063035) plus one part anti-FLAG EZview anti-FLAG affinity resin (RRID:AB_2616449). Immunoblots were imaged and quantitated using a Bio-Rad ChemiDoc MP system and associated Image Lab software (RRID:SCR_014210). Biotin-labeled BiP was detected using a streptavidin-Alexa Fluor 647 conjugate (RRID:AB_2336066). BiP was visualized with a rabbit anti- BiP (Kar2) serum (RRID:AB_2636950) and a goat anti-rabbit IgG secondary antibody conjugated to an Alexa Fluor 488 (RRID:AB_2535792). Immunoblots shown are representative images, which are typical of the results obtained from a minimum of two independent experiments.

REFERENCES

Anttonen, A. K., Mahjneh, I., Hämäläinen, R. H., Lagier-Tourenne, C., Kopra, O., Waris, L. et al. (2005). The gene disrupted in Marinesco-Sjögren syndrome encodes SIL1, an HSPA5 cochaperone. *Nat Genet*, *37*(12), 1309-1311.

Brachmann, C. B., Davies, A., Cost, G. J., Caputo, E., Li, J., Hieter, P. et al. (1998). Designer deletion strains derived from Saccharomyces cerevisiae S288C: a useful set of strains and plasmids for PCR-mediated gene disruption and other applications. *Yeast*, *14*(2), 115-132.

Bulleid, N. J., & Ellgaard, L. (2011). Multiple ways to make disulfides. *Trends Biochem Sci*, *36*(9), 485-492.

de Keyzer, J., Steel, G. J., Hale, S. J., Humphries, D., & Stirling, C. J. (2009). Nucleotide binding by Lhs1p is essential for its nucleotide exchange activity and for function in vivo. *J Biol Chem*, *284*(46), 31564-31571.

Depuydt, M., Leonard, S. E., Vertommen, D., Denoncin, K., Morsomme, P., Wahni, K. et al. (2009). A periplasmic reducing system protects single cysteine residues from oxidation. *Science*, *326*(5956), 1109-1111.

Ezgu, F., Krejci, P., Li, S., de Sousa, C., Graham, J. M., Hansmann, I. et al. (2014). Phenotype-genotype correlations in patients with Marinesco-Sjögren syndrome. *Clin Genet*, *86*(1), 74-84.

Goto, M., Okada, M., Komaki, H., Sugai, K., Sasaki, M., Noguchi, S. et al. (2014). A nationwide survey on Marinesco-Sjögren syndrome in Japan. *Orphanet J Rare Dis*, *9*, 58.

Gross, E., Sevier, C. S., Vala, A., Kaiser, C. A., & Fass, D. (2002). A new FAD-binding fold and intersubunit disulfide shuttle in the thiol oxidase Erv2p. *Nat Struct Biol*, *9*(1), 61-67.

Kakihana, T., Nagata, K., & Sitia, R. (2012). Peroxides and peroxidases in the endoplasmic reticulum: integrating redox homeostasis and oxidative folding. *Antioxid Redox Signal*, *16*(8), 763-771.

Krieger, M., Roos, A., Stendel, C., Claeys, K. G., Sonmez, F. M., Baudis, M. et al. (2013). SIL1 mutations and clinical spectrum in patients with Marinesco-Sjogren syndrome. *Brain*, *136*(Pt 12), 3634-3644.

Larkin, M. A., Blackshields, G., Brown, N. P., Chenna, R., McGettigan, P. A., McWilliam, H. et al. (2007). Clustal W and Clustal X version 2.0. *Bioinformatics*, *23*(21), 2947-2948.

Lu, J., & Holmgren, A. (2014). The thioredoxin superfamily in oxidative protein folding. *Antioxid Redox Signal*, *21*(3), 457-470.

Marino, S. M., & Gladyshev, V. N. (2010). Cysteine function governs its conservation and degeneration and restricts its utilization on protein surfaces. *J Mol Biol*, *404*(5), 902-916.

Senderek, J., Krieger, M., Stendel, C., Bergmann, C., Moser, M., Breitbach-Faller, N. et al. (2005). Mutations in SIL1 cause Marinesco-Sjögren syndrome, a cerebellar ataxia with cataract and myopathy. *Nat Genet*, *37*(12), 1312-1314.

Sevier, C. S., & Kaiser, C. A. (2006). Disulfide transfer between two conserved cysteine pairs imparts selectivity to protein oxidation by Ero1. *Mol Biol Cell*, *17*(5), 2256-2266.

Sevier, C. S., Qu, H., Heldman, N., Gross, E., Fass, D., & Kaiser, C. A. (2007). Modulation of cellular disulfide-bond formation and the ER redox environment by feedback regulation of Ero1. *Cell*, *129*(2), 333-344.

Sikorski, R. S., & Hieter, P. (1989). A system of shuttle vectors and yeast host strains designed for efficient manipulation of DNA in Saccharomyces cerevisiae. *Genetics*, *122*(1), 19-27.

Steel, G. J., Fullerton, D. M., Tyson, J. R., & Stirling, C. J. (2004). Coordinated activation of Hsp70 chaperones. *Science*, *303*(5654), 98-101.

Stothard, P. (2000). The sequence manipulation suite: JavaScript programs for analyzing and formatting protein and DNA sequences. *Biotechniques*, *28*(6), 1102, 1104.

Tyson, J. R., & Stirling, C. J. (2000). LHS1 and SIL1 provide a lumenal function that is essential for protein translocation into the endoplasmic reticulum. *EMBO J*, *19*(23), 6440-6452.

Wang, J., Pareja, K. A., Kaiser, C. A., & Sevier, C. S. (2014). Redox signaling via the molecular chaperone BiP protects cells against endoplasmic reticulum-derived oxidative stress. *Elife*, *3*, e03496.

Wang, J., & Sevier, C. S. (2016). Formation and Reversibility of BiP Protein Cysteine Oxidation Facilitate Cell Survival during and post Oxidative Stress. *J Biol Chem*, *291*(14), 7541-7557.

Wei, P. C., Hsieh, Y. H., Su, M. I., Jiang, X., Hsu, P. H., Lo, W. T. et al. (2012). Loss of the oxidative stress sensor NPGPx compromises GRP78 chaperone activity and induces systemic disease. *Mol Cell*, *48*(5), 747-759.

Williams, J. M., Inoue, T., Chen, G., & Tsai, B. (2015). The nucleotide exchange factors Grp170 and Sil1 induce cholera toxin release from BiP to enable retrotranslocation. *Mol Biol Cell*, *26*(12), 2181-2189.

Xu, M., Marsh, H. M., & Sevier, C. S. (2016). A Conserved Cysteine within the ATPase Domain of the Endoplasmic Reticulum Chaperone BiP is Necessary for a Complete Complement of BiP Activities. *J Mol Biol*, *428*(20), 4168-4184.

Yan, M., Li, J., & Sha, B. (2011). Structural analysis of the Sil1-Bip complex reveals the mechanism for Sil1 to function as a nucleotide-exchange factor. *Biochem J*, *438*(3), 447-455.

CHAPTER 3

PDI MATCHES BIP FUNCTION TO THE ER REDOX STATUS BOTH DIRECTLY AND VIA REGULATION OF THE REDUCTANT SIL1

ABSTRACT

Sil1 has been shown to act as a reductant which deactivates the oxidative stress-induced activities of the ER lumenal chaperone BiP. However, the electron donor which presumably regulates Sil1 and thereby matches BiP activity to the ER redox status has remained unknown. Here we show that protein disulfide isomerase (PDI), the primary factor that catalyzes the formation of disulfide bonds within folding proteins, drives BiP reduction both directly and by reduction of Sil1. PDI-mediated regulation of BiP oxidation provides a means of synchronizing BiP function to the current oxidative protein folding burden and the ER redox status since the oxidation state of PDI is tightly linked to the ER redox status.

INTRODUCTION

Relative to the cytosol, the endoplasmic reticulum (ER) maintains a slightly oxidizing environment (Oka & Bulleid, 2018). This is evident from the differing ratios of the reduced and oxidized form of the cellular redox buffer, glutathione. In the ER, the ratio of GSH to GSSG (reduced to oxidized) has been reported to range from 1:1 to 35:1 which is a stark contrast from the highly reducing ratio of ~100:1 thought to exist in the cytosol (Hwang, Sinskey, & Lodish, 1992; Chai, Ashraf, Rokutan, Johnston, & Thomas, 1994). These conditions are necessary to allow for the oxidation of cysteine pairs to disulfide bonded states which add stability to folding proteins (Pace, Grimsley, Thomson, & Barnett, 1988). The ER oxidoreductase (Ero1) drives oxidative folding by generating disulfide bonds de novo (Frand & Kaiser, 1998). Since Ero1 is unable to directly oxidize folding proteins, protein disulfide isomerase (PDI) serves as a disulfide bridge and passes a disulfide bond from Ero1 to a folding substrate (Frand & Kaiser, 1999). PDI is comprised of four thioredoxin-like domains, two of which possess cysteine-based active sites that enable PDI to function as an oxidoreductase (Wilkinson & Gilbert, 2004). In addition to acting as an oxidase by catalyzing the addition of disulfide bonds, PDI also reduces mismatched cysteine pairs to facilitate the isomerization of incorrect disulfide linkages (Wilkinson & Gilbert, 2004). While oxidation by Ero1 and reduction by folding proteins help establish a balance of oxidized and reduced PDI in the lumen, the redox state of PDI is also responsive to changing glutathione ratios. GSH leads to PDI reduction both directly and by reducing ER substrates that must subsequently be reoxidized by PDI (Chakravarthi, Jessop, & Bulleid, 2006). Thus, the opposing oxidase activity of Ero1 and reducing capacity of the lumenal glutathione pool dictate the oxidation state of PDI.

The process of oxidative protein folding also poses a challenge to cells as rapid disulfide bond formation can induce oxidative stress (Tu & Weissman, 2004). In order to generate a disulfide bond, Ero1 reduces oxygen (via a flavin cofactor) and produces hydrogen peroxide, which is a reactive oxygen species (ROS) with the potential to cause macromolecular damage (Tu & Weissman, 2002; Gross et al., 2006). Thus, high levels of ROS are generated in the ER lumen in response to increased secretory loads. Staggering estimates of peroxide production have been made based on back-of-the-envelope calculations involving prevalent disulfide-containing substrates. For instance, a stimulated beta-cell could produce as many as three million peroxide molecules per minute (Shimizu & Hendershot, 2009). This peroxide causes a net oxidation of the lumenal reduced glutathione pool, thus decreasing the [GSH]:[GSSG] ratio (Chakravarthi et al., 2006).

To prevent irreparable levels of ROS-induced damage to the ER, the oxidative protein folding machinery is regulated in response to the fluctuating ER redox status. This regulation is in large part accomplished by PDI (Kim, Sideris, Sevier, & Kaiser, 2012). When the ER becomes overly oxidized, PDI catalyzes the formation of regulatory disulfide bonds in Ero1 which temporarily inactivates the protein and stems peroxide production (Sevier et al., 2007). Once a stable [GSH]:[GSSG] ratio is reestablished, the PDI equilibrium will shift to favor the reduced form of the protein. PDI will then reduce the Ero1 regulatory bonds, activating the enzyme and reinitiating the process of oxidative protein folding (Kim et al., 2012). Notably, Ero1 displays minimal reactivity with glutathione (Tu, Ho-Schleyer, Travers, & Weissman, 2000; Sevier & Kaiser, 2006; Kim et al., 2012), so the oxidoreductase activity of PDI provides an elegant mechanism for balancing oxidative protein folding with the environment of the ER.

Aside from altering glutathione ratios, peroxide directly interferes with protein folding by misoxidizing substrates and preventing the proteins from achieving a native conformation (Korovila et al., 2017). Damaged proteins tend to form aggregates that have the potential to disrupt ER proteostasis by futilely engaging ER chaperones. We have previously described a mechanism that mitigates protein aggregation involving the activation of a thiol-based redox switch within the molecular chaperone BiP (Wang, Pareja, Kaiser, & Sevier, 2014; Wang & Sevier, 2016). BiP is the ER-resident Hsp70 chaperone which regulates numerous facets of protein folding within the lumen. BiP ordinarily acts as protein foldase which transiently binds and then releases peptides. However, ROS accumulation leads to oxidation of a conserved cysteine residue within BiP which locks the chaperone in a perpetually high affinity state for peptides (Wang et al., 2014). The modified BiP activity is proposed to facilitate the sequestration of proteins in a folding-competent state until the ER reduction potential is restored (Wang et al., 2014).

While BiP oxidation provides a protective phenotype during oxidative stress, the holdase activity of oxidized BiP appears detrimental under non-stressed conditions (Wang & Sevier, 2016). We previously demonstrated that the BiP nucleotide exchange factor Sil1 can reduce and restore BiP foldase activity post stress and serves to limit the accumulation of oxidized BiP in cells (Siegenthaler, Pareja, Wang, & Sevier, 2017). However, upon reduction of BiP, the catalytic cysteines in Sil1 will be left in an oxidized disulfide state and will require reduction before they can act on another BiP molecule. The electron source that drives Sil1 reductant activity and other possible mechanisms for regulating Sil1 have remained unknown. Here we show that Sil1 and BiP are tuned to redox status of the ER via PDI. PDI drives reduction of BiP both by directly reducing the chaperone and by reducing/activating Sil1. The involvement of PDI

in the regulation of BiP and Sil1 provides a means of linking BiP-mediated protein folding to the process of oxidative protein folding and associated reduction potential of the ER.

RESULTS AND DISCUSSION

In order for Sil1 to function as a reductant, the catalytic cysteines in the protein's N-terminus must be in a reduced dithiol state. Thus, a source of electrons is necessary to continually recycle Sil1 to a reduced state. We reasoned that Sil1 reduction was likely accomplished by either glutathione or a protein reductase coupled to another electron source. To test whether Sil1 is susceptible to reduction by glutathione, we monitored the redox state of purified Sil1 after treatment with a molar excess of reduced glutathione. Following incubation with GSH, the reaction was stopped with trichloroacetic acid (TCA) which both protonates reduced thiols minimizing their continued reactivity and precipitates the protein. Precipitated protein was then washed and treated with MM(PEG)12. MM(PEG12) contains a maleimide group which alkylates reduced thiols and adds a PEG group which causes a size shift detectable by SDS-PAGE. Thus, proteins display a size shift proportional to the number of reduced cysteines they contain. *Saccharomyces cerevisiae* Sil1 contains a total of 4 cysteines (**Figure 3.1A**). Two cysteines in the N-terminal region of Sil1 (Cys-52 and Cys-57) comprise the active site which regulates BiP while two other cysteines (Cys-203 and Cys-373) are located within the armadillo core of the NEF and are not reported to have any function (Siegenthaler et al., 2017). The mobility of wild-type Sil1 decreased slightly upon treatment with GSH indicating that at least some of the protein's thiols are reduced by GSH (**Figure 3.1B** compare lanes 1 and 5). To distinguish which residues were being reduced in our assay, we compared mutants lacking either the redox active cysteines or the armadillo core cysteines. A Sil1-C52A-C57A mutant displayed a mobility shift matching the wild-type protein (**Figure 3.1B** compare lane 2 and lane 6) suggesting that the shift seen for the wild-type protein is primarily caused by reduction of the non-catalytic cysteines. Additionally, a Sil1-C203A-C373A mutant did not shift upon treatment with GSH (**Figure 3.1B**

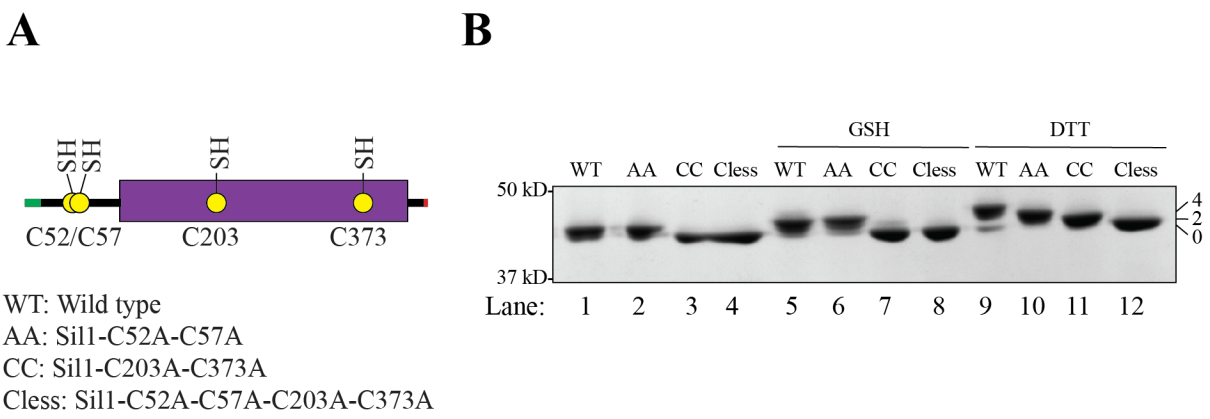

Figure 3.1 Sil1 catalytic cysteines are not reduced by glutathione. (A) Schematic depicting cysteine distribution in Sil1. Active site cysteines -52 and -57 are located in an unstructured region N-terminal to the armadillo repeat core (purple). Cysteines -203 and -373 are located within the core. Signal sequence: green. ER retention motif: red. (B) Reduction of Sil1 was followed by assaying number of free thiols in various mutants. Recombinant Sil1 was reacted with a molar excess of GSH or DTT for one hour before proteins were precipitated with TCA. Washed pellets were suspended in buffer containing MM(PEG)12. Samples were resolved by SDS-PAGE and visualized with Coomassie blue. Proteins containing reduced thiols display a size shift. Numbering on the right side of the panel denotes the size shifts observed for a given number of reduced cystines as inferred from the DTT-reduced mobility controls.

compare lanes 3 and 7). Thus, GSH does not seem capable of directly reducing the catalytic cysteines in Sil1.

The inability of GSH to reduce Sil1 suggested that the NEF is most likely reduced by an ER protein. To identify potential candidates, we mutated individual cysteines in the Sil1 catalytic site to prevent resolution of mixed disulfide intermediates. This approach is commonly used to identify interactors of proteins possessing thiol-based redox activity (Walker, Lyles, & Gilbert, 1996). Wild-type Sil1 and Sil1 mutants containing a 6xFLAG tag within a loop devoid of secondary structure to facilitate immunoprecipitation. Actively dividing cells were metabolically labeled with an ^{35}S-cysteine/methionine mixture and were then treated with TCA followed by *N*-ethylmalemide (NEM) to help preserve mixed-disulfide bonds formed within cells and also to

minimize the post-lysis formation of disulfide bonds (Le Moan, Tacnet, & Toledano, 2008). Sil1 was immunoprecipitated from the treated lysates under non-reducing conditions, and proteins were separated by either reducing or non-reducing SDS-PAGE. Notably, the isolated Sil1 migrated as a doublet. We speculate that the lower band represents truncated Sil1 protein as the N-terminus of the protein is thought to be unstructured and therefore is likely susceptible to proteolysis. We observed that expression of either active site mutant, Sil1-C52A or Sil1-C57A, resulted in the accumulation of high molecular weight species under non-reducing conditions that were absent if both Cys-52 and Cys-57 were mutated to alanine (**Figure 3.2**). These bands were confirmed to represent Sil1-containing mixed disulfide bonds as they were not present under reducing conditions. However, no additional band was immediately visible upon resolution of the mixed disulfides under reducing conditions. The resolved protein may not be abundant enough to detect in our assay, or the inability to detect a second resolved band could indicate that the high-molecular weight species are Sil1-Sil1 mixed disulfides.

To determine the identity of the mixed disulfide species, Sil1-trapping mutants were immunoprecipitated as before, and the bands were excised from Coomassie-stained gel and sent for mass spectrometry (MS) protein ID. The strongest obtained hit (besides Sil1) was protein disulfide isomerase (PDI) (data not shown). To confirm the results of the MS analysis, the samples were prepared as before but were subjected to a secondary IP against PDI. Thus, the mixed disulfide bands will only be visible if they contain both Sil1 and PDI. As expected, the high molecular weight species were present in the PDI immunoprecipitations (data not shown).

BiP represented the second strongest hit from our MS analysis although considerably fewer BiP peptides were detected than PDI (data not shown). This is unsurprising given the established ability of Sil1 to reduce BiP. A Sil1 trapping mutant would still possess a single thiol capable of

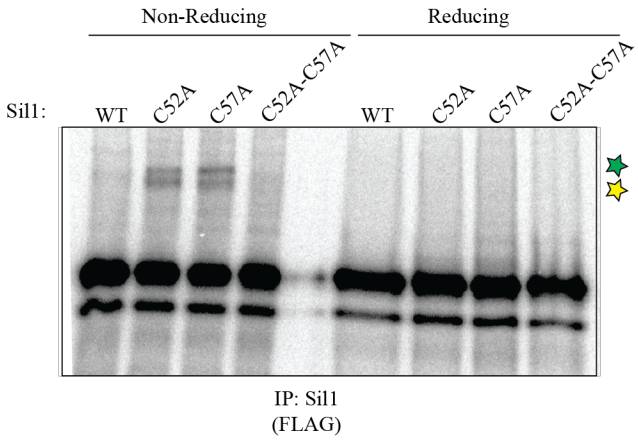

Figure 3.2 Sil1 cysteine mutants trap mixed disulfides. (A) CSY448 transformed with pKS65, pKS68, pKS69 or pCS922 were grown to mid-log phase before treatment with a S^{35}-labeled cysteine/methionine mixture for one hour. Cells were lysed in the presence of TCA and neutralized in the presence of NEM to preserve mixed disulfides. Sil1 was immunoprecipitated from the lysates, and samples were resolved by non-reducing and reducing SDS-PAGE. Mixed disulfide bands are indicated with green and yellow stars.

reducing BiP, but the resulting Sil1-BiP mixed disulfide intermediate would not be resolved since the second Sil1 cysteine would ordinarily be responsible for attacking the temporary mixed disulfide bond. We have previously shown that a Sil1 trapping mutant does form a Sil1-BiP complex *in vitro* (Siegenthaler et al., 2017). However, we were unable to detect a Sil1-BiP mixed disulfide in cells either by radiolabel or by western blot. We speculate that prevalence of the Sil1-PDI mixed disulfide over the Sil1-BiP mixed disulfide reflects the higher abundance of reactive PDI thiols compared to oxidized BiP thiols in a cell making a Sil1-PDI trap the kinetically favorable species.

PDI was a logical candidate to regulate Sil1 reducing activity since PDI can both oxidize and reduce protein thiols in the ER lumen (Wilkinson & Gilbert, 2004). Thus, PDI could reduce/activate Sil1 when BiP must be reduced or oxidize/deactivate Sil1 when a cell requires BiP to be oxidized. Furthermore, the doublet nature of the mixed disulfide bands was consistent

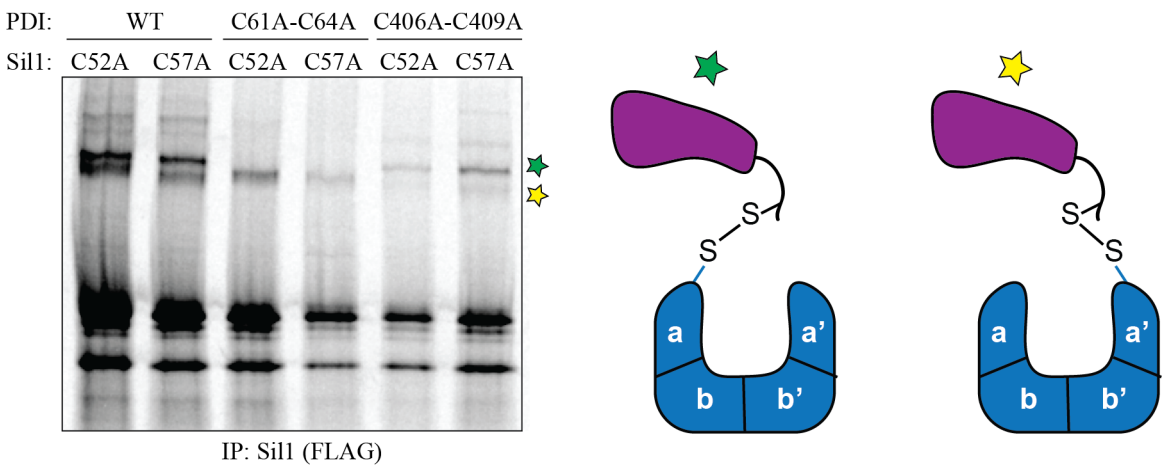

Figure 3.3 Both PDI active sites can react with Sil1. CSY804 (*pdi1*Δ *sil1*Δ [pCS463]), CSY901 (*pdi1*Δ *sil1*Δ [pCS464]), and CSY902 (*pdi1*Δ *sil1*Δ [pCS465]) transformed with pKS68 or pKS69 were grown to mid-log phase before treatment with a S^{35}-labeled cysteine/methionine mixture for one hour. Cells were lysed in the presence of TCA and neutralized in the presence of NEM to preserve mixed disulfides. Sil1 was immunoprecipitated from the lysates, and samples were resolved by non-reducing SDS-PAGE. Sil1-PDI mixed disulfide through the PDI a site (green) and a' site (yellow) are indicated. Resolving thiols are omitted from PDI in the protein schematics for simplicity. Sil1: purple. PDI: blue.

with previous reports that PDI often migrates as a doublet (Frand & Kaiser, 1999). The doublet likely results from the presence of two active sites present within two separate domains of PDI. In support of our hypothesis, the doublet collapsed into individual bands in strains containing PDI mutants lacking either the a or a' site (**Figure 3.3**) through the PDI a domain while the bottom band represents a mixed disulfide between Sil1 and the PDI a' domain (**Figure 3.3**).

The Sil1-PDI trap confirms that electrons are exchanged between the two proteins *in vivo*, so we next sought to determine if PDI is capable of reducing the Sil1 catalytic cysteines. We first tested if an equimolar concentration of PDI was able to drive reduction of oxidized Sil1. To this end, we reduced PDI with a molar excess of DTT and oxidized Sil1 with an excess of diamide. Both proteins were then desalted to remove the excess oxidant and reductants before the proteins were mixed to initiate a reaction. At specific times, a portion of the reaction was removed and added to sample buffer containing MM(PEG)12 which reacts with free cysteines thus stopping

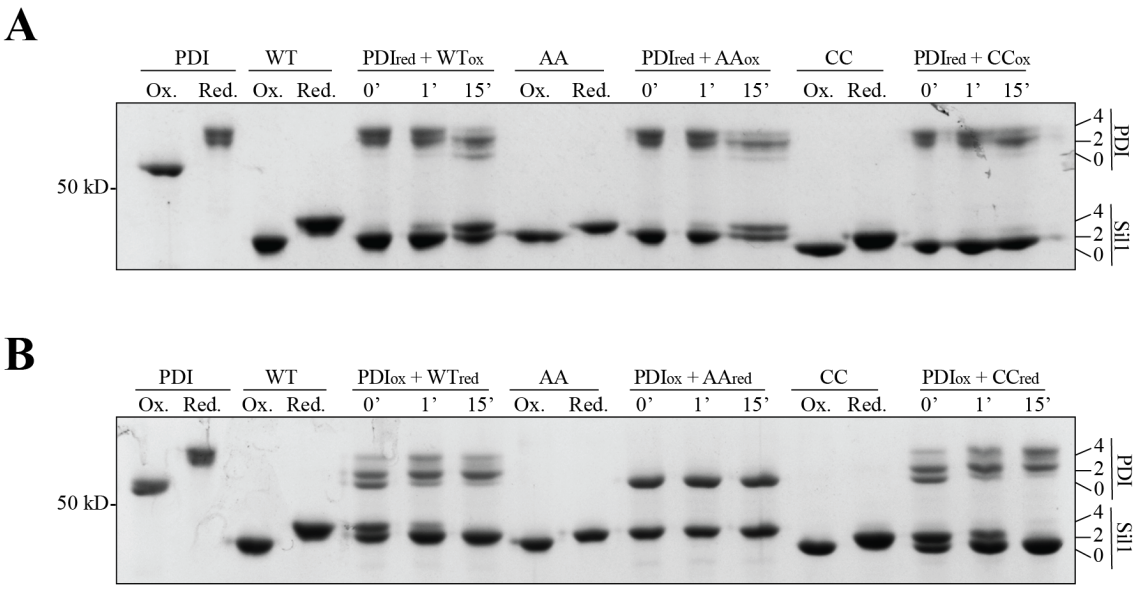

Figure 3.4 Stoichiometric concentrations of PDI oxidizes cysteines 52/57 and reduces cysteines 203/373 in Sil1. (A) Reaction of Reduced PDI with oxidized Sil1. The reactions were stopped at indicated timepoints with MM(PEG)12, separated by reducing SDS-PAGE and stained with Coomassie blue. Proteins containing reduced thiols display a size shift. Numbers on the right side of the panels indicate the expected size shift for a given number of reduced cysteines in PDI and Sil1. (B) Reaction of oxidized PDI and reduced Sil1. Samples were processed as in (A). WT: wild type. AA: Sil1-C52A-C57A. CC: Sil1-C203A-C373A.

the reaction and causing reduced proteins to display a size shift. An equimolar concentration of PDI was able to drive the reduction of wild-type Sil1 as the protein shifted to a higher molecular weight over time (**Figure 3.4A**). Notably, PDI showed a corresponding decrease in size indicating it is becoming oxidized during the course of the reaction with Sil1 (**Figure 3.4A**). The reaction between oxidized Sil1-C52A-C57A and reduced PDI displayed trends matching the reaction with wild-type Sil1 (**Figure 3.4A**). This suggests that most of the reduction observed in the wild-type reaction resulted from reduction of Csy-203 and Cys-373. Consistent with this, Sil1-C203A-C373A mutant seemed resistant to reduction in our assay as only a small fraction of the protein was reduced by the end of the time course (**Figure 3.4A**). Interestingly, when the reaction conditions were reversed and oxidized PDI was reacted with reduced Sil1, PDI was able

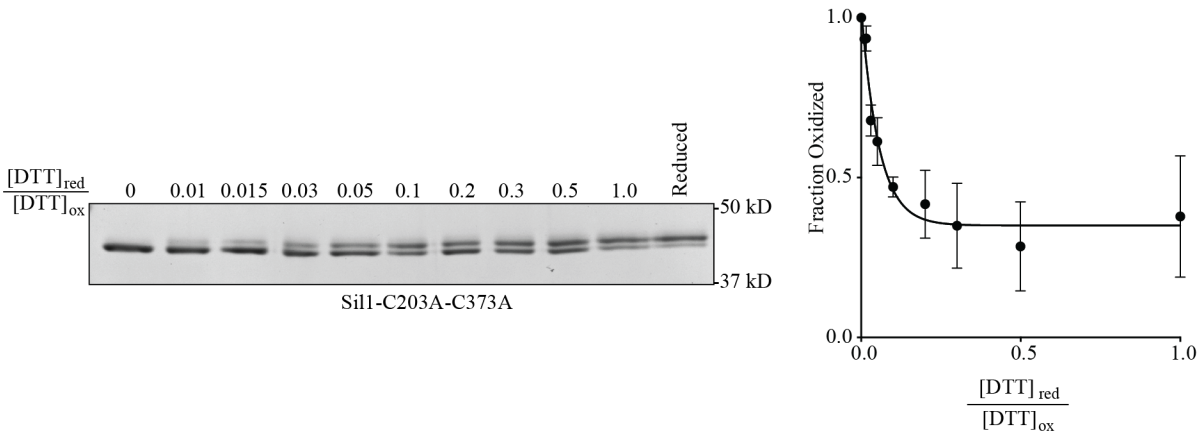

Figure 3.5 Determination of Sil1 reduction potential. Recombinant Sil1-C203A-C373A was reacted in varied ratios of oxidized and reduced DTT before addition of TCA and precipitation of protein. Washed pellets were solubilized in buffer containing mal-PEG2K to add a size shift to protein containing reduced cysteines. Samples were resolved by reducing SDS-PAGE and visualized with Coomassie blue. A representative image is displayed in the left panel. The mean fraction of oxidized Sil1 measured in three replicates was plotted against each DTT ratio. A one phase decay curve was fit to the data and the K_{OX} was determined to be 0.03836 M. From this, the reduction potential of the Sil1 C52/C57 pair was calculated to be -270 mV (Gilbert, 1997).

to oxidize the Sil1 active site cysteines. We observed that reaction of oxidized PDI with wild-type Sil1 or the Sil1-C203A-C373A mutant resulted in a shift to a lower molecular weight form (**Figure 3.4B**). In contrast, PDI seemed unable to oxidize the other two cysteines as the Sil1-C52A-C57A mutant did not display a size shift throughout the course of the assay (**Figure 3.4B)**. This is unsurprising as these cysteines are not surface accessible in the published Sil1 structure (Yan, Li, & Sha, 2011). To confirm the favored direction of electron flow between Sil1 and PDI, we measured the reduction potential Sil1. To do this, we allowed purified Sil1 protein possessing only the active site cysteines to equilibrate in different ratios of reduced and oxidized dithiothreitol (DTT) and determined the fraction of the protein that was oxidized at each ratio. Consistent with our data, the K_{ox} for Sil1 was measured to be 0.03836 M which corresponds to a reduction potential of -270 mV (**Figure 3.5A** and **B**) (Gilbert, 1997). This suggests that Sil1 is a more potent reductant than PDI which possesses reduction potentials of -194 mV and -164 mV

for the a and a' sites respectively (Vitu et al., 2010) and predicts that electrons would tend to flow from Sil1 to PDI.

While these data suggest PDI would predominately oxidize the Sil1 catalytic cysteines, the propensity for electron flow does not necessarily reflect the intracellular equilibrium reached between PDI and Sil1 in the presence of other driving factors. For instance, it is known that the *E. coli* periplasmic oxidoreductase DsbB oxidizes DsbA to allow for disulfide bond formation in a system analogous to the Ero1/PDI oxidative protein folding machinery. However, in the absence of ubiquinone (which serves as the final electron acceptor of the system) DsbA is unable to reduce DsbB (Inaba & Ito, 2002). This highlights the critical contribution of cellular factors in driving the equilibrium of intracellular electron flow reactions.

We therefore modified our *in vitro* assay to more accurately recapitulate the conditions of the ER. Since PDI is one of the most abundant proteins in the ER (Määttänen, Gehring, Bergeron, & Thomas, 2010), the PDI concentration was increased ten-fold over Sil1. Additionally, reduced glutathione was added to the reaction to drive the reduction of PDI since the oxidoreductase is expected to be primarily reduced during recover from oxidative stress (Mezghrani et al., 2001). As established in earlier assays (**Figure 3.1**), GSH alone is unable to reduce the catalytic cysteines of Sil1; two of the four cysteines are reduced in the presence of GSH (lane 1), and these cysteines correspond to the armadillo repeat cysteines (**Figure 3.6**, lanes 2-3). Yet the combination of GSH and PDI could drive the reduction of the Sil1 active site cysteines. The addition of PDI resulted in the appearance of a new band in the wild type lane which corresponds to the reduction of four cysteines (**Figure 3.6** lane 5). Furthermore, this is supported by the increased level of the band corresponding to a two-cysteine reduction in the Sil1-C203A-C373A

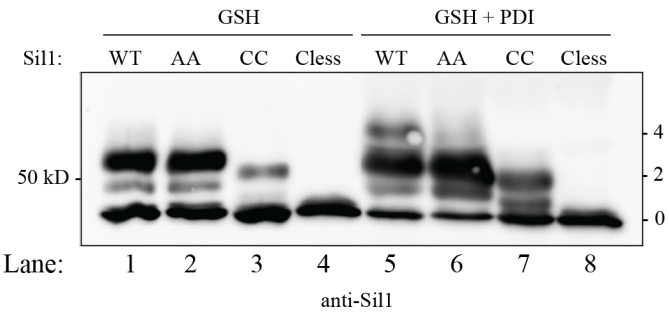

Figure 3.6 A molar excess of PDI and GSH drive reduction of Sil1 cysteines -52 and -57. Recombinant Sil1 mutants were incubated with a molar excess of GSH or PDI and GSH for one hour before proteins were precipitated with TCA. Pellets were washed and resuspended in the presence of mal-PEG2K to assay the number of reduced cysteines present in each protein. The expected shifts for Sil1 molecules with a given number of reduced cysteines is indicated on the right of the panel. AA: Sil1-C52A-C57A. CC: Sil1-C203A-C373A. Cless: Sil1-C52A-C57A-C203A-C373A.

sample (**Figure 3.6** lane 7) while no change is observed with the addition of PDI to a Sil1-C52A-C57A mutant (**Figure 3.6** lane 6).

Given the capacity of PDI to reduce Sil1 under reducing (high GSH) conditions, we speculate that the redox activity of Sil1 may be influenced by redox changes within the ER lumen. We reason that under increasing levels of oxidative stress, the increased oxidation of GSH to yield GSSG (Cuozzo & Kaiser, 1999; Chakravarthi et al., 2006) may skew the [GSH]:[GSSG] ratio, leading to a net oxidation of PDI within the ER and in turn causes the oxidation of the Sil1 catalytic cysteines (Raturi & Mutus, 2007). Upon restoration of an unstressed state in the ER, the increase in reduced GSH should increase the fraction of reduced PDI (Raturi & Mutus, 2007) which would allow PDI to reduce Sil1 and thereby drive reduction of BiP.

We next sought to establish the interdependence of Sil1 and PDI activity in cells via assaying the redox state of BiP. If PDI does provide the electrons for Sil1 to reduce BiP, we would expect loss of either Sil1 or BiP to result in accumulation of oxidized BiP. As PDI is essential, we required conditional alleles to inactivate the oxidoreductase (Wilkinson & Gilbert,

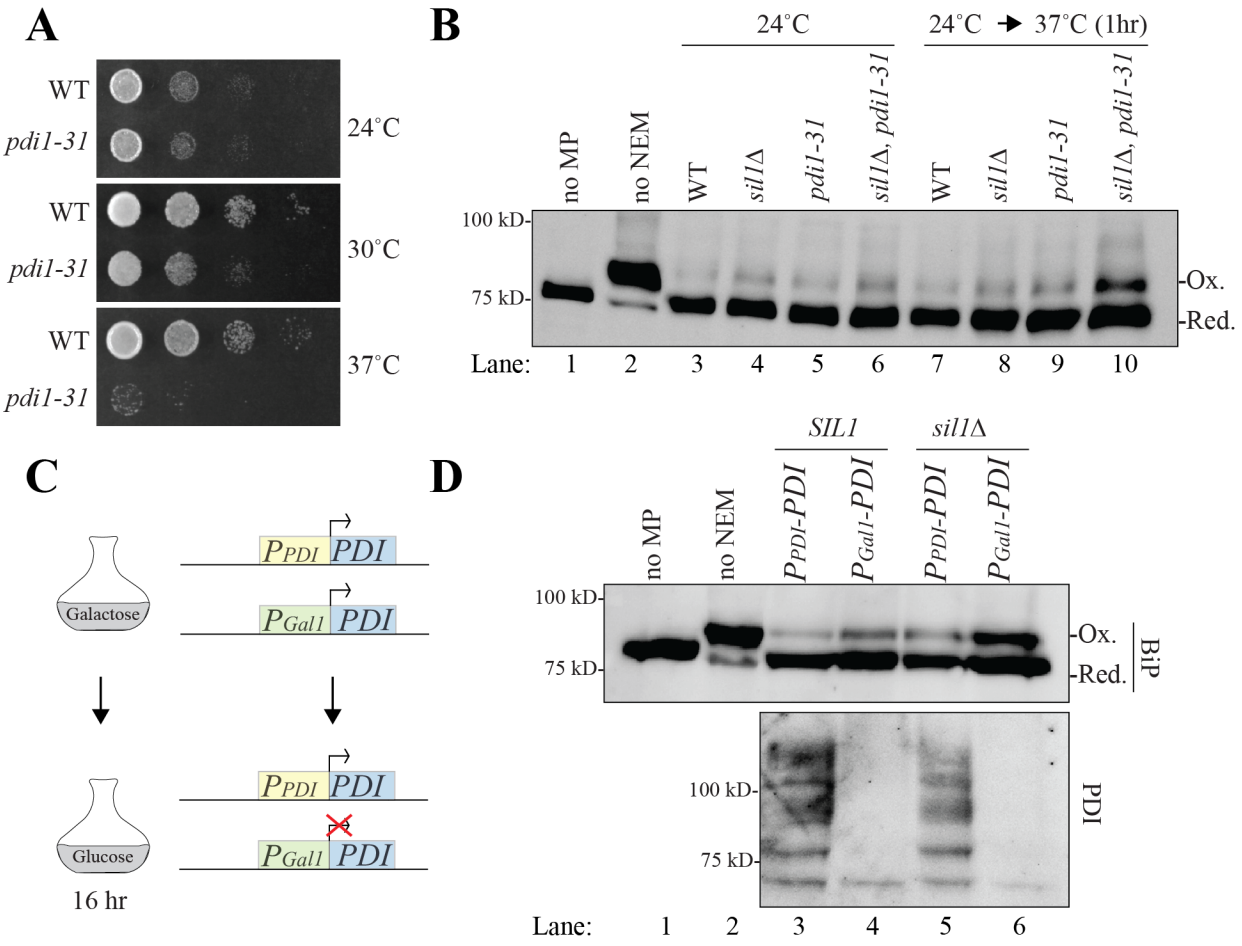

Figure 3.7 Depletion of PDI exacerbates the accumulation of oxidized BiP in Δ*sil1* cells. (A) CSY5 and CSY928 were spotted onto YPD plates and incubated for 2 d at the indicated temperature. (B) The redox state of BiP was assayed using a maleimide-PEG gel shift assay. CSY5, CSY448, CSY928 and CSY936 were grown in YPD until mid-log phase at 24˚C. Cells were either left at 24˚C or shifted to 37˚C for one hour before sample preparation. Cells were lysed in TCA to minimize thiol reactivity and neutralized in the presence of NEM to alkylate free thiols. Oxidized thiols were reduced with BME before proteins were again precipitated and neutralized in the presence of mal-PEG(2K) so that proteins containing newly reduced thiols (those oxidized at the time of lysis) display a size shift. The reduced and oxidized forms of BiP are indicated. (C) Schematic for glucose-mediated depletion of PDI. Cells were initially grown in galactose to support viability before shifting to glucose containing media (SMM) for 16 hrs. to deplete PDI. (D) CSY795, CSY796, CSY803, and CSY804 were grown as described in (C) and BiP oxidation was assayed as described in (B).

2004). To this end, we randomly mutagenized the *PDI1* gene and screened for mutants that were nonfunctional at 37˚C. The temperature sensitive mutant *pdi1-31* was integrated into the genome

to function as the only cellular copy of PDI. While the *pdi1-31* strain was viable at a permissive temperature of 24˚C and partially viable at the semi-permissive temperature of 30˚C, the strain was dead at 37˚C (**Figure 3.7A**). To inactivate PDI, strains were grown to mid-log phase at the permissive temperature before shifting to 37˚C for one hour. To assay the redox state of BiP, cells were lysed under acidic conditions to preserve cysteine oxidation. Then, the samples were neutralized in the presence of NEM which alkylates reduced thiols before oxidized thiols were reduced with BME. Following TCA precipitation and washing to remove excess BME, pellets were solubilized in the presence of Mal-PEG(2K) to alkylate newly reduced thiols. Thus, protein thiols oxidized at the time of lysis display a size shift. Mobility controls were generated by either omitting the mal-PEG or the NEM which results in standards that migrate at the minimum and maximum sizes respectively.

As previously reported, we observed a strain lacking Sil1 (*sil1*Δ cells) displayed increased levels of oxidized BiP; more oxidized BiP was detected when cells were grown at either 24˚C or 37˚C (Siegenthaler et al., 2017). Interestingly, cells carrying the *pdi1-31* allele also showed an accumulation of oxidized BiP after the inactivation of PDI at high temperature (**Figure 3.7B** compare lane 5 and lane 9). An accumulation of oxidized BiP upon inactivation of PDI is consistent with a role for PDI in regulating the oxidation state of BiP. We reasoned if PDI acts to reduce Sil1 and activate Sil1 reducing activity, that a strain lacking both Sil1 and PDI activities would show no additive impact on BiP oxidation state beyond that seen with the inactivation of either individual protein. Instead, strikingly, we observed that a *sil1*Δ *pdi1-31* double mutant strain displayed a much larger increase in oxidized BiP upon shift to high temperature relative to either individual mutant strain (**Figure 3.7B** lane 10). Notably, a similar result was seen also when PDI was depleted from cells using a glucose repressible promoter (**Figure 3.7C** and **D**). As

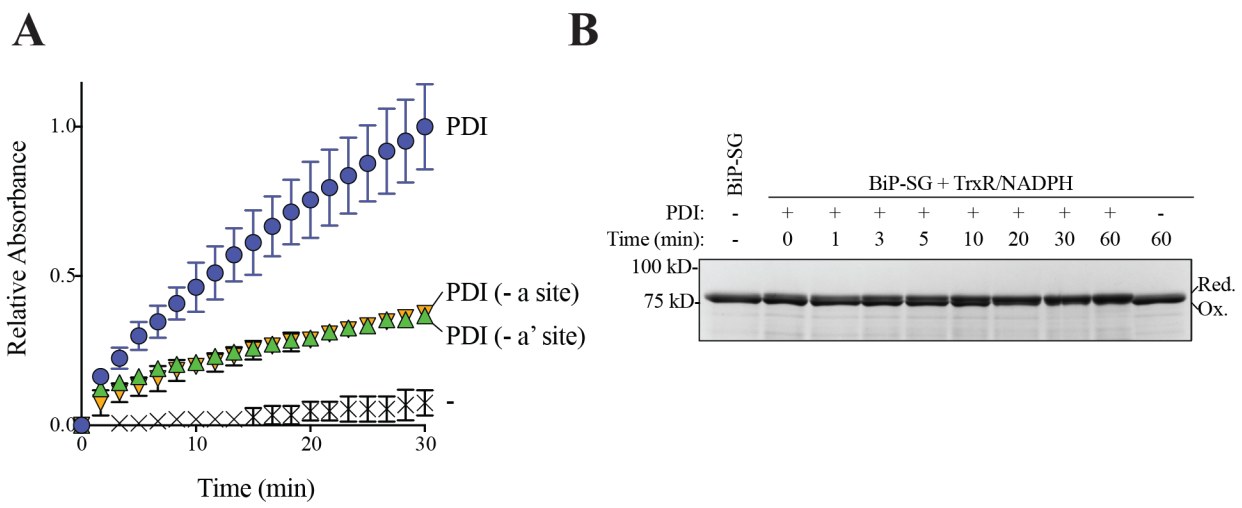

Figure 3.8 PDI can reduce BiP. (A) Reduction of recombinant BiP oxidized by DTNB (BiP-TNB) was followed by monitoring the change in absorbance at 412 nm (indicative of TNB release) in the presence of sub-stoicheometric concentrations of PDI or PDI mutants. TrxR and an excess of NADPH were included to continually reduce PDI. Mean values of three independent experiments are shown. Error bars depict the standard error of the mean. (B) Reduction of glutathionylated BiP was monitored by MM(PEG)12 -induced size shift. BiP-SG was reacted with a sub-stoicheometric concentration of PDI and TrxR along with an excess of NADPH. At indicated timepoints, reactions were stopped with mal-PEG, samples were resolved by reducing SDS-PAGE and visualized with Coomassie blue.

was observed with the temperature sensitive allele, depletion of PDI caused an increase in levels of oxidized BiP (**Figure 3.7D** compare lanes 3 and 4) which was further compounded by deletion of *SIL1* (**Figure 3.7D** lane 6). Importantly, PDI was not detectable in strains possessing the glucose-repressible PDI confirming we efficiently depleted the oxidoreductase in our assay. Altogether, our data suggest the potential for PDI to influence BiP oxidation via modulation of Sil1 redox state as well as the capacity of PDI to work independently to influence BiP oxidation.

Interestingly, the enhanced BiP oxidation upon loss of Sil1 and PDI compared to loss of either protein individually suggest that the proteins may regulate BiP independently of each other. One possible explanation for this would be that PDI is able to reduce BiP in addition to Sil1. We therefore tested the ability of PDI to reduce BiP *in vitro*. Catalytic amounts of PDI

reduced a BiP-TNB adduct in the presence of a thioredoxin reductase regeneration system (**Figure 3.8A**). Both PDI active sites proved reactive toward BiP as mutants lacking either the a or a' site reduce BiP albeit at a slower rate than the wild-type protein (**Figure 3.8 A**). While TNB modification is often used as a substitute for sulfenylation due to its stability and traceability, it is an artificial modification with the potential to behave differently than physiological modifications (Rudyk & Eaton, 2014). We therefore tested the ability of PDI to reduce glutathionylated BiP as this species has been detected in cells (Wang & Sevier, 2016). Consistent with our TNB assay, PDI reduced glutathionylated BiP as demonstrated by the size shift observed in a mal-PEG gel shift assay (**Figure 3.8B**).

Importantly, the ability of PDI to reduce BiP does not diminish the importance of Sil1 in mediating the redox state of the chaperone. To the contrary, the increase in BiP oxidation upon loss of either Sil1 or PDI highlights the individual role of each protein in BiP regulation (**Figure 3.7B** and **D**). Moreover, the synergistic increase in the fraction of oxidized BiP observed upon simultaneous loss of PDI and Sil1 implies that each reductant can compensate for the loss of the other. It also must be noted that PDI reactivity towards BiP does not preclude the possibility that PDI also regulates BiP via reduction of Sil1.

Our data clearly suggest that Sil1 and PDI interact in cells and that PDI is able to reduce Sil1. However, it also seems that Sil1 plays a role in regulating BiP oxidation independent of PDI. This is evidenced by the fact that depletion/inactivation of PDI alone resulted in the accumulation of less oxidized BiP than is seen for cells lacking both Sil1 and PDI activity (**Figure 3.7B** and **D**). If Sil1 were only able to reduce BiP using electrons from PDI, we would expect the levels of oxidized BiP to be equivalent in all strains where PDI is inactivated regardless of the presence or absence of Sil1. The unexpectedly elevated levels of oxidized BiP

may suggest that other disulfide isomerase family members are able to reduce Sil1 (albeit less efficiently) in the absence of PDI. *S. cerevisiae* possesses four other disulfide isomerase family members which are non-essential but may carry out some PDI functions in the absence of the primary disulfide isomerase (Nørgaard et al., 2001). Additionally, our data may point to a role for Sil1 in regulating BiP oxidation independent of its catalytic cysteines. We have previously demonstrated that while deletion of *SIL1* provides resistance to oxidative stress (induced by diamide treatment), strains possessing a *sil1-C52A-C57A* gene do not display the same stress resistance (Siegenthaler, et al., 2017). Thus, Sil1 NEF activity may also play a role in regulating BiP oxidation. It is possible that BiP is more likely to become oxidized in an ADP-bound form, and thus, loss of Sil1 increases the fraction of ADP-bound BiP and thereby the levels of oxidized BiP. Alternatively, the structural perturbations observed in BiP upon Sil1 binding may enhance the accessibility of the BiP cysteine to other potential reductants such as glutathione. While more studies are needed to establish the relative contributions of Sil1 NEF activity, Sil1 reductant activity, and PDI reductase activity in regulating BiP oxidation, the culmination of our data clearly indicate all three pathways play a role in governing BiP.

At first glance, the apparent redundant activities of PDI and Sil1 may seem puzzling, but the combined activities of the two proteins seem to allow for optimal regulation of BiP oxidation. We have previously shown that the half-life of oxidized BiP increased over 7-fold in cells lacking Sil1 (Siegenthaler et al., 2017). The eventual reduction of BiP in the Δ*sil1* cells is likely caused by PDI. Thus, Sil1 can be viewed as an enhancer of BiP reduction by serving as an electron bridge between PDI and BiP and also by regulating BiP oxidation through a mechanism(s) independent of the NEF's N-terminal cysteines.

Based on the published structures of BiP and PDI, it is not immediately clear how either PDI active site would gain access to the oxidized BiP cysteine (Tian, Xiang, Noiva, Lennarz, & Schindelin, 2006; Yang, Nune, Zong, Zhou, & Liu, 2015). PDI is comprised of four thioredoxin like domains that assume a "twisted U" shape. The catalytic cysteines of each active site are positioned on the top interior of the "U (Tian et al., 2006)." Thus, it seems that there would be considerable steric constraint preventing PDI from reaching the redox labile cysteine within the interior of the BiP nucleotide binding domain (NBD). It remains possible that oxidation of BiP causes partial unfolding of the BiP NBD. This would increase the accessibility of the cysteine allowing PDI to reduce it. More structural studies are necessary to reconcile the reactivity of PDI and BiP with known structures.

As a protein folding catalyst, PDI recognizes a large number of substrates in unfolded states (Hatahet & Ruddock, 2007). While no complete structure of Sil1 exists, the N-terminal region containing the catalytic cysteines is thought to be devoid of major structural elements and bear resemblance to a peptide substrate (Yan et al., 2011; Rosam et al., 2018). This feature of the N-terminus which is thought to facilitate Sil1 NEF activity (Rosam et al., 2018) may also mark Sil1 as a PDI substrate and thereby also facilitate the role of Sil1 as a BiP reductant. Also, the high affinity with which Sil1 binds BiP (K_d of 120 nM) helps make Sil1 an ideal BiP reductase (Pareja, et al., in preparation). In contrast, PDI possesses low affinity for substrates in order to facilitate the transient interactions with numerous peptides characteristic of factors involved with protein folding (Hatahet & Ruddock, 2007). While this is likely partially offset by the relatively high concentration of PDI in the ER compared to Sil1, large fractions of PDI will also be

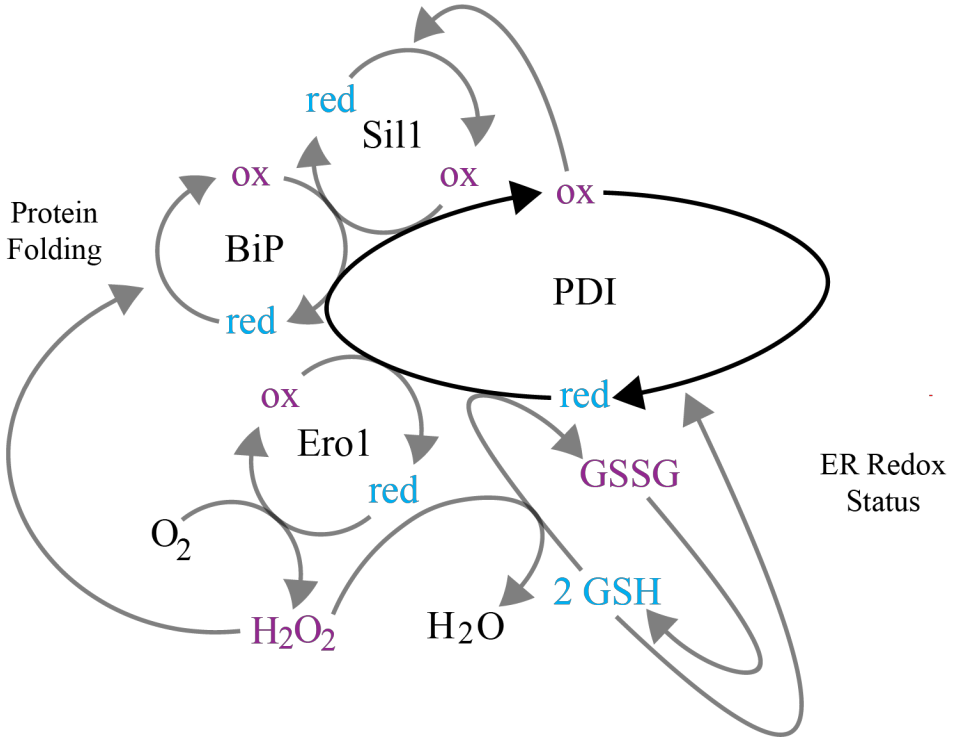

Figure 3.9 PDI balances the redox-regulated foldase/holdase functions of BiP in response to fluctuating lumenal reduction potentials. Oxidative protein folding generates hydrogen peroxide by the activity of Ero1. Peroxide oxidizes BiP to induce the protective holdase function of the chaperone. Ero1 oxidase activity increases oxidation of PDI both directly and indirectly via GSSG production. Oxidized PDI catalyzes formation of regulatory bonds in Ero1 stopping oxidative protein folding and peroxide production. Stabilization of the ER reduction potential (indicated by increasing GSH levels) leads to reduction of PDI. PDI reduces BiP either directly or via reduction/activation of Sil1 reinitiating the foldase activity of BiP. PDI reduces the Ero1 regulatory bonds enabling the oxidase to resume oxidative protein folding. Oxidized species are highlighted in purple. Reduced species are highlighted in blue.

for PDI to be a weak BiP-reductase compared to Sil1. If PDI possessed as high of an affinity for BiP as Sil1, BiP oxidation may be reversed too quickly to benefit from the protective functions of oxidized chaperone. Employment of a more targeted reductase that is harder to occupied for oxidative protein folding (Kozlov, Määttänen, Thomas, & Gehring, 2010; Behnke, Feige, & Hendershot, 2015). Furthermore, given the high abundance of PDI, it may be necessary reduce therefore expands the range in which BiP can be oxidized. Therefore, differential reduction by PDI or Sil1 likely enhances the regulation of BiP amidst the changing redox state of the ER.

It is also possible that PDI and Sil1 act on different forms of oxidized BiP. To date, BiP has been detected in sulfenylated and glutathionylated forms (Wang et al., 2014; Wang & Sevier, 2016) yet multiple other modes of oxidation may still occur. As alluded to earlier, it is currently unknown if or how oxidation affects the structure of BiP. Differential oxidation may change the chaperone structure in varying ways and therefore distinguish the chaperone as a better substrate for either PDI or Sil1. Our assay for detecting BiP oxidation in cells is unable to distinguish modes of oxidation as long as they are reducible by BME. PDI is oxidized by both Ero1 and GSSG to facilitate disulfide addition to secretory proteins. However, when peroxide buildup in the ER threatens proteostasis, PDI oxidizes a pair of regulatory disulfide bonds in Ero1 (Sevier et al., 2007). Regulatory bond oxidation deactivates Ero1 and restoration of a stable ER environment, rising GSH concentrations reduce PDI, and PDI in turn reduces Ero1 to resume oxidative protein folding (Appenzeller-Herzog et al., 2010; Kim et al., 2012). Thus, the responsiveness of PDI to fluctuating glutathione ratios and the intricate roles PDI plays in governing oxidative protein folding make the oxidoreductase an ideal intermediary between the ER redox state and the activities of the primary lumenal chaperone, BiP. Sil1 appears to increase the efficiency of BiP reduction by bridging electron flow and allows for an expanded range of BiP oxidation by serving as a more targeted reductase than PDI.

MATERIALS AND METHODS

Plasmid and strain construction

Plasmids are listed in **Table 3.1**. To construct pKP134, sequence coding for a start methionine and Kar2 residues 43-682 was cloned into pET-28a SUMO vector using BamHI and XhoI restriction sites. Yeast expression plasmids are derived from the pRS vector series (Sikorski & Hieter, 1989). To generate pKS28, a BamHI restriction site was inserted into pJW7 using QuikChange mutagenesis (Agielent Technologies). The BamHI site was inserted immediately after the nucleotides encoding Sil1 residue T257 as this region of the protein is devoid of major secondary structure (Yan et al., 2011). Sequence encoding a 3xFLAG tag flanked by BamHI restriction sites was ligated into pKS28 to generate a *SIL1* gene containing an epitope tag. A clone was selected containing two sequential 3xFLAG tags in the proper orientation to yield pKS35. To form pHS79, the *SIL1* gene was amplified from yeast genomic DNA including 759 bp 5' UTR and a 685 bp 3' UPR, and this fragment was ligated into pRS426 digested with KpnI and SacI. A fragment of the tagged *SIL1* gene was digested from pKS35 using KpnI and SacII restriction enzymes and ligated into the vector piece of pHS79 digested with the same enzymes to make pKS65. Mutations were inserted with QuikChange mutagenesis to form pKP160, pKS248, pKS280, pKS68, pKS69, and pCS922.

Yeast strains used in this study are listed in **Table 3.2** and are of the S288C background. Strains CSY795 and CSY796, were generated by transforming pSK65 and pCS463 into CSY125 followed by counterselection of pCS213 with 5-fluoroorotic acid (5-FOA). To make CSY802, CSY448 was crossed with CSY125. Subsequent construction of CSY803, CSY804, CSY901 and CSY902 was accomplished by transforming CSY802 with pSK65, pCS463, pCS464 or pCS465

Table 3.1. Plasmids

Plasmid	Description	Marker	Source
pKP136	*His6-SUMO-sil1-(19-421)*	KAN	(Pareja, et al., in preparation)
pKP160	*His6-SUMO-sil1-(19-421)-C52A-C57A*	KAN	This study
pKS248	*His6-SUMO-sil1-(19-421)-C203A-C373A*	KAN	This study
pKS280	*His6-SUMO-sil1-(19-421)-C52A-C57A-C203A-C373A*	KAN	This study
pCS637	*sil1-(20-407)-His6*	AMP	(Siegenthaler, et al., 2017)
pCS877	*sil1-(20-407)-C52A-C57A-His6*	AMP	(Siegenthaler, et al., 2017)
pCS948	*sil1-(20-407)-C203A-C373A-His6*	AMP	(Siegenthaler, et al., 2017)
pCS895	*sil1-(20-407)-C52A-C57A-C203A-C373A-His6*	AMP	(Siegenthaler, et al., 2017)
pKP134	*His6-SUMO-kar2-(43-682)*	KAN	This study
pJW7	*Sil1*	*CEN*, *URA3*	(Siegenthaler, et al., 2017)
pKS28	*Sil1* (with BamHI site after T257)	*CEN*, *URA3*	This study
pKS35	*SIL1-6xFLAG*	*CEN*, *URA3*	This study
pKS79	*Sil1*	*2μ*, *URA3*	This study
pKS65	*SIL1-6xFLAG*	*2μ*, *URA3*	This study
pKS68	*sil1-C52A-6xFLAG*	*2μ*, *URA3*	This study
pKS69	*sil1-C57A-6xFLAG*	*2μ*, *URA3*	This study
pCS922	*sil1-C52A-C57A-6xFLAG*	*2μ*, *URA3*	This study
pKK10	*His6-SUMO-PDI-(29-518)*	KAN	This study
pKK11	*His6-SUMO-PDI-(29-518)-C406S-C409S*	KAN	This study
pKK12	*His6-SUMO-PDI-(29-518)-C61S-C64S*	KAN	This study
pCS213	*PDI1*	*CEN*, *URA3*	(Vitu, et al., 2010)
pCS463	*PDI1*	*CEN*, *LEU2*	(Vitu, et al., 2010)
pCS464	*PDI1-C406A-C409A*	*CEN*, *LEU2*	(Vitu, et al., 2010)
pCS465	*PDI1-C61A-C64A*	*CEN*, *LEU2*	(Vitu, et al., 2010)
pSK65	*PGal1-PDI1*	*CEN*, *LEU2*	(Kim, et al., 2012)

Table 3.2. Strains

Strain	Genotype	Source
CSY5	*MATa GAL2 ura3-52 leu2-3,112*	(Wang, et al., 2014)
CSY448	*MATalpha GAL2 ura3 leu2 sil1Δ::KanMX*	(Siegenthaler, et al., 2017)
CSY125	*MATa GAL2 ura3-52 leu2-3,112 pdi1Δ::KanMX* [pCS213]	(Vitu, et al., 2010)
CSY795	*MATa GAL2 ura3-52 leu2-3,112 pdi1Δ::KanMX* [pSK65]	This study
CSY796	*MATa GAL2 ura3-52 leu2-3,112 pdi1Δ::KanMX* [pCS463]	This study
CSY802	*MATalpha GAL2 ura3-52 leu2-3,112 sil1Δ::KanMX pdi1Δ::KanMX* [pCS213]	This study
CSY803	*MATalpha GAL2 ura3-52 leu2-3,112 sil1Δ::KanMX pdi1Δ::KanMX* [pSK65]	This study
CSY804	*MATalpha GAL2 ura3-52 leu2-3,112 sil1Δ::KanMX pdi1Δ::KanMX* [pCS463]	This study
CSY901	*MATalpha GAL2 ura3-52 leu2-3,112 sil1Δ::KanMX pdi1Δ::KanMX* [pCS465]	This study
CSY902	*MATalpha GAL2 ura3-52 leu2-3,112 sil1Δ::KanMX pdi1Δ::KanMX* [pCS465]	This study
CSY928	*MATa GAL2 ura3-52 leu2-3,112 pdi11-31*	This study
CSY936	*MATa GAL2 ura3-52 leu2-3,112 pdi11-31 sil1Δ::KanMX*	This study

followed by counterselection of pCS213 with 5-FOA. To construct CSY936, CSY928 was crossed with CSY448.

Generation of temperature sensitive pdi1 alleles

To generate a temperature sensitive (TS) PDI, we screened a library of randomly mutagenized *PDI1* genes and selected clones that were unable to support growth as the only copy of PDI at 37˚C. The mutagenized library was made via an error-prone PCR approach using *pdi1-C406A-C409A* gene (pCS464) as template for the PCR. We elected to use a mutant lacking one of the two PDI active site as we reasoned this would eliminate a possible need to inactivate

both active sites which may increase the frequency of obtaining TS mutations. Importantly, pCS464 supports strain growth at 37˚C. The PCR product was amplified using 0.5 µM of PDI1_A primer (GTCGTTATTGTTATTTCCCGTTTT) to replicate the forward strand and 0.5 µM of T7 primer (TAATACGACTCACTATAGGG) to amplify the reverse strand. The reaction was carried out in the presence of 1x Taq buffer Mg free (BioLabs), 7 mM $MgCl_2$, 0.2 mM $MnCl_2$, 0.2 mM dGTP and dATP, 1 mM dTTP and dCTP, and 50 U/mL Taq (BioLabs). Initial denaturation was carried out at 94˚C for 2 minutes followed by 28 cycles of denaturation at 94˚C for 1.5 minutes, annealing at 57˚C for 2 minutes and extension at 72˚C for 3 minutes. A final extension was carried out at 72˚C for 10 minutes.

The mutagenized PCR was transformed into CSY125 along with the large fragment obtained from digestion of pCS464 with BamHI and SacII at an ~5:1 molar ratio. The transformed cells were shaken at room temperature overnight in YPD to allow for the mutagenized *pdi1* gene to recombine with the *LEU2* marked vector backbone from the digested pCS464. Transformants were then plated on S_{MM}-Leu and allowed to grow at 24˚C for several days. The colonies were frogged onto duplicate plates containing 5-FOA and left at 24˚C and 37˚C. Clones that supported growth at 24˚C, but not 37˚C were selected and the plasmids were isolated. The mutagenized *pdi1* genes were moved from the pRS315 vector into a pRS306 vector using KpnI and SacI sites in order to facilitate pop-in/pop-out integration of the TS alleles. The new plasmids were linearized by digestion with SpeI and transformed into CSY5. The cells were allowed to recover overnight in YPD at 24˚C and were then plated on S_{MM}-URA plates to select for clones that integrated a mutagenized *pdi1* gene. The obtained colonies were grown overnight in YPD at 24˚C to allow for pop-out of recombined *URA3*-marked wild-type genes. The cells

were then frogged onto duplicate YPD plates left at 24˚C and 37˚C, and a clone alive at the permissive temperature but dead at the restrictive temperature was selected as CSY928.

Yeast growth conditions

Cultures were grown in rich medium (1% Bacto-yeast extract and 2% Bacto-peptone containing 2% dextrose; YPD) or minimal medium (0.67% nitrogen base without amino acids supplemented with 16 amino acids not including cysteine) containing 2% dextrose (SMM), 2% galactose (SMM Gal) or 2% raffinose (SMM Raf). Uracil or leucine supplements were removed from minimal media to select for plasmids as needed. Methionine was omitted from media when cells were grown for metabolic labeling experiments.

Protein expression and purification

His_6-tagged Sil1 proteins were purified as previously described (Siegenthaler et al., 2017). His_6-SUMO tagged proteins were expressed into BL21 (DE3) and grown overnight at 37˚C in Luria-Bentani (LB) media containing 15 µg/mL kanamycin. The following day, cultures were diluted 100-fold into LB + Kan and were grown at 37˚C until an OD_{600} of ~1.0 was reached. At this point, the cultures were shifted to 18˚C and 0.5 mM isopropyl-b-D-thiogalactopyranoside (IPTG) was added to induce protein expression. Cells were harvested 16-20 hours post-induction and cell pellets were stored at -80˚C until purification. Cell pellets were thawed and solubilized in 20 mL of lysis buffer [20 mM HEPES, pH 8, 0.5 M NaCl, 10 mM Imidazole, 10% glycerol with EDTA-free protease inhibitor (Pierce), 1 mM betamercaptoethanol (BME), benzonase (Pierce) and 20 mg lysozyme (VWR)] per liter of harvested cells. The suspension was sonicated, and insoluble material was removed by centrifugation at 23,700 g for

30 minutes at 4˚C. Soluble material was loaded onto a HiTrap chelating column (GE Healthcare) charged with nickel. The column was washed with 40 column volumes of wash buffer 1 (20 mM HEPES, pH 7.4, 0.5 M NaCl, 10 mM imidazole, 10% glycerol) and 20 cv of wash buffer 2 (20 mM HEPES, pH 7.4, 0.5 M NaCl, 20 mM imidazole, 10% glycerol). The protein was eluted with elution buffer (20 mM HEPES, pH 7.4, 0.5 M NaCl, 0.5 M imidazole, 10% glycerol) and fractions containing protein were pooled. To cleave the SUMO tag, 50 µg/mL ULP was added to the pooled protein and the sample was dialyzed against dialysis buffer (20 mM HEPES, pH 7.4, containing 0.5 M NaCl, 10% glycerol) for at least 4 hours at 4˚C to dilute the imidazole. The sample was run over a HiTrap chelating column charged with nickel again to separate ULP and the cleaved His_6-SUMO tag from the prep. To ensure purification of the apo form of BiP, BiP preps only were loaded onto a HiTrap Blue HP (GE Healthcare) column and washed with low salt buffer (20 mM HEPES, pH 7.4, 10% glycerol) for five cv and then eluted with wash buffer 1. Cleaved, BiP, PDI and Sil1 proteins were run over a HiLoad™ 16/60 Superdex 200 pg (GE Healthcare) equilibrated with freshly made gel filtration buffer (20 mM HEPES, 0.1 M NaCl, 10 mM TCEP, pH 7.4) and protein were exchanged into desalting buffer (10 mM Tris-HCl pH 7.4, 50 mM NaCl, 10% glycerol) using a PD-10 column (GE Helathcare). Protein was concentrated to ~20-40 mg/mL using a vivaspin-15 (GE Healthcare) or an Ultra-4centrifugal filter (Amicon) and was flash frozen in liquid nitrogen before storage at -80˚C. Concentrations were determined by BCA protein assay (Thermo Fisher Scientific) using bovine serum albumin as a standard.

Sil1 mixed disulfide detection

CSY448, CSY804, CSY901 and CSY902 transformed with pKS65, pKS68, pKS69 or pCS922 were grown overnight at 30˚C in S_{MM}-Ura-Met. The following day, cells were diluted

into fresh media and grown to mid-log phase at 30˚C. Cells (10 OD_{600} equivalents) were pelleted and then suspended in 1 mL of media containing 30 µCi/OD_{600} equivalent of S^{35}-labeled cysteine methionine and incubated at room temperature for two hours. Cells were again pelleted and washed with 1 mL of 10% TCA. Cell pellets were suspended in 100 µL of 10% TCA and zirconium beads added. The cells were lysed with a FastPrep 24 instrument (MP Biomedical) and samples were diluted with 1 mL of 10% TCA. The suspension was transferred to a new tube and protein was precipitated by centrifugation at 21,000 x g form 10 minutes. Pellets were washed once with 1 mL of 5% TCA and twice with 1 mL of ethanol. Pellets were allowed to dry for 30 minutes at room temperature and were then suspended in 100 µL sample buffer containing 0.1 M NEM and complete ultra protease inhibitor cocktail (Roche). Sample were rotated at room temperature for 30 minutes before 1 mL of IP buffer (50 mM Tris-HCl, pH 7.4, 0.15 M NaCl, 1% Triton-X-100) was added and samples were rotated for an additional 15 minutes. Insoluble material was pelleted and the supernatant was added to 30 µL of 50% anti-FLAG M2 bead slurry (Sigma-Aldrich). Samples were rotated for one hour at room temperature and washed three times with IP buffer and once with IP buffer lacking detergent. Protein was eluted by the addition of 50 µL 2xESB followed by boiling for 5 minutes at 100˚C. For secondary immunoprecipitations, the samples were diluted again in 1 mL of IP buffer and immunoprecipitated with anti-PDI serum and SureBeads™ Protein A Magnetic Beads. Beads were washed as before and eluted with 50 µL of 2xESB. For reducing samples, 5% BME was added. Proteins separated by SDS-PAGE and the gel was dried onto a sheet of filter paper. Protein signal was detected with a phosphorimager.

Determination of BiP redox state

CSY5, CSY448, CSY928, and CSY936 were grown to mid-log phase at 24˚C in YPD. One set of samples were shaken for the final hour in a 37˚C water bath to allow for time to inactivate temperature sensitive PDI. Cells (10 OD_{600} equivalents) were harvested and washed immediately in 10% TCA. Cell pellets were suspended in 100 µL of 10% TCA and zirconium beads added. The cells were lysed with a FastPrep 24 5G instrument (MP Biomedical) and samples were diluted with 1 mL of 10% TCA. The suspension was transferred to a new tube and proteins were precipitated by centrifugation at 21,000 x g for 10 minutes at 4˚C. Pellets were washed with 1 mL of 5% TCA followed by 1 mL of ethanol before resuspension in cysteine modification buffer (CMBU) (0.1M HEPES-NaOH, pH 7.4, 1% SDS, 10 mM DTPA, 6 M Urea) containing 0.1 M NEM and complete ultra protease inhibitor cocktail (Roche). Samples were incubated at room temperature for 30 minutes before the addition of 1% BME to reduce oxidized cysteines. Proteins were again precipitated by the addition of 10% TCA followed by incubation on ice for 5 minutes and centrifugation as described above. Pellets were washed twice with 1 mL of ethanol before resuspension in 100 µL of CMBU containing 1 mM maleimide-PEG (mal-PEG2K: Lysan Bio Inc.). Samples were vortexed at room temperature for 30 minutes before an equal volume of sample buffer containing 10% BME was added. Proteins were separated by SDS-PAGE, transferred to nitrocellulose and probed with Kar2 (BiP) antiserum (RRID:AB_2636950) followed by an Alexa Fluor 488 conjugated anti-rabbit IgG (RRID:AB_2535792). For mobility controls, samples were prepared with the omission of either NEM or PEG-maleimdie to indicate the maximum and minimum shifts for BiP. For glucose-mediated depletion of PDI, CSY795, CSY796, CSY803 and CSY804 were grown on plates

containing galactose at 30˚C. Cells were diluted into S_{MM}-Leu and grown to mid-log phase (16 hours) at 30˚C. Cells were then harvested and BiP oxidation was assayed as described above.

In vitro reduction assays

Sil1 and PDI were oxidized or reduced by reaction of 50 µM protein with 10 mM diamide or 10 mM DTT respectively for one hour at room temperature. Modified proteins were desalted and exchanged into assay buffer (10 mM Tris-HCl, pH 8.0, 50 mM NaCl, 1 mM EDTA) using a NAP-5 column (GE Healthcare) that had been equilibrated with assay buffer. For gel-based based redox assays, 5 µM PDI and Sil1 were mixed in assay buffer and at the indicated timepoints, an equal volume of sample buffer containing 2 mM MM(PEG)12 (Thermo Fisher Scientific). Samples were incubated for 30 minutes at room temperature before 5% BME was added to stop further reaction of the maleimide. Proteins were resolved by SDS-PAGE and gels were visualized with Coomassie blue.

For BiP reduction assays, 50 µM BiP was reacted with 1 mM DTNB or 10 mM diamide and 1.4 mM GSH for one hour at room temperature. Oxidized BiP was desalted into assay buffer using a NAP-5 column (GE Healthcare). BiP-TNB reduction was monitored by following the change in absorbance at 412 nm with a Beckman Coulter DU730 UV/Vis spectrophotometer. Samples containing 0.25 µM PDI, 0.25 µM thioredoxin reductase (Sigma-Aldrich), 200 µM NADPH in assay buffer, and reactions were started with the addition of 5 µM BiP-TNB. Glutathionylated BiP reduction was monitored in a similar way except reactions were stopped at different times by the addition of an equal volume of sample buffer containing 2 mM MM(PEG)12 (Thermo Fisher Scientific). Samples were resolved by SDS-PAGE, and gels were visualized with Coomassie blue.

To monitor Sil1 reduction by glutathione and PDI, Sil1 was diluted to 20 µM in assay buffer. The samples were then diluted 10-fold with the addition of assay buffer containing 10 mM GSH, 10 mM GSH and 25 µM PDI or 10 mM DTT to provide reduced mobility standards. Reactions were carried out for one hour at room temperature before ice cold 10% TCA was added, and protein was precipitated for 30 minutes at 4˚C. Protein was pelleted by centrifugation at 21,00 x g for 15 minutes at 4˚C. Pellets were washed gently with ice-cold acetone and were then suspended in 1x ESB containing 1 M Urea and 2 mM MM(PEG)12 (Thermo Fisher Scientific). Samples were vortexed for 30 minutes before the addition of 5% BME to prevent further reaction of the maleimide. Proteins were separated by SDS-PAGE, transferred to nitrocellulose and probed with Sil1 antiserum (RRID:AB_2636949) followed by an Alexa Fluor 488 conjugated anti-rabbit IgG (RRID:AB_2535792)

Reduction potential measurements

Purified Sil1-C203A-C373A (pKS258) was diluted to 20 µM in reduction potential buffer (100 mM sodium phosphate, pH 7.0, 300 mM NaCl, 1 mM EDTA). The proteins were further diluted 10-fold in assay buffer containing varied ratios of oxidized and reduced DTT so that the final DTT concentration was always 0.1 M. The samples were allowed to equilibrate for one hour at room temperature before 1 mL of ice cold 10% TCA was added and protein was precipitated for 30 minutes at 4˚C. The samples were then centrifuged at 21,000 x g for 15 minutes at 4˚C. Pellets were gently washed once with ice cold acetone and were then suspended in 1x ESB containing 1 M Urea and 2 mM MM(PEG)12 (Thermo Fisher Scientific). Samples were vortexed for 30 minutes before the addition of 5% BME to prevent further reaction of the maleimide. Samples were resolved by SDS-PAGE and visualized with a ChemiDoc MP System

(Bio-Rad) and the relative abundance of the oxidized and reduced forms were quantified using the device's software. The mean fraction of oxidized protein plotted against the ratio of reduced to oxidized DTT, and the data were fit with a one-phase decay curve. The K_{OX} was determined from the reported half-life of the curve. The reduction potential was calculated using the Nernst equation (**Equation 3.1**) with an E_{NADP} value of -327 mV and K_{GR} and K_{DTT} values of 800 M and 260 M respectively (Gilbert, 1997).

Equation 3.1

$$E_{Sil1} = E_{NADP} - \frac{R\,T}{n\,F} \ln\left(\frac{K_{OX} - K_{DTT}}{K_{GR}}\right)$$

REFERENCES

Appenzeller-Herzog, C., Riemer, J., Zito, E., Chin, K. T., Ron, D., Spiess, M. et al. (2010). Disulphide production by Ero1α-PDI relay is rapid and effectively regulated. *EMBO J*, *29*(19), 3318-3329.

Behnke, J., Feige, M. J., & Hendershot, L. M. (2015). BiP and its nucleotide exchange factors Grp170 and Sil1: mechanisms of action and biological functions. *J Mol Biol*, *427*(7), 1589-1608.

Chai, Y. C., Ashraf, S. S., Rokutan, K., Johnston, R. B., & Thomas, J. A. (1994). S-thiolation of individual human neutrophil proteins including actin by stimulation of the respiratory burst: evidence against a role for glutathione disulfide. *Arch Biochem Biophys*, *310*(1), 273-281.

Chakravarthi, S., Jessop, C. E., & Bulleid, N. J. (2006). The role of glutathione in disulphide bond formation and endoplasmic-reticulum-generated oxidative stress. *EMBO Rep*, *7*(3), 271-275.

Cuozzo, J. W., & Kaiser, C. A. (1999). Competition between glutathione and protein thiols for disulphide-bond formation. *Nat Cell Biol*, *1*(3), 130-135.

Frand, A. R., & Kaiser, C. A. (1998). The ERO1 gene of yeast is required for oxidation of protein dithiols in the endoplasmic reticulum. *Mol Cell*, *1*(2), 161-170.

Frand, A. R., & Kaiser, C. A. (1999). Ero1p oxidizes protein disulfide isomerase in a pathway for disulfide bond formation in the endoplasmic reticulum. *Mol Cell*, *4*, 469-477.

Gilbert, H. F. (1997). Thiol/disulfide exchange and redox potential of proteins. In G. Lenaz & G. Milazzo (Eds.), *Bioelectrochemistry of Biomacromolecules1997* (pp. 256-324). Birkauser Verlag Basel.

Gross, E., Sevier, C. S., Heldman, N., Vitu, E., Bentzur, M., Kaiser, C. A. et al. (2006). Generating disulfides enzymatically: reaction products and electron acceptors of the endoplasmic reticulum thiol oxidase Ero1p. *Proc Natl Acad Sci U S A*, *103*(2), 299-304.

Hatahet, F., & Ruddock, L. W. (2007). Substrate recognition by the protein disulfide isomerases. *FEBS J*, *274*(20), 5223-5234.

Hwang, C., Sinskey, A. J., & Lodish, H. F. (1992). Oxidized redox state of glutathione in the endoplasmic reticulum. *Science*, *257*(5076), 1496-1502.

Inaba, K., & Ito, K. (2002). Paradoxical redox properties of DsbB and DsbA in the protein disulfide-introducing reaction cascade. *EMBO J*, *21*(11), 2646-2654.

Kim, S., Sideris, D. P., Sevier, C. S., & Kaiser, C. A. (2012). Balanced Ero1 activation and inactivation establishes ER redox homeostasis. *J Cell Biol*, *196*(6), 713-725.

Korovila, I., Hugo, M., Castro, J. P., Weber, D., Höhn, A., Grune, T. et al. (2017). Proteostasis, oxidative stress and aging. *Redox Biol*, *13*, 550-567.

Kozlov, G., Määttänen, P., Thomas, D. Y., & Gehring, K. (2010). A structural overview of the PDI family of proteins. *FEBS J*, *277*(19), 3924-3936.

Le Moan, N., Tacnet, F., & Toledano, M. B. (2008). Protein-thiol oxidation, from single proteins to proteome-wide analyses. *Methods Mol Biol*, *476*, 181-198.

Määttänen, P., Gehring, K., Bergeron, J. J., & Thomas, D. Y. (2010). Protein quality control in the ER: the recognition of misfolded proteins. *Semin Cell Dev Biol*, *21*(5), 500-511.

Mezghrani, A., Fassio, A., Benham, A., Simmen, T., Braakman, I., & Sitia, R. (2001). Manipulation of oxidative protein folding and PDI redox state in mammalian cells. *EMBO J*, *20*(22), 6288-6296.

Nørgaard, P., Westphal, V., Tachibana, C., Alsøe, L., Holst, B., & Winther, J. R. (2001). Functional differences in yeast protein disulfide isomerases. *J Cell Biol*, *152*(3), 553-562.

Oka, B. V. O., & Bulleid, N. J. (2018). Disulfide Bond Formationin the Endoplasmic Reticulum. In M. J. Feige (Ed.), *Oxidative Folding of Proteins: Basic Principles, Cellular Regulationa nd Engineering. Vol. 9* (pp. 306-333). Royal Society of Chemistry.

Pace, C. N., Grimsley, G. R., Thomson, J. A., & Barnett, B. J. (1988). Conformational stability and activity of ribonuclease T1 with zero, one, and two intact disulfide bonds. *J Biol Chem*, *263*(24), 11820-11825.

Pareja, K. A., & Sevier, C. S. (in preparation). Auto-inhibition of Sil1 nucleotide exchange factor activity through a conserved N-terminal region.

Raturi, A., & Mutus, B. (2007). Characterization of redox state and reductase activity of protein disulfide isomerase under different redox environments using a sensitive fluorescent assay. *Free Radic Biol Med*, *43*(1), 62-70.

Rosam, M., Krader, D., Nickels, C., Hochmair, J., Back, K. C., Agam, G. et al. (2018). Bap (Sil1) regulates the molecular chaperone BiP by coupling release of nucleotide and substrate. *Nat Struct Mol Biol*, *25*(1), 90-100.

Rudyk, O., & Eaton, P. (2014). Biochemical methods for monitoring protein thiol redox states in biological systems. *Redox Biol*, *2*, 803-813.

Sevier, C. S., & Kaiser, C. A. (2006). Disulfide transfer between two conserved cysteine pairs imparts selectivity to protein oxidation by Ero1. *Mol Biol Cell*, *17*(5), 2256-2266.

Sevier, C. S., Qu, H., Heldman, N., Gross, E., Fass, D., & Kaiser, C. A. (2007). Modulation of cellular disulfide-bond formation and the ER redox environment by feedback regulation of Ero1. *Cell*, *129*(2), 333-344.

Shimizu, Y., & Hendershot, L. M. (2009). Oxidative folding: cellular strategies for dealing with the resultant equimolar production of reactive oxygen species. *Antioxid Redox Signal*, *11*(9), 2317-2331.

Siegenthaler, K. D., Pareja, K. A., Wang, J., & Sevier, C. S. (2017). An unexpected role for the yeast nucleotide exchange factor Sil1 as a reductant acting on the molecular chaperone BiP. *Elife*, *6*.

Sikorski, R. S., & Hieter, P. (1989). A system of shuttle vectors and yeast host strains designed for efficient manipulation of DNA in Saccharomyces cerevisiae. *Genetics*, *122*(1), 19-27.

Tian, G., Xiang, S., Noiva, R., Lennarz, W. J., & Schindelin, H. (2006). The crystal structure of yeast protein disulfide isomerase suggests cooperativity between its active sites. *Cell*, *124*(1), 61-73.

Tu, B. P., Ho-Schleyer, S. C., Travers, K. J., & Weissman, J. S. (2000). Biochemical basis of oxidative protein folding in the endoplasmic reticulum. *Science*, *290*(5496), 1571-1574.

Tu, B. P., & Weissman, J. S. (2002). The FAD- and O(2)-dependent reaction cycle of Ero1-mediated oxidative protein folding in the endoplasmic reticulum. *Mol Cell*, *10*(5), 983-994.

Tu, B. P., & Weissman, J. S. (2004). Oxidative protein folding in eukaryotes: mechanisms and consequences. *J Cell Biol*, *164*(3), 341-346.

Vitu, E., Kim, S., Sevier, C. S., Lutzky, O., Heldman, N., Bentzur, M. et al. (2010). Oxidative activity of yeast Ero1p on protein disulfide isomerase and related oxidoreductases of the endoplasmic reticulum. *J Biol Chem*, *285*(24), 18155-18165.

Walker, K. W., Lyles, M. M., & Gilbert, H. F. (1996). Catalysis of oxidative protein folding by mutants of protein disulfide isomerase with a single active-site cysteine. *Biochemistry*, *35*(6), 1972-1980.

Wang, J., Pareja, K. A., Kaiser, C. A., & Sevier, C. S. (2014). Redox signaling via the molecular chaperone BiP protects cells against endoplasmic reticulum-derived oxidative stress. *Elife*, *3*, e03496.

Wang, J., & Sevier, C. S. (2016). Formation and Reversibility of BiP Protein Cysteine Oxidation Facilitate Cell Survival during and post Oxidative Stress. *J Biol Chem*, *291*(14), 7541-7557.

Wilkinson, B., & Gilbert, H. F. (2004). Protein disulfide isomerase. *Biochim Biophys Acta*, *1699*(1-2), 35-44.

Yan, M., Li, J., & Sha, B. (2011). Structural analysis of the Sil1-Bip complex reveals the mechanism for Sil1 to function as a nucleotide-exchange factor. *Biochem J*, *438*(3), 447-455.

Yang, J., Nune, M., Zong, Y., Zhou, L., & Liu, Q. (2015). Close and Allosteric Opening of the Polypeptide-Binding Site in a Human Hsp70 Chaperone BiP. *Structure*, *23*(12), 2191-2203.

CHAPTER 4

CONCLUSIONS AND FUTURE DIRECTIONS

SUMMARY OF FINDINGS

The works presented here describe the mechanisms by which the Hsp70 chaperone, BiP, is regulated in response to the fluctuating redox environment of the endoplasmic reticulum (ER). I build upon the previous finding that a cysteine residue in *S. cerevisiae* BiP is oxidized in response to peroxide production. Oxidation of this cysteine decouples BiP peptide binding from the nucleotide hydrolysis cycle that ordinarily governs BiP activity; the modified peptide binding properties increase cell tolerance to oxidative stress (Wang, Pareja, Kaiser, & Sevier, 2014; Wang & Sevier, 2016; Sevier, 2018). Specifically, I have identified roles for the BiP NEF, Sil1, and protein disulfide isomerase (PDI) in reducing BiP, which reestablishes a coordinated chaperone nucleotide hydrolysis and peptide binding cycle (**Figure 4.1**). While the modified activity of oxidized BiP imparts a resistance to oxidative stress, it also decreases competitive fitness under non-stressed conditions necessitating a reliable means for matching BiP oxidation to the luminal redox status (Wang et al., 2014; Wang & Sevier, 2016; Sevier, 2018). My data illuminate the pathways for reversal of BiP oxidation and identify the infrastructure that matches BiP oxidation to the ER redox status.

In Chapter 2, I demonstrated a correlation between the oxidation state of BiP and the ability of the chaperone to interact with its nucleotide exchange factor Sil1. Upon deletion of *SIL1*, I detected increased levels of oxidized BiP in cells and a correspondent increase in resistance to oxidative stress. Following up on this finding, I identified a catalytic cysteine pair

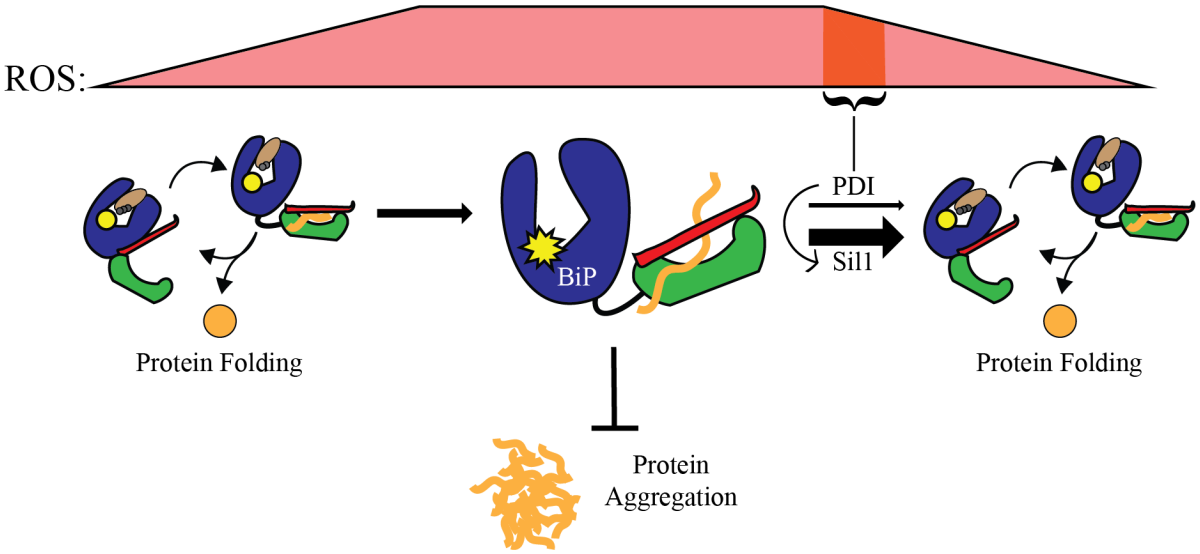

Figure 4.1. Regulation of BiP activity in response to fluctuating ER ROS levels. In the absence of high levels of ROS, BiP peptide binding activity is coupled to progression through a nucleotide hydrolysis cycle enabling BiP to function as a protein chaperone. Upon ROS accumulation, a cysteine residue in BiP is oxidized decoupling nucleotide hydrolysis and peptide binding. Oxidation causes BiP to bind peptides with constitutively high affinity mitigating proteotoxic effects of ROS. Once ROS levels decrease, PDI drives reduction of BiP (either directly or via reduction of the BiP-reductant, Sil1) to reestablish non-stressed BiP function.

located in the N terminus that was able to directly reduce BiP *in vitro*. This reduction restored progression through the BiP ATPase cycle and the associated peptide binding properties. Notably, yeast containing a cysteine-less Sil1 mutant as the only copy of Sil1 still maintain the ability to reduce BiP. These data suggest that the role of Sil1 in regulating BiP oxidation extends beyond the ability of the NEF to directly reduce the chaperone using its N-terminal cysteines. Alternatively, compensatory pathways may exist in a cysteine-less Sil1 mutant strain that allow for BiP reduction, and these pathways may be less active in a *sil1*Δ strain, where the capacity for BiP reduction is more severely compromised.

In Chapter 3, I described the identification of PDI as a mediator that acts to match BiP oxidation to the ER redox state. PDI was found to be an interactor of Sil1 leading us to hypothesize that PDI reduces Sil1 (thus activating the NEF as a BiP-reductant). In support of

this, PDI is able to drive reduction of the Sil1 catalytic cysteines in the presence of excess glutathione, which provides a continuous source of electrons. Furthermore, temporary inactivation of PDI in cells yielded increased levels of oxidized BiP. Surprisingly, I also demonstrated the ability of PDI to reduce BiP *in vitro* suggesting that PDI catalyzes the reduction of BiP through redundant pathways.

FUTURE DIRECTIONS

Distinguish the cysteine-dependent and cysteine-independent roles of Sil1 in regulating BiP

The data presented in Chapters 2 and 3 hint that Sil1 regulates BiP oxidation through multiple mechanisms. A complete understanding of the BiP-centric oxidative stress response therefore requires elucidation of all means by which Sil1 controls the redox state of BiP. Identification of these redundant pathways will further reveal how cells reverse BiP oxidation, provide insight on the physiological conditions when BiP oxidation is no longer and may help explain how BiP oxidation is misregulated in diseased cells.

While my *in vitro* data show that reduction of BiP is dependent on an N-terminal cysteine pair within Sil1, my *in vivo* data suggest Sil1 may also regulate BiP reduction through a cysteine-independent mechanism. In Chapter 2, I showed oxidized BiP accumulated in cells where *SIL1* has been deleted, but mutation of Cys-52 and Cys-57 did not yield the equal levels of BiP oxidation as was observed in the Δ*sil1* strain (data not shown). This implies that Sil1 mediates BiP reduction through a means not involving the N-terminal catalytic cysteines. Moreover, *sil1*Δ cells display enhanced resistance to the small molecule oxidant diamide relative to a wild type strain, which correlates with the increased levels of oxidized BiP observed in Δ*sil1* cells. Yet *sil1-C52A-C57A* cells showed the same sensitivity to diamide as wild-type cells again suggesting the Sil1 cysteines are not the only factor that causes BiP reduction. These data are puzzling because the diamide resistance imparted from deletion of *SIL1* is largely abrogated if the redox-sensitive cysteine of BiP is mutated to alanine indicating that the stress resistance acquired from loss of Sil1 does result from increased oxidation of BiP (**Chapter 2**). Together, these data support the importance of Sil1 in reduction of BiP and suggest the existence of unknown roles of Sil1 in regulation of BiP.

I believe the apparently conflicting data concerning the reducing activity of the Sil1 N-terminal cysteines likely result from the presence of redundant pathways through which Sil1 regulates BiP oxidation. While the C52/C57 pair may be critical to reverse BiP modification *in vitro*, the presence of unknown cellular factors may allow for reduction of BiP in the presence of Sil1. A cocrystal structure of the armadillo-repeat core of Sil1 bound to the BiP NBD suggests that Sil1 binding facilitates opening of the BiP NBD (Yan, Li, & Sha, 2011). This structural rearrangement would likely impact the accessibility of the oxidized cysteine within BiP and allow for another reductant to act upon the BiP cysteine. Thus, Sil1 binding may facilitate BiP reduction by either PDI or glutathione. While it may be difficult to identify unknown factors that could reduce BiP in the presence of Sil1, I intend to test candidates *in vitro*. Observation of increased BiP-reduction rates by GSH or PDI in the presence of a reductant-dead Sil1 would provide support for my hypothesis.

It is also possible that Sil1 NEF function indirectly impacts the redox state of BiP by maintaining ER proteostasis. Lhs1 can compensate for loss of Sil1 at least partially as *SIL1* is not essential in either yeast or humans (Bracher & Verghese, 2015; Behnke, Feige, & Hendershot, 2015), but it stands to reason that BiP-mediated protein folding will not be optimal in the absence of one NEF. Although I have not observed that deletion of Sil1 or mutation of Sil1 cysteines activates the unfolded protein response (UPR) in yeast (**Figure 4.2**), the UPR is activated in a $Sil1^{GT}$ mouse. Disruption of protein folding and subsequent activation of the UPR could potentially alter levels of oxidized BiP. Multiple redox signals act upstream of UPR activation, and correspondingly, many UPR outputs aim to alter the ER redox state (reviewed in

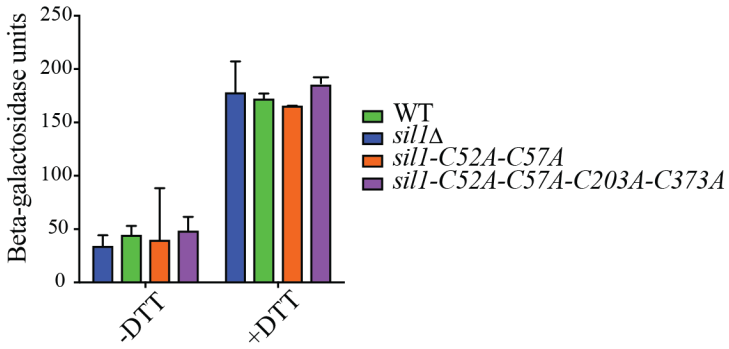

Figure 4.2. Loss of Sil1 or Sil1 cysteines does not affect UPR activation in *S. cerevisiae*. CSY448 transformed with pRS315, pHS116, pKS24 or pCS923 and a UPRE-lacZ reporter (pCS852) were grown to mid-log phase in SMM at 30˚C. For UPR activation controls, 2 mM DTT was added to the cells for the final 2.5 hours of growth. Beta galactosidase activity was measured as described in (Guarente, 1983). Error bars depict standard deviation of duplicate transformants.

Eletto et al., 2014). For instance, NADPH oxidases, which produce ROS, are induced by the UPR and lead to a more oxidizing environment, but glutathione synthesis enzymes that yield a more reducing environment also are upregulated by the UPR (Eletto, Chevet, Argon, & Appenzeller-Herzog, 2014). Moreover, Ero1 and PDI are both UPR targets (Frand & Kaiser, 1998; Wilkinson & Gilbert, 2004). Thus, increased levels of peroxide generated by Ero1 could cause BiP oxidation, but increased levels of PDI could result in more efficient reduction of BiP. While the existence of both oxidizing and reducing functions of the UPR likely allow for nuanced regulation of the ER redox poise, the seemingly contradictory UPR outputs make it difficult to predict exactly how UPR activation will affect BiP oxidation. Nevertheless, it remains possible that loss of Sil1 NEF activity influences the redox state of BiP in some organisms.

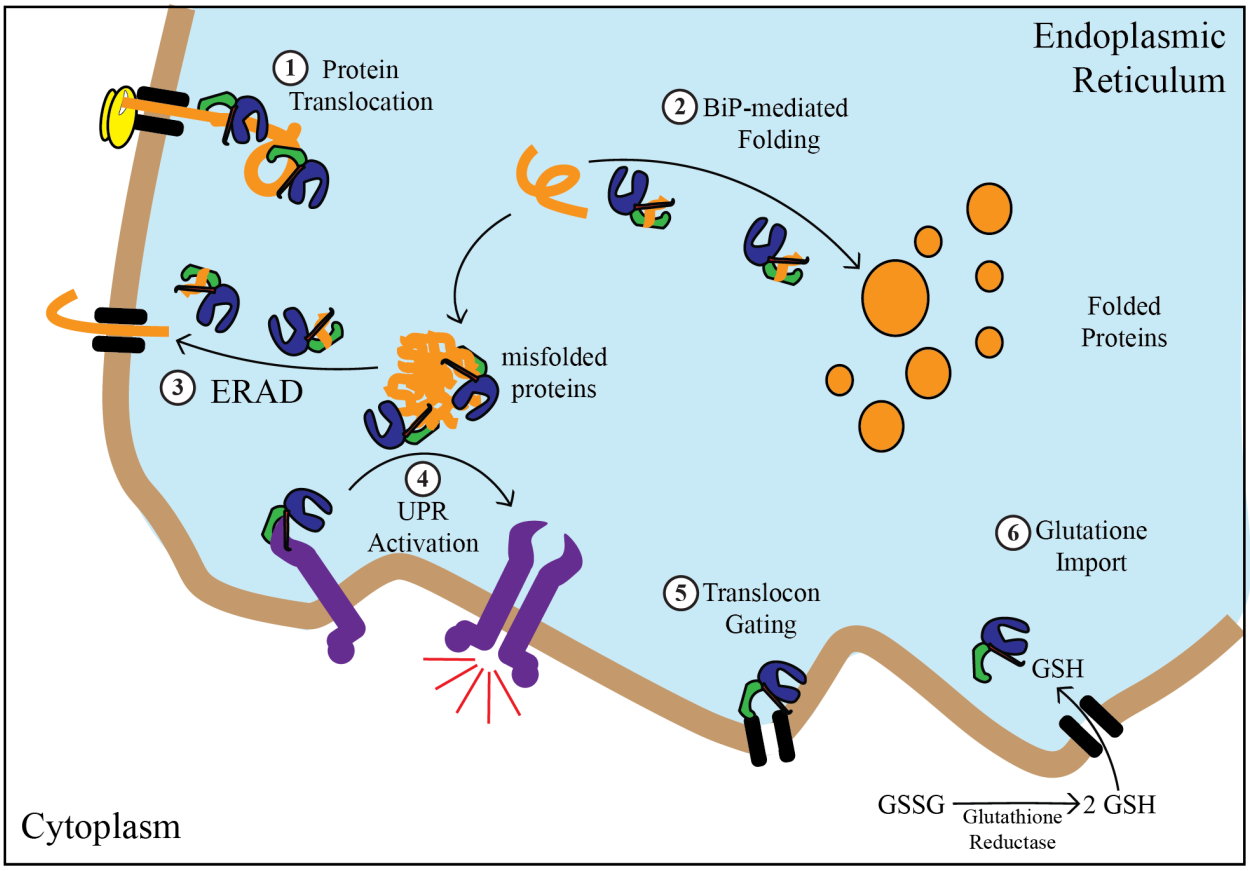

Figure 4.3. Potentially redox regulated BiP functions. The peptide binding properties of BiP enable the chaperone to regulate a variety of processes in the ER lumen (reviewed in (Hendershot, 2004) and discussed in Chapter 1). (1) BiP assists with the translocation of proteins into the ER lumen. (2) BiP acts as a chaperone and folds translocated peptides. (3) BiP delivers misfolded peptides for retrotranslocation into the cytosol. ERAD: ER-associated degradation (4) BiP allows for activation of UPR transmitters in response to unfolded protein accumulation. (5) BiP binds to channels in the ER membrane to regulate exchange of molecules between the ER and cytosol. (6) BiP binding to the translocon regulates GSH diffusion into the ER lumen (Ponsero et al., 2017).

Determine the effects of BiP oxidation on global ER function

BiP is involved in many processes that maintain ER homeostasis (**Figure 4.3**), but it remains to be tested how oxidation of the chaperone affects most of these functions. Aside from acting as a chaperone, BiP has also been shown to play roles in facilitating the translocation of substrates into the ER, assisting with the export of terminally misfolded proteins to the cytosol,

maintaining the permeability barrier of the ER and regulating activation of the unfolded protein response (Hamman, Hendershot, & Johnson, 1998; Gething, 1999; Kimata et al., 2003; Gething, 1999; Dudek et al., 2009; Walter & Ron, 2011; Clerico, Tilitsky, Meng, & Gierasch, 2015) (**Figure 4.3**). To fully understand the protective effects of this post-translational modification, it must be determined how all BiP-governed processes are influenced by BiP oxidation. It has been proposed that the enhanced "holdase" activity of oxidized BiP benefits the cell by mitigating protein aggregation during oxidative stress (Wang et al., 2014; Wang & Sevier, 2016), but all BiP activities rely on the peptide binding properties of the chaperone (Behnke, Feige, & Hendershot, 2015). It therefore stands to reason that all BiP activities could be changed by the modified peptide binding properties induced by BiP oxidation.

BiP has been shown to play a key role in gating the translocon through which peptides are imported into the ER (Hendershot, 2004). The chaperone binds to the luminal side of the pore and serves as a physical barrier preventing the passage of proteins or other molecules into the ER lumen (Vogel, Misra, & Rose, 1990; Hamman et al., 1998). Thus, the increased peptide binding properties caused by oxidation would likely block the efflux of molecules into the lumen. In support of this, multiple lines of evidence suggest that BiP oxidation may influence the rate at which peptides are imported into the ER (Wang et al., 2014; Xu, Marsh, & Sevier, 2016). First, expression of BiP mutants which mimic the oxidized form of the chaperone results in the accumulation of untranslocated protein precursors in cells (Wang et al., 2014; Xu et al., 2016). Furthermore, the induction of high ROS levels using a hyperactive version of Ero1 (Ero1*) produces the same phenotype when the UPR is compromised (Sevier et al., 2007; Wang et al., 2014). Since Ero1*-induced oxidative stress has been shown to increase BiP oxidation (Wang et al., 2014), these data support the idea that oxidation of BiP causes a decrease protein flux into the

ER. This would decrease the folding burden placed on the ER chaperones thereby enhancing the cell's ability to cope with oxidative stress.

While a model in which oxidized BiP blocks the translocon and thereby decreases the ER folding burden is appealing, more direct evidence is needed to solidify this claim. The hypothesis can be assessed by tracking the import of multiple secreted proteins in cells experiencing oxidative stress. Furthermore, the uncovered roles of Sil1 and PDI in regulating BiP oxidation can be exploited to verify this hypothesis. For instance, I have demonstrated that Δ*sil1* cells display a striking lag in the reduction of BiP after stress (**Chapter 2**). If BiP oxidation does attenuate secretory protein import, deletion of *SIL1* should also slow the rate at which normal secretory protein import occurs after stress. Similarly, expression of PDI mutants possessing differing reduction potentials should impact the propensity of BiP to become oxidized or reduced, so such mutants also could be utilized to monitor the block of translocation.

Oxidized BiP has also been proposed to regulate glutathione homeostasis in the ER (Ponsero et al., 2017). Since the ER lacks a glutathione reductase, GSH is imported from the cytosol, and the translocon is thought to provide the channel through which GSH diffuses into the lumen (Ponsero et al., 2017). Similar to a model in which BiP oxidation attenuates protein import into the ER, BiP oxidation may also serve to regulate glutathione import from the cytosol. Consistent with this, BiP oxidation mimetic mutants have been shown to block the import of GSH into the ER (Ponsero et al., 2017). This is proposed to enhance the cell's ability to regulate the ER redox milieu by limiting the activation of the Ero1 thereby minimizing ROS production. To investigate this claim, the GSH:GSSG ratio of the ER should be monitored during recovery from oxidative stress. While mutation of PDI would likely affect the ER glutathione pool in

multiple ways because of its roles in oxidative protein folding and Ero1 regulation, assessment of the rate at which lumenal glutathione ratios recover in Sil1 mutants should be informative.

BiP also influences the protein folding capacity of the endoplasmic reticulum by its regulation of the UPR transmitters (Reviewed in Walter and Ron, 2011). In *S. cerevisiae*, the luminal domain of the UPR transmitter IRE1 is bound by BiP, which prevents activation of the UPR. Upon unfolded protein accumulation, BiP releases IRE1, allowing the transmitter to initiate UPR signaling (Walter & Ron, 2011). Metazoans contain two additional transmitters, PERK and ATF6, which are similarly repressed by BiP binding (Walter & Ron, 2011). The increased peptide affinity of oxidized BiP may increase the fraction of UPR transmitters bound by BiP and thereby decrease UPR signaling. As stated above, the UPR can lead to ROS production through multiple outputs (Eletto et al., 2014), so UPR dampening may be beneficial during oxidative stress. Alternatively, the increased abundance of unfolded proteins expected during oxidative stress may outcompete the UPR transmitter binding sites ultimately leading to UPR activation. Notably, UPR activation has been assessed in strains possessing BiP alleles where the redox-sensitive cysteine has been mutated to all other amino acids, and the majority of strains displayed an elevated UPR (Xu et al., 2016). The observed UPR induction may suggest BiP oxidation leads to increased activation of the UPR transmitters, but it also may reflect the decreased folding activity of the BiP mutants. Determining how loss of Sil1 reducing activity affects UPR activation may facilitate this process, but as noted earlier, this may be species specific. While UPR induction is observed in mice lacking Sil1(Ichhaporia et al., 2018), I have not observed UPR activation upon deletion of Sil1 in yeast (**Figure 4.2**).

Assess the conservation of BiP redox regulation

The studies presented here were exclusively conducted in the model organism *S. cerevisiae*, but I expect that redox regulation of BiP and the reductant activity of Sil1 are conserved in higher eukaryotes. The redox-sensitive cysteine in the BiP NBD is nearly universally conserved (Wang et al., 2014). Also, most mammalian Sil1 orthologs possess an N-terminal cysteine pair corresponding to the C52/C57 pair present in yeast (See Chapter 2 for BiP and Sil1 alignments). It has been reported that Cys-41 of human BiP can form an intramolecular disulfide bond with Cys-420 found within the BiP SBD (Wei et al., 2012). The authors showed that formation of the BiP disulfide bond is catalyzed by the glutathione peroxidase NPGPx in response to peroxide and demonstrated that oxidation enhances BiP chaperone activity (Wei et al., 2012). Thus, the conservation of prosurvival functions activated by oxidation of BiP seems likely. However, a more detailed characterization of BiP oxidation in mammals is necessary as are studies testing for reductant function in mammalian Sil1 orthologs.

It is interesting to speculate if loss of Sil1 reductant function impacts the progression of Sil1-associated pathologies. Sil1 mutations have been repeatedly linked to Marinesco-Sjögren syndrome (MSS) as well as cancer and amyotrophic lateral sclerosis (ALS) (Van Raamsdonk, 2006; Xu, Xu, Zhang, Xin, & Pang, 2018; Filézac de L'Etang et al., 2015). Progression of the disease has been assumed to stem from a loss of Sil1 NEF activity and the ensuing impairment of BiP chaperone function. However, inefficient reduction of BiP after oxidative stress also may jeopardize ER proteostasis and therefore result in disease symptoms. It may be informative to study how targeted disruption of BiP redox regulation impacts mammalian systems. For instance, functional deletion of *SIL1* causes mice to display a phenotype that resembles the symptoms of MSS (Zhao, Longo-Guess, Harris, Lee, & Ackerman, 2005; Ichhaporia et al., 2018). If

mutation of the BiP redox-sensitive cysteine or mutation of the Sil1 catalytic cysteines in mice yielded pups that display a similar phenotype, it may point to a role for Sil1 reductant activity MSS progression.

The works presented here establish a framework for the oxidative regulation of the ER chaperone BiP in *S. cerevisiae*. Going forward, more work will be necessary to dissect the overlapping roles of PDI and Sil1 in reversing BiP oxidation and to determine the effect oxidation has on the numerous BiP activities that regulate ER function. Also, while existing data provide optimism that redox regulation of BiP occurs in higher eukaryotes, the extent to which this post-translational modification is conserved and the potential impact improper oxidation of BiP plays in disease progression need further assessment. More broadly, I hope my findings will prompt further studies aimed to increase our understanding of endoplasmic reticulum redox homeostasis and to identify novel cellular regulatory mechanisms utilizing oxidative modification events.

REFERENCES

Behnke, J., Feige, M. J., & Hendershot, L. M. (2015). BiP and its nucleotide exchange factors Grp170 and Sil1: mechanisms of action and biological functions. *J Mol Biol*, *427*(7), 1589-1608.

Bracher, A., & Verghese, J. (2015). The nucleotide exchange factors of Hsp70 molecular chaperones. *Front Mol Biosci*, *2*, 10.

Clerico, E. M., Tilitsky, J. M., Meng, W., & Gierasch, L. M. (2015). How hsp70 molecular machines interact with their substrates to mediate diverse physiological functions. *J Mol Biol*, *427*(7), 1575-1588.

Dudek, J., Benedix, J., Cappel, S., Greiner, M., Jalal, C., Müller, L. et al. (2009). Functions and pathologies of BiP and its interaction partners. *Cell Mol Life Sci*, *66*(9), 1556-1569.

Eletto, D., Chevet, E., Argon, Y., & Appenzeller-Herzog, C. (2014). Redox controls UPR to control redox. *J Cell Sci*, *127*(Pt 17), 3649-3658.

Filézac de L'Etang, A., Maharjan, N., Cordeiro Braña, M., Ruegsegger, C., Rehmann, R., Goswami, A. et al. (2015). Marinesco-Sjögren syndrome protein SIL1 regulates motor neuron subtype-selective ER stress in ALS. *Nat Neurosci*, *18*(2), 227-238.

Frand, A. R., & Kaiser, C. A. (1998). The ERO1 gene of yeast is required for oxidation of protein dithiols in the endoplasmic reticulum. *Mol Cell*, *1*(2), 161-170.

Gething, M. J. (1999). Role and regulation of the ER chaperone BiP. *Semin Cell Dev Biol*, *10*(5), 465-472.

Guarente, L. (1983). Yeast promoters and lacZ fusions designed to study expression of cloned genes in yeast. *Methods Enzymol*, *101*, 181-191.

Hamman, B. D., Hendershot, L. M., & Johnson, A. E. (1998). BiP maintains the permeability barrier of the ER membrane by sealing the lumenal end of the translocon pore before and early in translocation. *Cell*, *92*(6), 747-758.

Hendershot, L. M. (2004). The ER function BiP is a master regulator of ER function. *Mt Sinai J Med*, *71*(5), 289-297.

Ichhaporia, V. P., Kim, J., Kavdia, K., Vogel, P., Horner, L., Frase, S. et al. (2018). SIL1, the endoplasmic-reticulum-localized BiP co-chaperone, plays a crucial role in maintaining skeletal muscle proteostasis and physiology. *Dis Model Mech*, *11*(5).

Kimata, Y., Kimata, Y. I., Shimizu, Y., Abe, H., Farcasanu, I. C., Takeuchi, M. et al. (2003). Genetic evidence for a role of BiP/Kar2 that regulates Ire1 in response to accumulation of unfolded proteins. *Mol Biol Cell*, *14*(6), 2559-2569.

Ponsero, A. J., Igbaria, A., Darch, M. A., Miled, S., Outten, C. E., Winther, J. R. et al. (2017). Endoplasmic Reticulum Transport of Glutathione by Sec61 Is Regulated by Ero1 and Bip. *Mol Cell*, *67*(6), 962-973.e5.

Sevier, C. S. (2018). Redox Regulation of Hsp70 Chaperone Function in the Endoplasmic Reticulum. In M. J. Feige (Ed.), *Oxidative Folding of Proteins: Basic Principles, Cellular Regulation and Engineering. Vol. 9* (pp. 334-354). Royal Society of Chemistry.

Sevier, C. S., Qu, H., Heldman, N., Gross, E., Fass, D., & Kaiser, C. A. (2007). Modulation of cellular disulfide-bond formation and the ER redox environment by feedback regulation of Ero1. *Cell*, *129*(2), 333-344.

Van Raamsdonk, J. M. (2006). Loss of function mutations in SIL1 cause Marinesco-Sjögren syndrome. *Clin Genet*, *69*(5), 399-400.

Vogel, J. P., Misra, L. M., & Rose, M. D. (1990). Loss of BiP/GRP78 function blocks translocation of secretory proteins in yeast. *J Cell Biol*, *110*(6), 1885-1895.

Walter, P., & Ron, D. (2011). The unfolded protein response: from stress pathway to homeostatic regulation. *Science*, *334*(6059), 1081-1086.

Wang, J., Pareja, K. A., Kaiser, C. A., & Sevier, C. S. (2014). Redox signaling via the molecular chaperone BiP protects cells against endoplasmic reticulum-derived oxidative stress. *Elife*, *3*, e03496.

Wang, J., & Sevier, C. S. (2016). Formation and Reversibility of BiP Protein Cysteine Oxidation Facilitate Cell Survival during and post Oxidative Stress. *J Biol Chem*, *291*(14), 7541-7557.

Wei, P. C., Hsieh, Y. H., Su, M. I., Jiang, X., Hsu, P. H., Lo, W. T. et al. (2012). Loss of the oxidative stress sensor NPGPx compromises GRP78 chaperone activity and induces systemic disease. *Mol Cell*, *48*(5), 747-759.

Wilkinson, B., & Gilbert, H. F. (2004). Protein disulfide isomerase. *Biochim Biophys Acta*, *1699*(1-2), 35-44.

Xu, H., Xu, S., Zhang, R., Xin, T., & Pang, Q. (2018). SIL1 functions as an oncogene in glioma by AKT/mTOR signaling pathway. *Onco Targets Ther*, *11*, 3775-3783.

Xu, M., Marsh, H. M., & Sevier, C. S. (2016). A Conserved Cysteine within the ATPase Domain of the Endoplasmic Reticulum Chaperone BiP is Necessary for a Complete Complement of BiP Activities. *J Mol Biol*, *428*(20), 4168-4184.

Yan, M., Li, J., & Sha, B. (2011). Structural analysis of the Sil1-Bip complex reveals the mechanism for Sil1 to function as a nucleotide-exchange factor. *Biochem J*, *438*(3), 447-455.

Zhao, L., Longo-Guess, C., Harris, B. S., Lee, J. W., & Ackerman, S. L. (2005). Protein accumulation and neurodegeneration in the woozy mutant mouse is caused by disruption of SIL1, a cochaperone of BiP. *Nat Genet*, *37*(9), 974-979.